POPULATION PHARMACOKINETICS OF INTRAVENOUS ACETAMINOPHEN (PARACETAMOL) AND ITS METABOLITES IN NEONATES

by

Sarah Fogley Cook

A dissertation submitted to the faculty of
The University of Utah
in partial fulfillment of the requirements for the degree of

Doctor of Philosophy

Department of Pharmacology and Toxicology

The University of Utah

December 2015

The University of Utah Graduate School

STATEMENT OF DISSERTATION APPROVAL

The dissertation of **Sarah Fogley Cook**

has been approved by the following supervisory committee members:

Michael R. Franklin	, Chair	**10/02/2015** Date Approved
Diana G. Wilkins	, Member	**10/02/2015** Date Approved
Catherine M. Sherwin	, Member	**10/02/2015** Date Approved
Philip J. Moos	, Member	**10/02/2015** Date Approved
Lawrence D. McGill	, Member	**10/02/2015** Date Approved

and by **Karen S. Wilcox** , Chair/Dean of

the Department/College/School of **Pharmacology and Toxicology**

and by David B. Kieda, Dean of The Graduate School.

ABSTRACT

Pain management is a critical component of neonatal intensive care, not only for ethical reasons, but also because the failure to provide adequate analgesia during early life has been associated with poor outcomes. Intravenous acetaminophen is an attractive option for treatment of neonatal pain; however, there is a lack of consensus regarding optimal dosing guidelines, and safety data are limited. A principal safety concern is acetaminophen-induced hepatotoxicity, which depends highly on drug metabolism. Unfortunately, neonatal pharmacokinetic data for acetaminophen metabolites are scarce. The objective of this dissertation was to explore maturational changes in the pharmacokinetics of intravenous acetaminophen and its metabolites in neonates. This goal was achieved by completion of three major aims that centered on a prospective clinical trial. Neonates with a clinical indication for intravenous analgesia received multiple doses of intravenous acetaminophen, and pharmacokinetic samples were collected throughout a 72-h study period. Aim 1 focused on development and validation of a novel high-performance liquid chromatography–tandem mass spectrometry method for simultaneous quantification of acetaminophen and the metabolites derived from acetaminophen glucuronidation, sulfation, and oxidation. Suitability of the assay was demonstrated by analysis of plasma and urine samples from the neonatal pharmacokinetic study. In Aim 2, a population pharmacokinetic model was developed from the parent drug concentration–time data. In extremely preterm to full-term neonates, body weight

was the principal predictor of intravenous acetaminophen pharmacokinetics. External evaluation with a dataset from an independent study suggested that these findings should be generalizable to other similar patient populations. Aim 3 focused on development of a parent–metabolite population pharmacokinetic model using the data obtained from the neonatal pharmacokinetic study. As part of model development, an extensive covariate analysis was performed to identify patient characteristics that influenced metabolite pharmacokinetic parameters, with a particular focus on formation clearance of metabolites derived from acetaminophen oxidation. Maturational changes in the fraction of acetaminophen undergoing oxidation were small relative to between-subject variability. Collectively, these results improve understanding of the factors influencing acetaminophen disposition during the neonatal period, and these findings inform appropriate dosing strategies for intravenous acetaminophen in this vulnerable patient population.

For our study patients and their families, who so generously contributed to scientific progress, even in the face of immense personal challenges

TABLE OF CONTENTS

LIST OF FIGURES

Figure

LIST OF TABLES

Table

LIST OF ABBREVIATIONS

AIC	Akaike information criterion
APAP	acetaminophen; paracetamol; *N*-acetyl-*p*-aminophenol
APAP-cys	acetaminophen-cysteine
APAP-gluc	acetaminophen-glucuronide
APAP-glut	acetaminophen-glutathione
APAP-NAC	acetaminophen-*N*-acetylcysteine
APAP-sulf	acetaminophen-sulfate
BIC	Bayesian information criterion
BMI	body mass index
BSV	between-subject variability
CI	confidence interval
CL	clearance
$CL_{formation}$	formation (hepatic) clearance
CV	coefficient of variation
CYP	cytochrome P450
ECD	electrochemical detection
ESI	electrospray ionization
GA	gestational age
GFR	glomerular filtration rate

HPLC	high-performance liquid chromatography
IS	internal standard(s)
LC	liquid chromatography
LLOQ	lower limit of quantification
MRM	multiple reaction monitoring
MS/MS	tandem mass spectrometry
NAPQI	*N*-acetyl-*p*-benzoquinone imine
NBup-D_3	norbuprenorphine-D_3
NCT	national clinical trial
NICU	neonatal intensive care unit
NONMEM	nonlinear mixed effects modeling
NPDE	normalized prediction distribution error
OFV	objective function value
PARANEO	paracetamol in neonates
PCA	postconceptional age
PMA	postmenstrual age
PNA	postnatal age
PsN	Perl-speaks-NONMEM
QC	quality control
RSE	relative standard error
RUV	residual unexplained variability
SD	standard deviation
SRM	selective reaction monitoring

SULT	sulfotransferase
UGT	UDP-glucuronosyltransferase
ULOQ	upper limit of quantification
UV	ultraviolet
V_d	volume of distribution

GLOSSARY OF COMMON TERMS

Akaike information criterion: An indicator of the goodness of fit for a model to a set of data observations. The Akaike information criterion is equal to the objective function value plus twice the number of model parameters. Thus, it is an indicator of model fit that includes a penalty for increased model complexity (i.e., more parameters). The number itself is not meaningful, but changes in the Akaike information criterion are informative. A decrease in Akaike information criterion indicates an improvement in model fit that exceeds the complexity penalty. Unlike comparisons of objective function values, comparisons of Akaike information criteria have no statistical interpretation.

Bayesian information criterion: An indicator of the goodness of fit for a model to a set of data observations. The Bayesian information criterion is equal to the objective function value plus the product of the number of model parameters and the natural log of the number of data observations. Thus, it is an indicator of model fit that includes a penalty for increased model complexity (i.e., more parameters). The number itself is not meaningful, but changes in the Bayesian information criterion are informative. A decrease in Bayesian information criterion indicates an improvement in model fit that exceeds the complexity penalty. Unlike comparisons of objective function values, comparisons of Bayesian information criteria have no statistical interpretation. Model discrimination based on Bayesian information criteria tends to be more conservative than that based on Akaike information criteria; i.e., it tends to select the simpler model.

Between-subject variability: A type of random-effect parameter in a population pharmacokinetic model. Between-subject variability describes the magnitude of the differences in pharmacokinetic parameter values that occur across individuals. In model equations, the random effect for an individual on a given pharmacokinetic parameter is typically denoted with the Greek letter *eta* (η), and the between-subject variability for a given pharmacokinetic parameter is described by the variance of the eta distribution, which is typically denoted as the square of the Greek letter *omega* (ω^2). In the modeling software program NONMEM, the omega (Ω) matrix is used to indicate which between-subject variance parameters should be estimated.

Conditional weighted residual: A statistic that is used to evaluate nonlinear mixed effects models. The calculation of conditional weighted residuals involves standardization of the prediction errors (i.e., the difference between predicted and observed concentrations) in order to account for the variability in the predictions as well as the correlation between multiple prediction errors from the same individual. Conditional weighted residuals should be normally distributed with a mean of 0 and a variance of 1. Therefore, most conditional weighted residuals are expected to fall between −3 and +3 (i.e., within

3 standard deviations of the observation).

Covariate: Any variable that is specific to an individual and may explain pharmacokinetic variability. Covariates describe predictable sources (fixed effects) of variability. Incorporation of a useful covariate into a pharmacokinetic model is expected to reduce the amount of unpredictable variability (random effects). Examples of potential covariates include body weight, age, sex, and genotype.

Extremely preterm: Gestational age <28 weeks.

Fixed effects: Pharmacokinetic model parameters that take on a single value for all individuals in a study population. Fixed-effect parameters include structural pharmacokinetic parameters, which describe the shape of the typical concentration time course in a population, and covariate parameters, which describe pharmacokinetic variability that can be predicted by subject characteristics. In model equations, fixed-effect parameters are typically denoted with the Greek letter *theta* (θ).

Full term: Gestational age ≥37 weeks and <42 weeks.

Gestational age: The time elapsed between the first day of a mother's last normal menstrual period and the day of delivery. Gestational age is usually expressed in completed weeks; e.g., a 30-week, 6-day fetus is considered to have a gestational age of 30 weeks.

Individual prediction: A pharmacokinetic model prediction that is based on fixed-effect parameters and also incorporates the between-subject random effects.

Infant: A child with a postnatal age <365 days. Infancy includes the neonatal period.

Neonate: A child with a postnatal age <28 days.

Nested models: Two models are considered nested, or hierarchical, when one model is a subset of the other; i.e., when setting one (or more) parameter(s) in the larger model to the null hypothesis value(s) makes the models identical.

Nonlinear mixed effects modeling: A modeling approach that simultaneously analyzes all data for a study population while still accounting for intra-individual observations. *Nonlinear* refers to the fact that the dependent variable (e.g., concentration) is nonlinearly related to the independent variable (e.g., time) and model parameters; *mixed effects* refers to the incorporation of fixed and random effects. One of the most popular software programs for nonlinear mixed effects modeling is an acronym of the term (NONMEM). In the field of pharmacokinetics, this approach is often more specifically described as population pharmacokinetic modeling.

Normalized prediction distribution error: A simulation-based statistic that is used to evaluate nonlinear mixed effects models. Normalized prediction distribution errors take into account the full predictive distribution of each observation and account for the correlation between multiple observations from the same individual. By construction,

normalized prediction distribution errors should be normally distributed with a mean of 0 and a variance of 1.

Objective function value: An indicator of the goodness of fit for a model to a set of data observations. The number itself is not meaningful, but changes in objective function value are informative. A decrease in objection function value indicates an improvement in model fit. If two models are nested, the difference in objective function values is approximately asymptotically chi-squared distributed with degrees of freedom equal to the difference in the number of parameters; e.g., for two competing models that differ by one parameter, a difference of >3.84 units in objective function values is considered a significant difference in model fit at $p < 0.05$.

Pharmacokinetic parameter: Structural parameters that mathematically describe the shape of a concentration time course (e.g., clearance and volume of distribution).

Population prediction: A pharmacokinetic model prediction that is based only on fixed-effect parameters (i.e., the structural and covariate parameters).

Postconceptional age: The time elapsed between the day of conception and the day of delivery (i.e., conceptional age) plus the time elapsed since birth (i.e., postnatal age). In pregnancies resulting from assisted reproductive technologies, a precise conceptional age can be determined; in other cases, conceptional age is assumed to be 2 weeks less than gestational age. The American Academy of Pediatrics has recommended that *postconceptional age* should not be used in clinical pediatrics, so the term has largely fallen out of favor but still appears in some literature.

Postmenstrual age: The time elapsed between the first day of a mother's last normal menstrual period and birth (i.e., gestational age) plus the time elapsed since birth (i.e., postnatal age). Postmenstrual age is usually expressed in weeks; e.g., an infant with a gestational age of 32 weeks and a postnatal age of 4 days has a postmenstrual age of 32.6 weeks.

Postnatal age: The time elapsed since birth. Also referred to as chronological age.

Post term: Gestational age ≥42 weeks.

Preterm: Gestational age <37 weeks.

Random effects: Pharmacokinetic model parameters that vary across individuals in a study population. Random-effect parameters describe unpredictable pharmacokinetic variability, for instance, between-subject variability, between-occasion variability, and residual unexplained variability.

Residual unexplained variability: A type of random-effect parameter in a population pharmacokinetic model. Residual unexplained variability describes the magnitude of the unexplained differences between the predicted and observed concentrations. In model equations, the random effect for an observation is typically denoted with the Greek letter *epsilon* (ε), and the residual unexplained variability is described by the variance of the

epsilon distribution, which is typically denoted as the square of the Greek letter *sigma* (σ^2). In the modeling software program NONMEM, the sigma (Σ) matrix is used to indicate which residual unexplained variance parameters should be estimated.

Very preterm: Gestational age $\geq$28 weeks and <32 weeks.

ACKNOWLEDGMENTS

This dissertation reflects the efforts and contributions of many individuals. I thank, first and foremost, the members of my dissertation committee for their outstanding guidance and support. I was incredibly fortunate to have opportunities to work closely with each one of them during different stages of my graduate career and to learn from their unique expertise and research styles. Diana Wilkins, my committee co-chair, provided me with a perfect balance of independence and supervision. Michael Franklin, also a co-chair, kept me focused on the big picture and never lacked constructive suggestions for ways to improve my work. Catherine Sherwin introduced me to the wonderful world of population modeling and displayed a remarkable commitment to serving as my mentor. Philip Moos perpetually amazed me with his breadth and depth of knowledge, from which I benefited greatly. Lawrence McGill generously shared his time and helpful perspective long after the completion of histopathology analysis. Douglas Rollins graciously took time out of his well-deserved retirement to stay involved in my project.

My deepest thanks go to Amber King of the Center for Human Toxicology in the Department of Pharmacology and Toxicology at the University of Utah for her vast contributions to the analytical work presented in this dissertation. I am also grateful for the help and friendship provided by many others at the Center for Human Toxicology, especially David Andrenyak, Bobbie Smith, Olga Averin, Wendy Fang, David Anderson,

and Fenyun Liu.

Pediatrics became my adoptive home during the latter portion of my research, and I owe a great deal to many people in that department. Jessica Roberts and Chris Stockmann provided invaluable guidance and encouragement throughout my pharmacokinetic modeling efforts. Much-appreciated support and camaraderie were supplied by many others, particularly Jonathan Constance, Matthew Linakis, Tian Yu, Alfred Balch, Nicole Mihalopoulos, and Amy Adams.

I am immensely grateful to John van den Anker of Children's National Health System, who so generously allowed me to work with the data from his clinical trial. I would also like to acknowledge John's colleagues and staff at Children's National Health System, namely, Elaine Williams, Nina Deutsch, Samira Samiee-Zafarghandy, and Syamala Mankala, for their contributions to the execution of the trial and the collection of study data. I am indebted, as well, to Karel Allegaert of KU Leuven for the dataset he so graciously shared. His collaborative spirit enabled our external model evaluation.

My thanks also go to all those in the Department of Pharmacology and Toxicology who have supported me throughout graduate school: to the chairs, Karen Wilcox and William Crowley, for their leadership; to the Graduate Training Committee for their continued guidance; to the staff, Debra Gillett, Linda Wright, Sandy Hiskey, and Sheila Merrill, for their administrative assistance; to the faculty, who not only taught me pharmacology but taught me how to think critically about pharmacology; and to my fellow students for their support and friendship.

I have been incredibly fortunate to receive stipend support through several predoctoral fellowship programs, and my gratitude, therefore, goes to the Willard L.

Eccles Foundation, the American Foundation for Pharmaceutical Education, and the Howard Hughes Medical Institute and University of Utah Med Into Grad Program (U2M2G). This research was also made possible by a contract for analytical laboratory services from McNeil Consumer Healthcare (to Diana Wilkins and Douglas Rollins) and by National Institutes of Health grants from the *Eunice Kennedy Shriver* National Institute of Child Health and Human Development (R01HD060543; to John van den Anker) and the National Center for Advancing Translational Sciences (UL1TR000075; to Children's National Health System).

Finally, I give heartfelt thanks to my family and friends for their extraordinary support and encouragement. Xiaoying He helped me realize that graduate school was the right path. Nela Zvereva has provided enduring friendship. My family have given their constant love and support — my parents, Anees and Karen Fogley; my sisters, Rebecca and Rachel Fogley; and my father- and mother-in-law, Fran and Donna Cook. Above all, I thank my husband, Tim, for his boundless support, patience, and utter faith in my abilities.

CHAPTER 1

INTRODUCTION

Pain Management in Neonates

Over the course of the 20th century, neonatal mortality in the United States decreased substantially [1, 2]. A recent report from the National Center for Health Statistics showed that the neonatal mortality rate, which is defined as the number of deaths before a postnatal age of 28 days per 1,000 live births, continued to decline from 2000 to 2011 [3]. Reductions in neonatal mortality rate that have occurred since 1970 have largely been attributed to advances in medical care [1, 2], but decreases in neonatal deaths have been accompanied by increases in the number of critically ill neonates requiring intensive care. In the United States, overall admission rates to neonatal intensive care units (NICUs) were recently estimated at 77.9 per 1,000 live births, and rates ranged from 43.0 per 1,000 live births for normal-birth-weight infants (2.5–4.0 kg) to 844.1 per 1,000 live births for very low-birth-weight infants (<1.5 kg) [4].

Neonatal intensive care often involves exposure to pain from surgery, disease state, or repeated procedures such as endotracheal intubation, heel puncture, indwelling arterial and venous catheter insertion, nasogastric tube insertion, and nasal, tracheal, and gastric suctioning [5, 6]. Estimates from prospective studies showed that newborns underwent a mean of 10–12 painful procedures per day during the first 14 days of NICU hospitalization [5, 7]. Consequently, pain management is a critical component of neonatal intensive care, not only for humanitarian reasons, but also because the failure to provide adequate analgesia during early life has been associated with poor short- and long-term outcomes [8].

As recently as the 1980s, neonates were assumed to have an inability or diminished capacity to perceive pain due to nervous system immaturity [8]. In 1987, a

paradigm-shifting paper by Anand and Hickey helped to establish that pain pathways are intact and functional in neonates [9]. In neonates, painful stimuli produce acute behavioral and physiological responses. Behavioral responses include crying and specific facial expressions and body movements [10-12]; physiological responses are reflected in cardiorespiratory, hormonal, and metabolic changes [8, 9, 12]. In neonates who received inadequate surgical anesthesia, acute physiological stress responses were accompanied by short-term circulatory and metabolic complications [13]. Long-term adverse outcomes associated with neonatal pain exposure are numerous and include neuromorphological effects [14, 15], growth impairments [16], cognitive and motor deficits [17], and altered pain thresholds [12]. Collectively, these findings highlight the importance of achieving effective neonatal analgesia.

Intravenous Acetaminophen

In neonates, acetaminophen (*N*-acetyl-*p*-aminophenol, paracetamol) is commonly used for treatment of mild to moderate procedural pain or as part of multimodal postoperative pain management [8, 18]. Acetaminophen was first synthesized in 1888 and has been widely used since it was first marketed to consumers in the mid-20th century [19]. Today, acetaminophen is one of the most commonly used medications in the United States, and the prevalence of use is high in both adults [20-22] and children [23]. It has been estimated that 26% of children <2 years of age use a product containing the drug each week [23]. Acetaminophen is used for its analgesic and antipyretic effects, which are thought to occur primarily via inhibition of cyclooxygenase activity and prostaglandin synthesis [24]. Very recently, the proposed use of acetaminophen for closure of patent

ductus arteriosus in preterm neonates has also piqued interest in a new potential indication [25].

Oral and rectal formulations of acetaminophen have long been available, but intravenous formulations are relatively new. The first intravenous formulation, propacetamol, is a prodrug that is rapidly hydrolyzed by plasma esterases to produce acetaminophen. Propacetamol has not been approved by the United States Food and Drug Administration but it is available in other countries. Unfortunately, propacetamol requires reconstitution and is associated with infusion-site discomfort [26, 27]. More recently, an intravenous formulation of the active drug was developed in a ready-to-use solution that elicits few infusion-site reactions [27, 28]. Intravenous acetaminophen was first approved in 2002 in Europe and is marketed under the trade name Perfalgan [29]. In the United States, intravenous acetaminophen was approved in 2010, and the formulation is marketed under the trade name Ofirmev [30]. Intravenous acetaminophen has been rapidly adopted into clinical practice and has been described as “a worthy addition to the analgesic armamentarium” [31]. The intravenous formulations allow for administration of the drug in situations when enteral delivery is unsuitable, for instance, during postoperative periods. Additionally, intravenous delivery provides predictable bioavailability and onset of action compared to enteral routes [32, 33].

In the United States, intravenous acetaminophen is only approved for use in adults and in children 2 years of age or older; it is indicated for management of mild to moderate pain, management of moderate to severe pain with adjunctive opioid analgesics, and fever reduction [30]. In other countries, intravenous acetaminophen is approved for use in term neonates [18, 29]. Both licensed and off-label administration of

intravenous acetaminophen to neonates occurs worldwide [18]. Intravenous acetaminophen is a particularly attractive option for neonatal analgesia because it has fewer side effects and is generally better tolerated than opioids [8, 34], and postoperative use of intravenous acetaminophen in neonates has been shown to reduce morphine requirements [35]. The licensed dose for patients weighing 10 kg or less, including term neonates, is 7.5 mg/kg every 4–6 h, with a maximum daily dose of 30 mg/kg [29]. In practice, diverse dosing regimens have been implemented [36-38]. Many of these regimens comprise higher-than-licensed doses, which have been suggested by neonatal pharmacokinetic studies (Table 1.1) [18, 36-39]. In the clinical trial that is the focus of this dissertation, 15-mg/kg doses were administered at 12-h intervals to neonates <28 weeks' gestation (30 mg/kg/day) and at 8-h intervals to neonates ≥28 weeks' gestation (45 mg/kg/day), and these total daily doses are roughly consistent with many of the suggested dosing regimens listed in Table 1.1.

Pharmacokinetics of Intravenous Acetaminophen in Neonates

Appropriate dose selection for neonates is complicated by developmental changes that occur during early life [40]. Acetaminophen is primarily eliminated by hepatic metabolism, so measures of hepatic maturation and function are critical for explanation of between-subject variability in acetaminophen pharmacokinetics [39, 41-44]. A number of recent neonatal studies have reported on the pharmacokinetics of intravenous acetaminophen [39, 42] and propacetamol [45-47]; however, there is still a lack of consensus regarding optimal dosing guidelines (Table 1.1) [18, 36-39]. Furthermore, pharmacokinetic data from extremely preterm neonates (<28 weeks' gestation) remain

Table 1.1 Suggested neonatal dosing regimens for intravenous acetaminophen.

Source	Description	Neonatal subgroup	Dose (mg/kg)	Interval (h)	Total daily dose (mg/kg)
[29]	Licensed dose for Perfalgan	Term neonates	Loading: n/s Maintenance: 7.5	4–6	30[a]
[36]	"Stockholm protocol"	28–32 wks PCA	Loading: 20 Maintenance: 7.5	8	22.5–35
		33–36 wks PCA	Loading: 20 Maintenance: 7.5	6	30–42.5
		>37 wks PCA	Loading: 20 Maintenance: 10–15	6	40–65
[37]	Allegaert et al. 2007	<31 wks PCA	Loading: 20 Maintenance: 10	12	20–30
		31–36 wks PCA	Loading: 20 Maintenance: 10	8	30–40
		>36 wks PCA	Loading: 20 Maintenance: 10	6	40–50
[48]	Neonatal formulary	<30 wks PMA	Loading: 20 Maintenance: 10	6	40–50
		31–36 wks PMA	Loading: 20 Maintenance: 12.5	6	50–57.5
		Term neonates	Loading: 20 Maintenance: 15	6	60–65
[18]	Dutch formulary	<31 wks PMA	Loading: 20 Maintenance: 10	n/s	20[b]
		31–36 wks PMA	Loading: 20 Maintenance: 10	n/s	30[b]
		Term neonates	Loading: 20 Maintenance: 10	n/s	40[b]
[39]	Allegaert et al. 2011	32–44 wks PMA	Loading: 20 Maintenance: 10	6	40–50

[a] Maximum daily dose limited to 30 mg/kg.

[b] Maximum amount from maintenance dosing per day.

n/s, not specified; PCA, postconceptional age; PMA, postmenstrual age.

scarce [18, 39, 42]. The age-based breakpoints in the dosing regimens listed in Table 1.1 are somewhat arbitrary but reflect the tendency of clinicians to recommend more conservative drug administration for less mature neonates.

Estimates for clearance of intravenous acetaminophen in neonates range from 0.090–0.21 L/h/kg, depending in part upon gestational, postmenstrual, or postconceptional age [39, 42, 45-47]. The distribution of intravenous acetaminophen in neonates has been described with both one- [45-47] and two-compartment [39, 42] pharmacokinetic models, and volume of distribution estimates range from 0.56–0.76 L/kg [42, 46]. Neonatal pharmacokinetic parameter estimates can be extrapolated to a standard 70-kg adult using allometric scaling exponents of 0.75 and 1 for clearance and volume of distribution, respectively [49]. Allometrically standardized estimates from neonatal studies of intravenous acetaminophen range from 70–76 L/70 kg for volume of distribution [39, 45, 47] and 2.9–7.1 L/h/70 kg for clearance. These standardized neonatal volumes of distribution are consistent with the typical adult range of 0.7–1.0 L/kg [50]. The standardized neonatal clearance values are approximately 20–40% of typical adult values [51], and this relatively low neonatal clearance can be attributed to incomplete maturation of hepatic drug metabolism pathways [44, 52-54]. Zuppa et al. have described the pharmacokinetics of intravenous acetaminophen across the pediatric age range and found that standardized clearance values increased from birth and plateaued near adult values by approximately 2 years of age [41]. The study by Zuppa et al. only included three full-term neonates; nevertheless, the findings are consistent with the studies that focused solely on neonatal subjects.

Body weight, as a correlate of body size, has been identified as the major patient

characteristic (covariate) influencing intravenous acetaminophen pharmacokinetics in neonates [39, 45, 47]. Postmenstrual age [39, 47], postconceptional age [45], and unconjugated bilirubin [39, 47] have also been shown to have minor effects on neonatal clearance of intravenous acetaminophen. More specifically, high unconjugated bilirubin has been associated with reduced clearance [39, 47], and correlation in concentrations of acetaminophen and unconjugated bilirubin might derive from the fact that both molecules undergo substantial clearance via glucuronidation.

Perhaps the most comprehensive study to date on the pharmacokinetics of intravenous acetaminophen in neonates is the pooled analysis performed by Allegaert et al. [39]. After identifying body weight as the principal predictor of intravenous acetaminophen pharmacokinetics in neonates with postmenstrual ages of 32–44 weeks, the authors proposed a parsimonious dosing regimen in which maturational changes in acetaminophen pharmacokinetics could be accommodated using only equivalent per-kilogram dosing, without requirements for different doses or dosing intervals dependent upon gestational or postmenstrual age [39]. The appropriateness of implementing such a dosing regimen in neonates of <32 weeks' postmenstrual age requires further investigation. Additionally, the efficacy of the proposed dosing regimen should be evaluated in pharmacodynamic studies. Finally, appropriate dosing should also be guided by safety data. The principal safety concern that accompanies use of acetaminophen is the risk of acetaminophen-induced hepatotoxicity, which depends highly on drug metabolism [24, 34].

Acetaminophen Metabolism and Acetaminophen-Induced Hepatotoxicity

When used as indicated, acetaminophen is well tolerated [24, 55, 56]. At supratherapeutic doses, however, the drug has long been known to produce liver necrosis [57-60], and acetaminophen overdose is currently the leading cause of acute liver failure in the United States [61]. Drug metabolism plays a key role in acetaminophen-induced hepatotoxicity, as illustrated in Figure 1.1 [62, 63]. Much of the present understanding of the relationship between acetaminophen metabolism and hepatotoxicity stems from research performed in the National Institutes of Health laboratory of James Gillette and B. B. Brodie. The results of their rodent model experiments were published in 1973 in a series of seminal papers by Mitchell et al. [64, 65], Jollow et al. [66], and Potter et al. [67].

Acetaminophen metabolism occurs primarily in the liver, where the drug undergoes glucuronidation and sulfation by UDP-glucuronosyltransferases (UGTs) and sulfotransferases (SULTs), respectively. The nontoxic glucuronide and sulfate metabolites are efficiently excreted in the urine. Acetaminophen can also be oxidized by hepatic cytochrome P450 enzymes (CYPs) to form the reactive intermediate *N*-acetyl-*p*-benzoquinone imine (NAPQI). At therapeutic doses, only a small portion (5–15%) of acetaminophen is bioactivated to yield NAPQI. This electrophilic species can be detoxified by conjugation with glutathione, either nonenzymatically or with the aid of glutathione *S*-transferase enzymes. The acetaminophen-glutathione conjugate undergoes rapid hydrolysis by hepatic gamma-glutamyl transpeptidase and dipeptidases to form acetaminophen-cysteine, and acetaminophen-cysteine is subsequently acetylated by *N*-

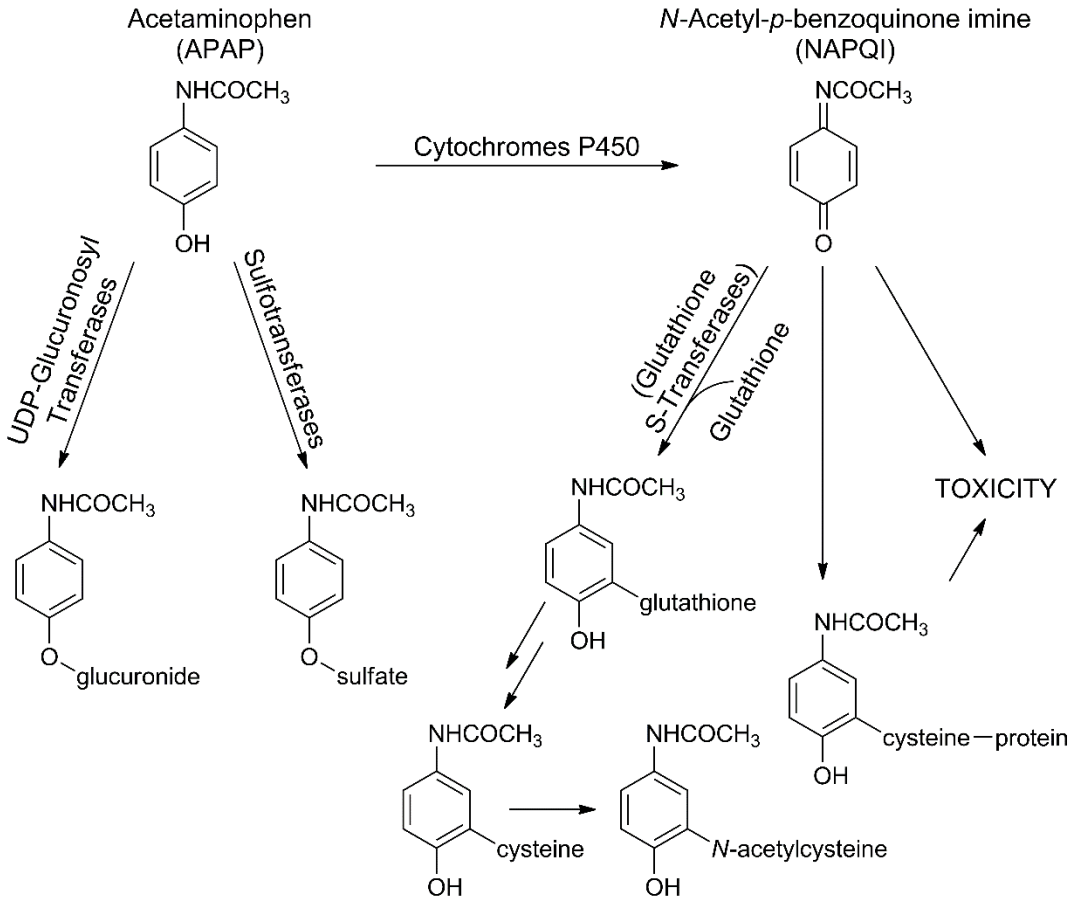

Figure 1.1 Major routes of hepatic metabolism for acetaminophen with relationship to hepatotoxicity.

acetyltransferases, thus producing acetaminophen-*N*-acetylcysteine [68, 69]. Given a sufficiently high dose of acetaminophen, the glutathione detoxification pathway can be saturated by NAPQI, and excess electrophile will instead bind covalently to hepatic proteins [62, 63]. Toxicity is thought to result from a combination of inactivation of critical hepatic proteins via NAPQI binding and oxidative stress [70, 71].

As illustrated in Figure 1.1, the balance between different metabolic pathways plays a critical role in influencing susceptibility to acetaminophen-induced hepatotoxicity. Furthermore, this balance can be influenced by individual characteristics (e.g., genetics, ethnicity, sex, age) as well as extrinsic factors (e.g., nutritional status, concomitant drug/xenobiotic exposure, circadian variation, repeated acetaminophen exposure). Ample evidence from rodent model studies illustrates the interplay between factors affecting acetaminophen metabolism and acetaminophen-induced hepatotoxicity, including age [72], sex [73], natural products exposure [74], fasting [75], diurnal variation [76], and repeated acetaminophen exposure [77]. In humans, it is difficult to obtain proof of causal relationships between metabolic effects of such factors and susceptibility to acetaminophen-induced hepatotoxicity; however, some associations have been noted. Court et al. found that a single nucleotide polymorphism in the UGT1A-3′ untranslated region (rs8330) was associated with enhanced *in vitro* acetaminophen glucuronidation, and also showed that this polymorphism was underrepresented in patients with acute liver failure following unintentional acetaminophen overdose compared to acute liver failure from other causes (intentional acetaminophen overdose or non-acetaminophen-induced acute liver failure) [78]. There is also evidence that acute alcohol (ethanol) exposure in humans reduces the risk of acetaminophen-induced

hepatotoxicity via inhibition of CYP2E1 and, conversely, that chronic alcohol exposure increases the risk of toxicity via induction of CYP2E1 expression, although the relationship between alcohol exposure and acetaminophen-induced hepatotoxicity is somewhat contentious [24, 62].

Acetaminophen Metabolism in Neonates

Children are generally thought to be more resistant to acetaminophen-induced hepatotoxicity than adults [79-81], but hepatic safety data for intravenous acetaminophen in neonates are quite limited. One retrospective study based on data collected from preterm neonates, term neonates, and young infants showed no significant increase in serum alanine aminotransferase, aspartate aminotransferase, or gamma-glutamyl transpeptidase during or up to 2 days after repeated administration of intravenous acetaminophen [82]. These observations were made during implementation of a dosing regimen that was more aggressive than the licensed schedule (see [37] in Table 1.1), and they suggest that such dosing is well tolerated. However, the analysis was only based on serum liver enzyme measurements, which suffer from well-documented limitations [83]. Additionally, these findings are based on retrospective data from a single study center.

As discussed in the previous section, inter-individual differences in acetaminophen metabolism are likely to influence susceptibility to acetaminophen-induced hepatotoxicity. Furthermore, substantial developmental changes in drug metabolism occur during the neonatal period [84, 85], and maturational differences might increase the risk of acetaminophen-induced hepatotoxicity in certain subgroups of neonates. Unfortunately, neonatal pharmacokinetic data for acetaminophen metabolites

remain scarce across all routes of administration, and previous studies that have incorporated metabolite data focused on the glucuronide and sulfate conjugates [42, 52, 53, 86-88].

Both early [52, 53] and recent [42, 86-88] studies on the neonatal pharmacokinetics of acetaminophen-sulfate and acetaminophen-glucuronide have generally relied on urinary excretion data. In neonates, sulfation is the predominant route of acetaminophen elimination [42, 52, 53, 86-88]. Glucuronidation accounts for the majority of acetaminophen clearance in adults, but glucuronidation capacity is immature in neonates [44, 89]. Van der Marel et al. modeled the pharmacokinetics of acetaminophen and its glucuronide and sulfate metabolites in infants and young children with an age range of approximately 5–20 months [90]. Weight-standardized formation (hepatic) clearance of acetaminophen-sulfate did not increase with age, but acetaminophen-glucuronide formation clearance increased with age from an extrapolated neonatal value of 2.7 L/h/70 kg to 6.6 L/h/70 kg at 20 months of age, which is approximately half of adult estimates.

Neonatal pharmacokinetic data for acetaminophen-sulfate and acetaminophen-glucuronide agree reasonably well with data from ontogenic expression and activity studies. In a panel of human fetal and postnatal liver cytosol preparations, acetaminophen sulfation exhibited a strong negative correlation with estimated gestational age during the earlier stages of development (10–25 weeks' estimated gestational age), but activity was relatively stable from an estimated gestational age of approximately 25 weeks through adolescence [91]. Results from experiments with human liver microsomes and recombinant human UGTs suggest that UGT1A1, UGT1A6, and UGT1A9 contribute to

acetaminophen glucuronidation [92]. A role for UGT2B15 in acetaminophen glucuronidation has also been supported by *in vivo* data [93]. In fetal liver samples (20 weeks' gestation), mRNA expression for these four UGT isoforms was undetectable [94]. By 6 months after birth, transcript levels for UGT1A1, UGT1A6, and UGT2B15 reached adult values, and by 7 months after birth, protein expression of UGT1A1 and UGT1A6 was also consistent with that in adults. For UGT1A9, mRNA expression was detectable at 6 months of age but did not approach adult values until 1.5 years after birth. *In vitro* activity for glucuronidation of bilirubin, a UGT1A1-specific substrate, are consistent with these mRNA and protein expression data: as a percentage of adult activity, bilirubin glucuronidation was 0.1% at 17–30 weeks' gestation and 1% at 30–40 weeks' gestation; a rapid age-dependent increase has been observed after birth, independent of gestational age, and adult activity values were reached by 8–15 weeks' postnatal age [89, 95-97].

Neonatal pharmacokinetic data for CYP-derived metabolites (acetaminophen-cysteine and acetaminophen-*N*-acetylcysteine) are lacking, but some information on the ontogeny of relevant CYP enzymes is available from expression and activity studies. In humans, CYP2E1 is primarily responsible for the oxidation of acetaminophen to NAPQI [62]. Vieira et al. were unable to detect CYP2E1 protein or enzyme activity in human fetal liver at >30 weeks' gestation but observed that both protein content and activity increased dramatically on the first day after birth, regardless of gestational age [98]. Protein expression and enzyme activity then followed similar, steady increases over the course of infancy, and values for 1–10 year olds approached those of adults. Measurements of hepatic CYP2E1 protein expression obtained by Johnsrud et al. were somewhat inconsistent with the aforementioned study. CYP2E1 protein was readily

detectable in many fetal liver samples obtained at >20 weeks' gestation. CYP2E1 protein content increased most markedly during the first few months after birth and approached adult values by about 90 days' postnatal age [99]. Birth was not always associated with a spike in CYP2E1 protein expression, and this inconsistency in the onset of expression contributed to substantial between-subject variability in neonatal samples (80-fold variation). Nevertheless, in a subset of samples from subjects with known gestational and postnatal ages, postnatal age was strongly correlated with CYP2E1 content ($p < 0.001$) and gestational age was not ($p = 0.07$). This observation is compatible with the notion that peripartum or postnatal factors play a significant role in initiating CYP2E1 protein expression, which is in line with the findings of Vieira et al.

Collectively, results from relevant enzyme ontogeny studies highlight the volatile and variable nature of neonatal drug metabolism, and these findings underscore the need for further studies of acetaminophen metabolism in this vulnerable patient population.

Utility of Population Pharmacokinetic Modeling for Neonatal Studies

Pediatric pharmacokinetic studies pose numerous challenges in terms of both physiological factors and study design considerations [100]. Physiologically, children exhibit substantial differences in the pharmacokinetic processes of absorption, distribution, metabolism, and excretion compared to adults. Furthermore, both inter- and intra-subject variability in these processes are often large because of substantial developmental changes that occur during early life [40, 101]. Historically, limitations on blood sampling volumes have presented a major study design challenge in pediatric

populations. For instance, based on neonatal volume restrictions, an overall maximum of 9 mL of blood may be collected over a 4-week period. These figures contrast sharply with acceptable collection volumes for adults, from whom such a volume could easily be collected in a matter of hours [100]. Fortunately, the exquisite sensitivity and specificity of modern analytical techniques has enabled quantification of drugs and metabolites in ever-decreasing sample volumes [102]. The introduction of population-based modeling to pediatric pharmacokinetic analysis in the 1980s has also proved critical to surmounting many challenges associated with pediatric study design.

Traditional pharmacokinetic analysis involves estimation of pharmacokinetic parameters for each individual in a study population based on individual concentration–time profiles. Individual pharmacokinetic parameters are then summarized with measures of central tendency, such as means or medians, and measures of variability, such as standard errors or interquartile ranges. In the traditional approach, a relatively large number of samples must be collected from each patient and the sample collection times must be quite consistent across individuals. Additionally, this statistical approach tends to overestimate the amount of between-subject variability in pharmacokinetic parameters because it has a poor ability to differentiate between between-subject and within-subject variability [103].

In contrast to traditional pharmacokinetic analysis, population pharmacokinetic modeling occurs simultaneously for an entire population but still accounts for intra-individual observations [104, 105]. The population approach is more generally referred to as *nonlinear mixed effects modeling*. *Nonlinear* refers to the fact that the dependent variable (e.g., concentration) is nonlinearly related to the independent variable (e.g., time)

and model parameters; *mixed effects* refers to the incorporation of fixed and random effects. Fixed-effect parameters take on a single value for all individuals in a study population and include the structural pharmacokinetic parameters, which describe the shape of the typical concentration time course in a population, and the covariate parameters, which describe pharmacokinetic variability that is predictable based on subject characteristics. Random-effect parameters vary across individuals in a study population and describe unpredictable pharmacokinetic variability, including between-subject variability and within-subject variability (e.g., residual unexplained variability). Importantly, population-based modeling allows for analysis of pharmacokinetic data that is both sparse (i.e., few samples per subject) and unbalanced (i.e., collected at inconsistent points on the concentration–time curve across individuals). Such data is typical of pediatric trials because of ethical and logistical constraints on sample collection. The ability to incorporate systematic covariate analyses for identification of influential patient characteristics is another feature that is particularly useful for studies in neonates, who often exhibit substantial pharmacokinetic variability due to a complex interplay between maturational processes.

Research Objective and Major Findings by Chapter

The overarching objective of this dissertation was to explore maturational changes in the pharmacokinetics of intravenous acetaminophen and its metabolites in neonates. This goal was achieved by completion of three major aims (Chapters 2–4) that were centered on a prospective clinical trial. The study was approved by the Institutional Review Board at Children's National Health System (Washington, DC) and was

conducted in accordance with good clinical practice. In brief, neonates with a clinical indication for intravenous analgesia received acetaminophen (15 mg/kg/dose) for 5 doses at 12-h intervals (<28 weeks' gestation) or for 7 doses at 8-h intervals (≥28 weeks' gestation). The breakpoint in dosing protocol at 28 weeks' gestation was somewhat arbitrary but is in line with other published regimens (Table 1.1), which generally incorporate more conservative dosing practices for less mature neonates. Plasma and urine samples were collected throughout a 72-h pharmacokinetic study period. Importantly, there was good representation of extremely preterm, preterm, and term neonates among the study subjects.

Chapter 2

In recent years, a number of liquid chromatography–tandem mass spectrometry methods have been published for the sensitive and specific quantification of acetaminophen and its metabolites in various human and rodent matrices [106-111]; however, most of these included only the parent drug and one or two metabolites as analytes [107-110]. One recently reported assay included acetaminophen and the glucuronide, sulfate, glutathione, cysteine, and *N*-acetylcysteine conjugates, but the method required two 16-min analytical injections per sample, one for each ionization mode, in order to achieve adequate sensitivity. Additionally, the assay was validated for analysis of rat plasma, not human matrices [106].

Chapter 2 focuses on the development and validation of methods for simultaneous quantification of acetaminophen, acetaminophen-glucuronide, acetaminophen-sulfate, acetaminophen-glutathione, acetaminophen-cysteine, and acetaminophen-*N*-acetyl-

cysteine in human plasma and urine by high-performance liquid chromatography–electrospray ionization–tandem mass spectrometry. Details of the methods are provided along with comprehensive validation results. Because study sample volumes from the neonatal pharmacokinetic trial were extremely limited, the sensitivity of the assays was optimized in order to minimize the amount of sample required for each assay. The utility and suitability of the assays are illustrated by a brief summary of the pharmacokinetic sample analysis. This work was not published prior to submission of the final version of this dissertation.

Chapter 3

Chapter 3 focuses on the development of a population pharmacokinetic model using the parent drug concentration–time data obtained from the neonatal pharmacokinetic study. Nonlinear mixed effects models were constructed in NONMEM 7.2. Potential covariates included body weight, gestational age, postnatal age, postmenstrual age, sex, race, total bilirubin, and estimated glomerular filtration rate. An external dataset was used to test the predictive performance of the model through calculation of bias and precision. In neonates ranging from extremely preterm to full-term gestational ages, body weight was the principal predictor of intravenous acetaminophen pharmacokinetics. Data were well described by a one-compartment model with first-order elimination. Clearance and volume of distribution were estimated as 0.348 L/h (5.5% relative standard error; 30.8% between-subject variability) and 2.46 L (3.5% relative standard error; 14.3% between-subject variability), respectively, at the mean subject weight of 2.30 kg. External evaluation suggested that these findings should be

generalizable to other similar patient populations. The median prediction error was 10.1% (95% confidence interval: 6.1–14.3%) and the median absolute prediction error was 25.3% (95% confidence interval: 23.1–28.1%). This work has been published in *Clinical Pharmacokinetics* [112].

Chapter 4

Chapter 4 focuses on the development of a parent–metabolite population pharmacokinetic model using the data obtained from the neonatal pharmacokinetic study. Concentration–time data for acetaminophen, acetaminophen-glucuronide, acetaminophen-sulfate, and the combined oxidative pathway metabolites (acetaminophen-cysteine and acetaminophen-*N*-acetylcysteine) were simultaneously modeled in NONMEM 7.2. As part of the model development process, an extensive covariate analysis was performed to identify patient characteristics that influenced metabolite pharmacokinetic parameters, with a particular focus on formation clearance of the oxidative pathway metabolites. Formation clearances for all metabolites increased with weight, and formation clearances for glucuronidation and oxidation also increased with postnatal age. At the mean weight (2.3 kg) and postnatal age (7.5 days), formation clearance estimates (bootstrap 95% confidence interval; between-subject variability) were 0.049 L/h (0.038–0.062; 62%) for glucuronidation, 0.21 L/h (0.17–0.24; 33%) for sulfation, and 0.058 L/h (0.044–0.078; 72%) for oxidation. Expression of individual oxidation formation clearance estimates as a fraction of total individual acetaminophen clearance estimates showed that, on average, fractional formation clearance for oxidation increased <15% when plotted against weight or postnatal age. Thus, maturational

changes in the fraction of drug undergoing oxidation were small relative to between-subject variability. This work was not published prior to submission of the final version of this dissertation.

Appendix

One potential limitation of the parent–metabolite model described in Chapter 4 is its failure to account for NAPQI that covalently binds proteins to form acetaminophen protein adducts. Although this fraction of NAPQI is expected to be small relative to the amount conjugated by glutathione, future studies could explore this point more thoroughly by measuring acetaminophen protein adducts in neonatal study samples and testing for covariate effects on the pharmacokinetics of circulating acetaminophen protein adducts. The material in this appendix has been included with such an application in mind. A novel procedure is reported for quantification of a biomarker of acetaminophen protein adducts in human serum by high-performance liquid chromatography–electrospray ionization–tandem mass spectrometry. Details of the method are provided along with validation results. The utility of the assay is illustrated by a brief summary of the analysis of serum samples collected from human subjects taking chronic, therapeutic doses of acetaminophen. This work has been published in the *Journal of Chromatography B* [113].

References

[1] Healthier mothers and babies, Morb. Mortal. Wkly. Rep. 48 (1999) 849.

[2] B. Guyer, M.A. Freedman, D.M. Strobino, E.J. Sondik, Annual summary of vital statistics: trends in the health of Americans during the 20th century, Pediatrics

106 (2000) 1307.

[3] M.F. MacDorman, D.L. Hoyert, T.J. Mathews, Recent declines in infant mortality in the United States, 2005-2011, NCHS Data Brief (2013) 1.

[4] W. Harrison, D. Goodman, Epidemiologic trends in neonatal intensive care, 2007-2012, JAMA Pediatr. 169 (2015) 855.

[5] S.H. Simons, M. van Dijk, K.S. Anand, D. Roofthooft, R.A. van Lingen, D. Tibboel, Do we still hurt newborn babies? A prospective study of procedural pain and analgesia in neonates, Arch. Pediatr. Adolesc. Med. 157 (2003) 1058.

[6] S.M. Vitaliti, G. Costantino, L. Li Puma, M.P. Re, B. Vergara, G. Pinello, Painful procedures in the NICU, J. Matern. Fetal Neonatal Med. 25 Suppl 4 (2012) 146.

[7] R. Carbajal, A. Rousset, C. Danan, S. Coquery, P. Nolent, S. Ducrocq, C. Saizou, A. Lapillonne, M. Granier, P. Durand, R. Lenclen, A. Coursol, P. Hubert, L. de Saint Blanquat, P.Y. Boelle, D. Annequin, P. Cimerman, K.J. Anand, G. Breart, Epidemiology and treatment of painful procedures in neonates in intensive care units, JAMA 300 (2008) 60.

[8] R.W. Hall, K.J. Anand, Pain management in newborns, Clin. Perinatol. 41 (2014) 895.

[9] K.J. Anand, P.R. Hickey, Pain and its effects in the human neonate and fetus, N. Engl. J. Med. 317 (1987) 1321.

[10] R.E. Grunau, T. Oberlander, L. Holsti, M.F. Whitfield, Bedside application of the Neonatal Facial Coding System in pain assessment of premature neonates, Pain 76 (1998) 277.

[11] L. Holsti, R.E. Grunau, Initial validation of the Behavioral Indicators of Infant Pain (BIIP), Pain 132 (2007) 264.

[12] S.M. Walker, Biological and neurodevelopmental implications of neonatal pain, Clin. Perinatol. 40 (2013) 471.

[13] K.J. Anand, W.G. Sippell, A. Aynsley-Green, Randomised trial of fentanyl anaesthesia in preterm babies undergoing surgery: effects on the stress response, Lancet 1 (1987) 243.

[14] S. Brummelte, R.E. Grunau, V. Chau, K.J. Poskitt, R. Brant, J. Vinall, A. Gover, A.R. Synnes, S.P. Miller, Procedural pain and brain development in premature newborns, Ann. Neurol. 71 (2012) 385.

[15] J.G. Zwicker, R.E. Grunau, E. Adams, V. Chau, R. Brant, K.J. Poskitt, A. Synnes, S.P. Miller, Score for neonatal acute physiology-II and neonatal pain predict corticospinal tract development in premature newborns, Pediatr. Neurol. 48

(2013) 123 e1.

[16] J. Vinall, S.P. Miller, V. Chau, S. Brummelte, A.R. Synnes, R.E. Grunau, Neonatal pain in relation to postnatal growth in infants born very preterm, Pain 153 (2012) 1374.

[17] R.E. Grunau, M.F. Whitfield, J. Petrie-Thomas, A.R. Synnes, I.L. Cepeda, A. Keidar, M. Rogers, M. Mackay, P. Hubber-Richard, D. Johannesen, Neonatal pain, parenting stress and interaction, in relation to cognitive and motor development at 8 and 18 months in preterm infants, Pain 143 (2009) 138.

[18] G.M. Pacifici, K. Allegaert, Clinical pharmacology of paracetamol in neonates: a review, Curr. Ther. Res. Clin. Exp. 77 (2015) 24.

[19] P. David Josephy, The molecular toxicology of acetaminophen, Drug Metab. Rev. 37 (2005) 581.

[20] D.W. Kaufman, J.P. Kelly, L. Rosenberg, T.E. Anderson, A.A. Mitchell, Recent patterns of medication use in the ambulatory adult population of the United States: the Slone survey, JAMA 287 (2002) 337.

[21] R. Paulose-Ram, R. Hirsch, C. Dillon, K. Losonczy, M. Cooper, Y. Ostchega, Prescription and non-prescription analgesic use among the US adult population: results from the third National Health and Nutrition Examination Survey (NHANES III), Pharmacoepidemiol. Drug Saf. 12 (2003) 315.

[22] R. Paulose-Ram, R. Hirsch, C. Dillon, Q. Gu, Frequent monthly use of selected non-prescription and prescription non-narcotic analgesics among U.S. adults, Pharmacoepidemiol. Drug Saf. 14 (2005) 257.

[23] L. Vernacchio, J.P. Kelly, D.W. Kaufman, A.A. Mitchell, Medication use among children <12 years of age in the United States: results from the Slone Survey, Pediatrics 124 (2009) 446.

[24] G.G. Graham, M.J. Davies, R.O. Day, A. Mohamudally, K.F. Scott, The modern pharmacology of paracetamol: therapeutic actions, mechanism of action, metabolism, toxicity and recent pharmacological findings, Inflammopharmacol. 21 (2013) 201.

[25] G. Terrin, F. Conte, M.Y. Oncel, A. Scipione, P.J. McNamara, S. Simons, R. Sinha, O. Erdeve, K.S. Tekgunduz, M. Dogan, I. Kessel, C. Hammerman, E. Nadir, S. Yurttutan, B. Jasani, S. Alan, F. Manguso, M. De Curtis, Paracetamol for the treatment of patent ductus arteriosus in preterm neonates: a systematic review and meta-analysis, Arch. Dis. Child. Fetal Neonatal Ed. DOI 10.1136/ archdischild-2014-307312 (2015).

[26] M. Depre, A. van Hecken, R. Verbesselt, T.B. Tjandra-Maga, M. Gerin, P.J. de Schepper, Tolerance and pharmacokinetics of propacetamol, a paracetamol

formulation for intravenous use, Fundam. Clin. Pharmacol. 6 (1992) 259.

[27] A. Tzortzopoulou, E.D. McNicol, M.S. Cepeda, M.B. Francia, T. Farhat, R. Schumann, Single dose intravenous propacetamol or intravenous paracetamol for postoperative pain, Cochrane Database Syst. Rev. DOI 10.1002/14651858.CD 007126.pub2 (2011) CD007126.

[28] S.T. Duggan, L.J. Scott, Intravenous paracetamol (acetaminophen), Drugs 69 (2009) 101.

[29] Bristol-Myers Squibb Pharmaceutical Limited, Summary of product characteristics: Perfalgan 10mg/ml solution for infusion, electronic Medicines Compendium. Available at: https://www.medicines.org.uk/emc/medicine/14288. Accessed 1 Sept 2015.

[30] Food and Drug Administration, Drug approval package: Ofirmev (acetaminophen) injection, 10 mg/mL. Available at: http://www.accessdata. fda.gov/drugsatfda_docs/nda/2010/022450_ofirmev_toc.cfm. Accessed 1 Sept 2015.

[31] J.D. Tobias, Acute pain management in infants and children-part 1: pain pathways, pain assessment, and outpatient pain management, Pediatr. Ann. 43 (2014) e163.

[32] S.A. Prins, M. Van Dijk, P. Van Leeuwen, S. Searle, B.J. Anderson, D. Tibboel, R.A. Mathot, Pharmacokinetics and analgesic effects of intravenous propacetamol vs rectal paracetamol in children after major craniofacial surgery, Paediatr. Anaesth. 18 (2008) 582.

[33] B.J. Anderson, G.A. Woollard, N.H. Holford, A model for size and age changes in the pharmacokinetics of paracetamol in neonates, infants and children, Br. J. Clin. Pharmacol. 50 (2000) 125.

[34] L. Cuzzolin, R. Antonucci, V. Fanos, Paracetamol (acetaminophen) efficacy and safety in the newborn, Curr. Drug Metab. 14 (2013) 178.

[35] I. Ceelie, S.N. de Wildt, M. van Dijk, M.M. van den Berg, G.E. van den Bosch, H.J. Duivenvoorden, T.G. de Leeuw, R. Mathot, C.A. Knibbe, D. Tibboel, Effect of intravenous paracetamol on postoperative morphine requirements in neonates and infants undergoing major noncardiac surgery: a randomized controlled trial, JAMA 309 (2013) 149.

[36] M. Bartocci, S. Lundeberg, Intravenous paracetamol: the 'Stockholm protocol' for postoperative analgesia of term and preterm neonates, Paediatr. Anaesth. 17 (2007) 1120.

[37] K. Allegaert, I. Murat, B.J. Anderson, Not all intravenous paracetamol formulations are created equal, Paediatr. Anaesth. 17 (2007) 811.

[38] E.M. Wilson-Smith, N.S. Morton, Survey of i.v. paracetamol (acetaminophen) use in neonates and infants under 1 year of age by UK anesthetists, Paediatr. Anaesth. 19 (2009) 329.

[39] K. Allegaert, G.M. Palmer, B.J. Anderson, The pharmacokinetics of intravenous paracetamol in neonates: size matters most, Arch. Dis. Child. 96 (2011) 575.

[40] G.L. Kearns, S.M. Abdel-Rahman, S.W. Alander, D.L. Blowey, J.S. Leeder, R.E. Kauffman, Developmental pharmacology--drug disposition, action, and therapy in infants and children, N. Engl. J. Med. 349 (2003) 1157.

[41] A.F. Zuppa, G.B. Hammer, J.S. Barrett, B.F. Kenney, N. Kassir, S. Mouksassi, M.A. Royal, Safety and population pharmacokinetic analysis of intravenous acetaminophen in neonates, infants, children, and adolescents with pain or fever, J. Pediatr. Pharmacol. Ther. 16 (2011) 246.

[42] C. van Ganzewinkel, L. Derijks, K.J. Anand, R.A. van Lingen, C. Neef, B.W. Kramer, P. Andriessen, Multiple intravenous doses of paracetamol result in a predictable pharmacokinetic profile in very preterm infants, Acta Paediatr. 103 (2014) 612.

[43] B.J. Anderson, R.A. van Lingen, T.G. Hansen, Y.C. Lin, N.H. Holford, Acetaminophen developmental pharmacokinetics in premature neonates and infants: a pooled population analysis, Anesthesiology 96 (2002) 1336.

[44] K. Allegaert, S. Vanhaesebrouck, R. Verbesselt, J.N. van den Anker, In vivo glucuronidation activity of drugs in neonates: extensive interindividual variability despite their young age, Ther. Drug Monit. 31 (2009) 411.

[45] K. Allegaert, B.J. Anderson, G. Naulaers, J. de Hoon, R. Verbesselt, A. Debeer, H. Devlieger, D. Tibboel, Intravenous paracetamol (propacetamol) pharmacokinetics in term and preterm neonates, Eur. J. Clin. Pharmacol. 60 (2004) 191.

[46] K. Allegaert, C.D. Van der Marel, A. Debeer, M.A. Pluim, R.A. Van Lingen, C. Vanhole, D. Tibboel, H. Devlieger, Pharmacokinetics of single dose intravenous propacetamol in neonates: effect of gestational age, Arch. Dis. Child. Fetal Neonatal Ed. 89 (2004) F25.

[47] G.M. Palmer, M. Atkins, B.J. Anderson, K.R. Smith, T.J. Culnane, C.M. McNally, E.J. Perkins, G.A. Chalkiadis, R.W. Hunt, I.V. acetaminophen pharmacokinetics in neonates after multiple doses, Br. J. Anaesth. 101 (2008) 523.

[48] E. Hey, Part 2: Drug monographs, Neonatal Formulary 6, Wiley-Blackwell, Chichester, UK, 2011, pp. 33-280.

[49] B.J. Anderson, N.H. Holford, Mechanism-based concepts of size and maturity in

pharmacokinetics, Annu. Rev. Pharmacol. Toxicol. 48 (2008) 303.

[50] L.F. Prescott, Paracetamol (acetaminophen): a critical bibliographic review, UK: Taylor & Francis, London, 1996.

[51] K. Allegaert, K.T. Olkkola, K.H. Owens, M. Van de Velde, M.M. de Maat, B.J. Anderson, Covariates of intravenous paracetamol pharmacokinetics in adults, BMC Anesthesiol. 14 (2014) 77.

[52] G. Levy, N.N. Khanna, D.M. Soda, O. Tsuzuki, L. Stern, Pharmacokinetics of acetaminophen in the human neonate: formation of acetaminophen glucuronide and sulfate in relation to plasma bilirubin concentration and D-glucaric acid excretion, Pediatrics 55 (1975) 818.

[53] R.P. Miller, R.J. Roberts, L.J. Fischer, Acetaminophen elimination kinetics in neonates, children, and adults, Clin. Pharmacol. Ther. 19 (1976) 284.

[54] B.J. Anderson, N.H. Holford, Mechanistic basis of using body size and maturation to predict clearance in humans, Drug Metab. Pharmacokinet. 24 (2009) 25.

[55] R.C. Dart, E. Bailey, Does therapeutic use of acetaminophen cause acute liver failure? Pharmacotherapy 27 (2007) 1219.

[56] A.M. Larson, Acetaminophen hepatotoxicity, Clin. Liver Dis. 11 (2007) 525, vi.

[57] E.M. Boyd, G.M. Bereczky, Liver necrosis from paracetamol, Br. J. Pharmacol. Chemother. 26 (1966) 606.

[58] D.G. Davidson, W.N. Eastham, Acute liver necrosis following overdose of paracetamol, Br. Med. J. 2 (1966) 497.

[59] J.S. Thomson, L.F. Prescott, Liver damage and impaired glucose tolerance after paracetamol overdosage, Br. Med. J. 2 (1966) 506.

[60] B. McJunkin, K.W. Barwick, W.C. Little, J.B. Winfield, Fatal massive hepatic necrosis following acetaminophen overdose, JAMA 236 (1976) 1874.

[61] A.M. Larson, J. Polson, R.J. Fontana, T.J. Davern, E. Lalani, L.S. Hynan, J.S. Reisch, F.V. Schiodt, G. Ostapowicz, A.O. Shakil, W.M. Lee, Acetaminophen-induced acute liver failure: results of a United States multicenter, prospective study, Hepatology 42 (2005) 1364.

[62] M.R. McGill, H. Jaeschke, Metabolism and disposition of acetaminophen: recent advances in relation to hepatotoxicity and diagnosis, Pharm. Res. 30 (2013) 2174.

[63] L.P. James, P.R. Mayeux, J.A. Hinson, Acetaminophen-induced hepatotoxicity, Drug Metab. Dispos. 31 (2003) 1499.

[64] J.R. Mitchell, D.J. Jollow, W.Z. Potter, D.C. Davis, J.R. Gillette, B.B. Brodie, Acetaminophen-induced hepatic necrosis. I. Role of drug metabolism, J. Pharmacol. Exp. Ther. 187 (1973) 185.

[65] J.R. Mitchell, D.J. Jollow, W.Z. Potter, J.R. Gillette, B.B. Brodie, Acetaminophen-induced hepatic necrosis. IV. Protective role of glutathione, J. Pharmacol. Exp. Ther. 187 (1973) 211.

[66] D.J. Jollow, J.R. Mitchell, W.Z. Potter, D.C. Davis, J.R. Gillette, B.B. Brodie, Acetaminophen-induced hepatic necrosis. II. Role of covalent binding in vivo, J. Pharmacol. Exp. Ther. 187 (1973) 195.

[67] W.Z. Potter, D.C. Davis, J.R. Mitchell, D.J. Jollow, J.R. Gillette, B.B. Brodie, Acetaminophen-induced hepatic necrosis. III. Cytochrome P-450-mediated covalent binding in vitro, J. Pharmacol. Exp. Ther. 187 (1973) 203.

[68] Z. Gregus, C. Madhu, C.D. Klaassen, Species variation in toxication and detoxication of acetaminophen in vivo: a comparative study of biliary and urinary excretion of acetaminophen metabolites, J. Pharmacol. Exp. Ther. 244 (1988) 91.

[69] P. Moldeus, C. von Bahr, A. Rane, Metabolism of a glutathione conjugate in human fetal and adult tissues, Dev. Pharmacol. Ther. 1 (1980) 83.

[70] H. Jaeschke, M.R. McGill, A. Ramachandran, Oxidant stress, mitochondria, and cell death mechanisms in drug-induced liver injury: lessons learned from acetaminophen hepatotoxicity, Drug Metab. Rev. 44 (2012) 88.

[71] J.A. Hinson, D.W. Roberts, L.P. James, Mechanisms of acetaminophen-induced liver necrosis, Handb. Exp. Pharmacol. DOI 10.1007/978-3-642-00663-0_12 (2010) 369.

[72] G.M. Adamson, J.M. Papadimitriou, A.W. Harman, Postnatal mice have low susceptibility to paracetamol toxicity, Pediatr. Res. 29 (1991) 496.

[73] K. Du, C. David Williams, M.R. McGill, H. Jaeschke, Lower susceptibility of female mice to acetaminophen hepatotoxicity: role of mitochondrial glutathione, oxidant stress and c-jun N-terminal kinase, Toxicol. Appl. Pharmacol. DOI 10.1016/j.taap.2014.09.002 (2014).

[74] H. Jaeschke, C.D. Williams, M.R. McGill, Y. Xie, A. Ramachandran, Models of drug-induced liver injury for evaluation of phytotherapeutics and other natural products, Food Chem. Toxicol. 55 (2013) 279.

[75] V.F. Price, M.G. Miller, D.J. Jollow, Mechanisms of fasting-induced potentiation of acetaminophen hepatotoxicity in the rat, Biochem. Pharmacol. 36 (1987) 427.

[76] X. Kakan, P. Chen, J. Zhang, Clock gene mPer2 functions in diurnal variation of acetaminophen induced hepatotoxicity in mice, Exp. Toxicol. Pathol. 63 (2011)

581.

[77] R.M. Shayiq, D.W. Roberts, K. Rothstein, J.E. Snawder, W. Benson, X. Ma, M. Black, Repeat exposure to incremental doses of acetaminophen provides protection against acetaminophen-induced lethality in mice: an explanation for high acetaminophen dosage in humans without hepatic injury, Hepatology 29 (1999) 451.

[78] M.H. Court, M. Freytsis, X. Wang, I. Peter, C. Guillemette, S. Hazarika, S.X. Duan, D.J. Greenblatt, W.M. Lee, The UDP-glucuronosyltransferase (UGT) 1A polymorphism c.2042C>G (rs8330) is associated with increased human liver acetaminophen glucuronidation, increased UGT1A exon 5a/5b splice variant mRNA ratio, and decreased risk of unintentional acetaminophen-induced acute liver failure, J. Pharmacol. Exp. Ther. 345 (2013) 297.

[79] R.G. Peterson, B.H. Rumack, Age as a variable in acetaminophen overdose, Arch. Intern. Med. 141 (1981) 390.

[80] M. Tenenbein, Acetaminophen: the 150 mg/kg myth, J. Toxicol. Clin. Toxicol. 42 (2004) 145.

[81] G.R. Bond, Reduced toxicity of acetaminophen in children: it's the liver, J. Toxicol. Clin. Toxicol. 42 (2004) 149.

[82] K. Allegaert, M. Rayyan, T. De Rijdt, F. Van Beek, G. Naulaers, Hepatic tolerance of repeated intravenous paracetamol administration in neonates, Paediatr. Anaesth. 18 (2008) 388.

[83] M.R. McGill, H. Jaeschke, Mechanistic biomarkers in acetaminophen-induced hepatotoxicity and acute liver failure: from preclinical models to patients, Expert Opin. Drug Metab. Toxicol. DOI 10.1517/17425255.2014.920823 (2014) 1.

[84] M.J. Blake, L. Castro, J.S. Leeder, G.L. Kearns, Ontogeny of drug metabolizing enzymes in the neonate, Semin. Fetal Neonatal Med. 10 (2005) 123.

[85] R.N. Hines, Developmental expression of drug metabolizing enzymes: Impact on disposition in neonates and young children, Int. J. Pharm. 452 (2013) 3.

[86] R.A. van Lingen, J.T. Deinum, J.M. Quak, A.J. Kuizenga, J.G. van Dam, K.J. Anand, D. Tibboel, A. Okken, Pharmacokinetics and metabolism of rectally administered paracetamol in preterm neonates, Arch. Dis. Child. Fetal Neonatal Ed. 80 (1999) F59.

[87] K. Allegaert, J. de Hoon, R. Verbesselt, C. Vanhole, H. Devlieger, D. Tibboel, Intra- and interindividual variability of glucuronidation of paracetamol during repeated administration of propacetamol in neonates, Acta Paediatr. 94 (2005) 1273.

[88] E.H. Krekels, S. van Ham, K. Allegaert, J. de Hoon, D. Tibboel, M. Danhof, C.A. Knibbe, Developmental changes rather than repeated administration drive paracetamol glucuronidation in neonates and infants, Eur. J. Clin. Pharmacol. DOI 10.1007/s00228-015-1887-y (2015).

[89] E.H. Krekels, M. Danhof, D. Tibboel, C.A. Knibbe, Ontogeny of hepatic glucuronidation; methods and results, Curr. Drug Metab. 13 (2012) 728.

[90] C.D. van der Marel, B.J. Anderson, R.A. van Lingen, N.H. Holford, M.A. Pluim, F.G. Jansman, J.N. van den Anker, D. Tibboel, Paracetamol and metabolite pharmacokinetics in infants, Eur. J. Clin. Pharmacol. 59 (2003) 243.

[91] A.A. Adjei, A. Gaedigk, S.D. Simon, R.M. Weinshilboum, J.S. Leeder, Interindividual variability in acetaminophen sulfation by human fetal liver: implications for pharmacogenetic investigations of drug-induced birth defects, Birth Defects Res. A Clin. Mol. Teratol. 82 (2008) 155.

[92] M.H. Court, S.X. Duan, L.L. von Moltke, D.J. Greenblatt, C.J. Patten, J.O. Miners, P.I. Mackenzie, Interindividual variability in acetaminophen glucuronidation by human liver microsomes: identification of relevant acetaminophen UDP-glucuronosyltransferase isoforms, J. Pharmacol. Exp. Ther. 299 (2001) 998.

[93] S.L. Navarro, Y. Chen, L. Li, S.S. Li, J.L. Chang, Y. Schwarz, I.B. King, J.D. Potter, J. Bigler, J.W. Lampe, UGT1A6 and UGT2B15 polymorphisms and acetaminophen conjugation in response to a randomized, controlled diet of select fruits and vegetables, Drug Metab. Dispos. 39 (2011) 1650.

[94] C.P. Strassburg, A. Strassburg, S. Kneip, A. Barut, R.H. Tukey, B. Rodeck, M.P. Manns, Developmental aspects of human hepatic drug glucuronidation in young children and adults, Gut 50 (2002) 259.

[95] N. Kawade, S. Onishi, The prenatal and postnatal development of UDP-glucuronyltransferase activity towards bilirubin and the effect of premature birth on this activity in the human liver, Biochem. J. 196 (1981) 257.

[96] S. Onishi, N. Kawade, S. Itoh, K. Isobe, S. Sugiyama, Postnatal development of uridine diphosphate glucuronyltransferase activity towards bilirubin and 2-aminophenol in human liver, Biochem. J. 184 (1979) 705.

[97] M.W. Coughtrie, B. Burchell, J.E. Leakey, R. Hume, The inadequacy of perinatal glucuronidation: immunoblot analysis of the developmental expression of individual UDP-glucuronosyltransferase isoenzymes in rat and human liver microsomes, Mol. Pharmacol. 34 (1988) 729.

[98] I. Vieira, M. Sonnier, T. Cresteil, Developmental expression of CYP2E1 in the human liver: hypermethylation control of gene expression during the neonatal period, Eur. J. Biochem. 238 (1996) 476.

[99] E.K. Johnsrud, S.B. Koukouritaki, K. Divakaran, L.L. Brunengraber, R.N. Hines, D.G. McCarver, Human hepatic CYP2E1 expression during development, J. Pharmacol. Exp. Ther. 307 (2003) 402.

[100] H.K. Batchelor, J.F. Marriott, Paediatric pharmacokinetics: key considerations, Br. J. Clin. Pharmacol. 79 (2015) 395.

[101] K. Allegaert, M. van de Velde, J. van den Anker, Neonatal clinical pharmacology, Paediatr. Anaesth. 24 (2014) 30.

[102] R.N. Xu, L. Fan, M.J. Rieser, T.A. El-Shourbagy, Recent advances in high-throughput quantitative bioanalysis by LC-MS/MS, J. Pharm. Biomed. Anal. 44 (2007) 342.

[103] E.I. Ette, P.J. Williams, J.R. Lane, Population pharmacokinetics III: design, analysis, and application of population pharmacokinetic studies, Ann. Pharmacother. 38 (2004) 2136.

[104] R.F. De Cock, C. Piana, E.H. Krekels, M. Danhof, K. Allegaert, C.A. Knibbe, The role of population PK-PD modelling in paediatric clinical research, Eur. J. Clin. Pharmacol. 67 Suppl 1 (2011) 5.

[105] C.A. Knibbe, M. Danhof, Individualized dosing regimens in children based on population PKPD modelling: are we ready for it? Int. J. Pharm. 415 (2011) 9.

[106] J.H. An, H.J. Lee, B.H. Jung, Quantitative analysis of acetaminophen and its six metabolites in rat plasma using liquid chromatography/tandem mass spectrometry, Biomed. Chromatogr. 26 (2012) 1596.

[107] T. Gicquel, J. Aubert, S. Lepage, B. Fromenty, I. Morel, Quantitative analysis of acetaminophen and its primary metabolites in small plasma volumes by liquid chromatography-tandem mass spectrometry, J. Anal. Toxicol. 37 (2013) 110.

[108] A.K. Hewavitharana, S. Lee, P.A. Dawson, D. Markovich, P.N. Shaw, Development of an HPLC-MS/MS method for the selective determination of paracetamol metabolites in mouse urine, Anal. Biochem. 374 (2008) 106.

[109] Q.Y. Tan, R.H. Zhu, H.D. Li, F. Wang, M. Yan, L.B. Dai, Simultaneous quantitative determination of paracetamol and its glucuronide conjugate in human plasma and urine by liquid chromatography coupled to electrospray tandem mass spectrometry: application to a clinical pharmacokinetic study, J. Chromatogr. B Analyt. Technol. Biomed. Life Sci. 893-894 (2012) 162.

[110] D. Tonoli, E. Varesio, G. Hopfgartner, Quantification of acetaminophen and two of its metabolites in human plasma by ultra-high performance liquid chromatography-low and high resolution tandem mass spectrometry, J. Chromatogr. B Analyt. Technol. Biomed. Life Sci. 904 (2012) 42.

[111] C. Bylda, R. Thiele, U. Kobold, D.A. Volmer, Simultaneous quantification of acetaminophen and structurally related compounds in human serum and plasma, Drug Test. Anal. 6 (2014) 451.

[112] S.F. Cook, J.K. Roberts, S. Samiee-Zafarghandy, C. Stockmann, A.D. King, N. Deutsch, E.F. Williams, K. Allegaert, D.G. Wilkins, C.M. Sherwin, J.N. van den Anker, Population pharmacokinetics of intravenous paracetamol (acetaminophen) in preterm and term neonates: model development and external evaluation, Clin. Pharmacokinet. DOI 10.1007/s40262-015-0301-3 (2015).

[113] S.F. Cook, A.D. King, Y. Chang, G.J. Murray, H.R. Norris, R.C. Dart, J.L. Green, S.C. Curry, D.E. Rollins, D.G. Wilkins, Quantification of a biomarker of acetaminophen protein adducts in human serum by high-performance liquid chromatography-electrospray ionization-tandem mass spectrometry: Clinical and animal model applications, J. Chromatogr. B Analyt. Technol. Biomed. Life Sci. 985 (2015) 131.

CHAPTER 2

SIMULTANEOUS QUANTIFICATION OF ACETAMINOPHEN AND FIVE ACETAMINOPHEN METABOLITES IN HUMAN PLASMA AND URINE BY HIGH-PERFORMANCE LIQUID CHROMATOGRAPHY–ELECTROSPRAY IONIZATION–TANDEM MASS SPECTROMETRY: METHOD VALIDATION AND APPLICATION TO A NEONATAL PHARMACOKINETIC STUDY

Abstract

Drug metabolism plays a key role in acetaminophen (APAP)-induced hepatotoxicity, and quantification of APAP metabolites provides critical information about factors influencing susceptibility to APAP-induced hepatotoxicity in clinical and experimental settings. The aims of this study were to develop, validate, and apply high-performance liquid chromatography–electrospray ionization–tandem mass spectrometry (HPLC–ESI–MS/MS) methods for simultaneous quantification of APAP, APAP-glucuronide, APAP-sulfate, APAP-glutathione, APAP-cysteine, and APAP-*N*-acetylcysteine in small volumes of human plasma and urine. In the reported procedures, APAP-d4 and APAP-d3-sulfate were utilized as internal standards (IS). Analytes and IS were recovered from human plasma (10 μL) by protein precipitation with acetonitrile. Human urine (10 μL) was prepared by fortification with IS followed only by sample dilution. Calibration concentration ranges were tailored to literature values for each analyte in each biological matrix. Prepared samples from plasma and urine were analyzed under the same HPLC–ESI–MS/MS conditions, and chromatographic separation was achieved through use of an Agilent Poroshell 120 EC–C18 column with a 20-min run time per injected sample. The analytes could be accurately and precisely quantified over 2.0–3.5 orders of magnitude. Across both matrices, mean intra- and inter-assay accuracies ranged from 85–112%, and intra- and inter-assay imprecision did not exceed 15%. Validation experiments included tests for specificity, recovery and ionization efficiency, inter-individual variability in matrix effects, stock solution stability, and sample stability under a variety of storage and handling conditions (room temperature, freezer, freeze-thaw, and postpreparative). The utility and suitability of the reported

procedures were illustrated by analysis of pharmacokinetic samples collected from neonates receiving intravenous APAP.

Introduction

Acetaminophen (APAP) has been widely used for nearly a century and is currently one of the most commonly used medications in the United States [1-4]. APAP is an effective and well-tolerated analgesic and antipyretic agent when used as indicated [5-7]. At supratherapeutic doses, however, the drug has long been known to produce liver injury [8-11], and APAP overdose is currently the leading cause of acute liver failure in the United States [12]. Consequently, APAP is frequently utilized as a model hepatotoxicant [13-15], and studies of the precise mechanistic pathways that ultimately result in APAP-induced liver injury are still underway [16, 17].

Drug metabolism plays a key role in APAP-induced hepatotoxicity (Figure 2.1) [18, 19]. APAP metabolism occurs primarily in the liver, where the drug undergoes glucuronidation and sulfation by UDP-glucuronosyltransferases and sulfotransferases, respectively. The nontoxic glucuronide (APAP-gluc) and sulfate (APAP-sulf) metabolites are efficiently excreted in the urine. APAP can also be oxidized by hepatic cytochrome P450 enzymes to form the reactive intermediate *N*-acetyl-*p*-benzoquinone imine (NAPQI). At therapeutic doses, only a small portion (5–15%) of APAP is bioactivated to yield NAPQI. This electrophilic species can be detoxified by conjugation with glutathione, either nonenzymatically or with the aid of glutathione *S*-transferase enzymes. The APAP-glutathione conjugate (APAP-glut) undergoes rapid hydrolysis by hepatic gamma-glutamyl transpeptidase and dipeptidases to form APAP-cysteine (APAP-cys),

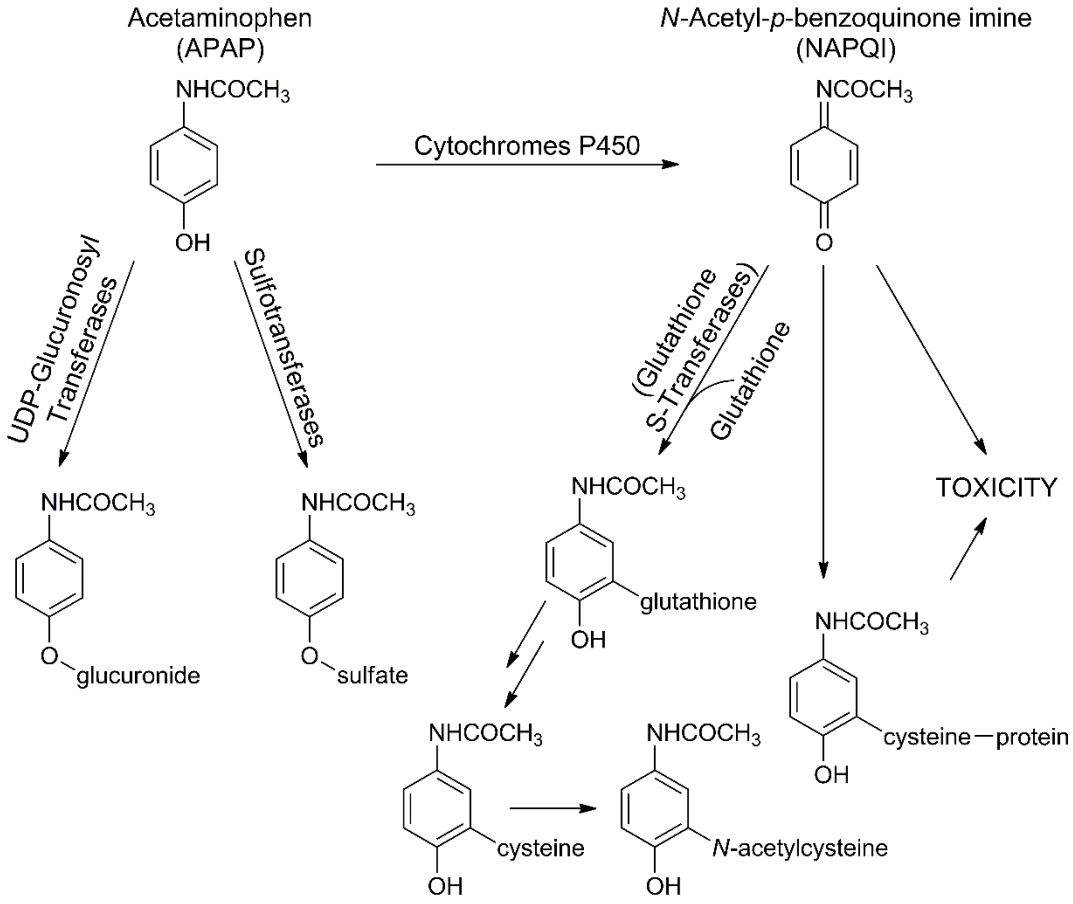

Figure 2.1 Major APAP metabolic pathways.

and APAP-cys is subsequently acetylated by *N*-acetyltransferases, thus producing APAP-*N*-acetylcysteine (APAP-NAC) [20, 21]. Given a sufficiently high dose of APAP, the glutathione detoxification pathway can be saturated by NAPQI, and excess electrophile will instead bind covalently to hepatic proteins [18, 19]. Toxicity is thought to result from a combination of inactivation of critical hepatic proteins via NAPQI binding and oxidative stress [13, 16].

Susceptibility to APAP-induced hepatotoxicity is likely to be influenced by variability in the major APAP metabolic pathways. Therefore, in both clinical and experimental settings, quantification of the major APAP metabolites is essential to achieve a thorough understanding of factors affecting hepatotoxicity risk. In recent years, a number of liquid chromatography–tandem mass spectrometry (LC–MS/MS) methods have been published for the sensitive and specific quantification of APAP and metabolites in various human and rodent matrices [22-27]; however, most of these included only the parent drug and one or two metabolites as analytes [23-26]. One recently reported assay included APAP, APAP-gluc, APAP-sulf, APAP-glut, APAP-cys, and APAP-NAC, but the method required two 16-min analytical injections per sample, one for each ionization mode, in order to achieve adequate sensitivity. Additionally, the assay was validated for analysis of rat plasma, not human matrices [22].

We sought to develop and validate methods for simultaneous quantification of APAP, APAP-gluc, APAP-sulf, APAP-glut, APAP-cys, and APAP-NAC in human plasma and urine by high-performance liquid chromatography–electrospray ionization–tandem mass spectrometry (HPLC–ESI–MS/MS). Furthermore, we aimed to optimize the sensitivity of the assays so that the required sample volume could be minimized. This

sample volume minimization was particularly important because the assays were intended for use in a neonatal pharmacokinetic study, an application where sample volumes are extremely limited.

Herein we report novel procedures for simultaneous quantification of APAP and five APAP metabolites in human plasma and urine by HPLC–ESI–MS/MS. Details of the methods are provided along with comprehensive validation results. The utility and suitability of the assays are illustrated by a brief summary of the analysis of pharmacokinetic plasma and urine samples collected from neonates receiving intravenous APAP.

Materials and Methods

Materials

Analyte-free human plasma (sodium heparin; from individual donors) was obtained from BioChemed Services (Winchester, VA). Analyte-free human urine was obtained from APAP-abstinent volunteers at the Center for Human Toxicology (CHT) in the Department of Pharmacology and Toxicology at the University of Utah. Human urine for matrix stability experiments was obtained from a volunteer at the CHT approximately 3 h after ingestion of 1 g of APAP (500-mg caplets, Kroger, Cincinnati, OH). The following reference standards and deuterated internal standards were obtained from Toronto Research Chemicals (Toronto, ON, Canada): acetaminophen (98%), 4-acetamidophenyl β-D-glucuronide sodium salt (98%), 4-acetaminophen sulfate potassium salt (98%), acetaminophen glutathione disodium salt (95%), 3-cysteinylacetaminophen trifluoroacetic acid salt (95%), 3-(*N*-acetyl-L-cystein-*S*-yl)-acetaminophen disodium salt

(95%), acetaminophen-d4 (APAP-d4, 98% chemical purity, 99% isotopic purity), and 4-acetaminophen-d3 sulfate (APAP-d3-sulf, 98% chemical purity, 99% isotopic purity). APAP (analytical standard) and ammonium acetate (≥98%) were obtained from Sigma–Aldrich (St. Louis, MO). Glacial acetic acid was obtained from Spectrum Chemicals (New Brunswick, NJ). Formic acid (88%) was obtained from Fisher Scientific (Pittsburgh, PA). LC–MS grade acetonitrile and methanol were obtained from Honeywell Burdick and Jackson (Morristown, NJ). Ultrapure water (18.2 MΩ) for preparation of aqueous solutions was obtained by passage of deionized water through a Milli-Q Gradient A10 filtration system equipped with a Q-Gard 2 purification pack (EMD Millipore, Billerica, MA). Silanized glassware was prepared by vapor-phase silanization with hexamethyldisilazane (Pierce, Rockford, IL) under vacuum in an oven at 250°C for 2 h.

Authentic clinical samples for assay verification

Clinical samples were collected from subjects enrolled in an Institutional Review Board-approved study (Children's National Health System, Washington, DC) in which APAP (Ofirmev, 10 mg/mL, Mallinckrodt Pharmaceuticals, Dublin, Ireland) was administered by 30-min intravenous infusions at 15 mg/kg/dose to neonates with a clinical indication for intravenous analgesia. Patients <28 weeks gestation received 5 doses at 12-h intervals; patients ≥28 weeks gestation received 7 doses at 8-h intervals. Pharmacokinetic samples were collected prior to the first APAP dose and throughout the 3-day study period, up to 24 h after the final dose. Blood samples (0.2 mL) were obtained from indwelling arterial lines and collected in sodium heparin Vacutainer tubes (BD,

Franklin Lakes, NJ). Blood samples were centrifuged at 4°C for 10–15 min at 1500 x *g*. Plasma supernatants were transferred to cryovials and stored at −70°C. Urine samples were collected from gel-free study diapers (Cuddle Buns Preemie diapers, Small Beginnings Inc., Hesperia, CA) and stored at −70°C. Batches of de-identified study samples were shipped overnight on dry ice to the CHT at the University of Utah and immediately stored at −80°C until the time of preparation for analysis.

Calibrator, quality control (QC), and internal standard (IS) solutions

Individual stock solutions of analyte reference standards and IS were prepared at concentrations ranging from 0.1 to 1 mg/mL in methanol/water (1/1, v/v) using a Mettler Toledo XS3DU microbalance (Columbus, OH) and silanized class-A volumetric flasks. For reference standards obtained in salt form, all specified concentrations reflect the concentration of free analyte. Individual stock solutions were then pooled and diluted to prepare a combined working solution with 100 µg/mL APAP, APAP-gluc, and APAP-sulf and 10.0 µg/mL APAP-glut, APAP-cys, and APAP-NAC in methanol/water (1/1, v/v). Lower concentration working solutions were subsequently prepared by 5 10-fold serial dilutions in methanol/water (1/1, v/v). Separate sets of analyte stock and working solutions were prepared for calibrator and QC applications. APAP reference material used for each set was obtained from two different chemical manufacturers. Metabolite reference standards of sufficient purity were generally not available from different manufacturers or lot numbers; however, calibrator and QC solution sets were prepared by different analysts. Individual IS stock solutions were pooled and diluted with water to

prepare IS working solutions with the concentrations indicated below. All stock and working solutions were stored at −20°C in silanized glass tubes.

Sample preparation

Calibrator and QC samples. Prior to use for preparation of calibrator or QC samples, individual lots of biological matrix were prepared without IS, analyzed, and confirmed to be negative for all analytes and IS. Calibration standards and triplicate sets of QC samples were freshly prepared in silanized glass tubes for concurrent analysis with each validation or study sample batch. Analyte- and IS-free matrix (10 µL plasma or urine) was fortified with analyte working solutions to yield the nominal matrix concentrations provided in Table 2.1. Two additional analyte-free matrix samples accompanied each batch for preparation with and without IS.

Plasma sample preparation. Study samples were thawed at ambient temperature and gently mixed by vortexing before transfer of 10-µL aliquots to silanized glass tubes. To maintain equivalence in preparation and control for the addition of solvent that occurred during fortification of calibrator and QC samples with analyte working solution, methanol/water (1/1, v/v) was used to bring all samples to a total volume of 110 µL. Samples were then fortified with 10 µL of IS working solution containing 0.20 and 25 µg/mL of APAP-d4 and APAP-d3-sulf, respectively, in water. Acetonitrile (600 µL) was added, and each sample was vortex mixed for 30 s before 15 min of centrifugation at 1100 x *g*, ambient temperature in an IEC FL40 swing-out rotor centrifuge (Thermo Fisher Scientific Inc., Waltham, MA). Sample supernatants were transferred to a clean set of silanized glass tubes, placed in a 35°C water bath, and evaporated to dryness under a 10–

Table 2.1 Nominal calibrator and QC concentrations.

Analyte(s)	Matrix	Calibrator concentrations (μg/mL)	QC concentrations (μg/mL)			
			Level 1	Level 2	Level 3	Level 4
APAP APAP-gluc APAP-sulf	plasma	0.050, 0.10, 0.25, 0.75, 1.0, 2.5, 7.5, 10, 50	0.15	0.80	8.0	40
APAP-glut	plasma	0.0050[a], 0.010[a], 0.025, 0.075, 0.10, 0.25, 0.75, 1.0, 5.0	0.015[c]	0.080	0.80	4.0
APAP-cys	plasma	0.0050[a], 0.010, 0.025, 0.075, 0.10, 0.25, 0.75, 1.0, 5.0	0.015	0.080	0.80	4.0
APAP-NAC	plasma	0.0050[a], 0.010, 0.025, 0.075, 0.10, 0.25, 0.75, 1.0, 5.0[b]	0.015	0.080	0.80	4.0[c]
APAP	urine	0.20, 1.0, 5.0, 10, 40, 70, 100, 400, 700, 1,000	7.5	50	500	n/a
APAP-gluc APAP-sulf	urine	0.20[a], 1.0, 5.0, 10, 40, 70, 100, 400, 700, 1,000	7.5	50	500	n/a
APAP-glut APAP-cys APAP-NAC	urine	0.020[a], 0.10, 0.50, 1.0, 4.0, 7.0, 10, 40, 70, 100	0.75	5.0	50	n/a

[a] Concentration present but excluded from analysis due to failure to meet LLOQ acceptance criteria.

[b] Concentration present but excluded from analysis due to nonlinearity.

[c] Concentration present but excluded from analysis; concentration falls outside calibration range.

n/a, not applicable.

15 psi air stream in a TurboVap LV Evaporator (Zymark). Sample residues were reconstituted in 400 µL of 0.1% aqueous formic acid, vortex mixed for 30 s, and centrifuged for 5 min at 1100 x *g*, ambient temperature in the swing-out rotor centrifuge. From the top of each centrifuged sample, 200 µL was carefully removed and transferred to a conical polypropylene autosampler vial.

Urine sample preparation. Study samples were thawed at ambient temperature and gently mixed by vortexing before transfer of 10-µL aliquots to silanized glass tubes. To maintain equivalence in preparation and control for the addition of solvent that occurred during fortification of calibrator and QC samples with analyte working solution, methanol/water (1/1, v/v) was used to bring all samples to a total volume of 110 µL. Samples were then fortified with 10 µL of IS working solution containing 10 and 100 µg/mL of APAP-d4 and APAP-d3-sulf, respectively, in water. Samples were diluted by addition of 380 µL of 0.1% aqueous formic acid followed by 20 s vortex mixing. To remove any solid particles that might be present, samples were centrifuged for 5 min at 1100 x *g*, ambient temperature in the swing-out rotor centrifuge. Sample supernatants (100 µL) were carefully transferred to a clean set of silanized glass tubes and diluted in an additional 300 µL of 0.1% aqueous formic acid. Following 20 s vortex mixing, 200 µL of each sample was transferred to a conical polypropylene autosampler vial.

HPLC–ESI–MS/MS analysis

HPLC–ESI–MS/MS was conducted on an Agilent 1260 Infinity HPLC system (inline solvent micro-degasser, binary LC pump, high-performance thermostatted autosampler, and 1290 Infinity thermostatted column compartment) interfaced with an

Agilent 6460 triple-quadrupole mass spectrometer (Agilent Technologies, Santa Clara, CA). MassHunter Workstation software (Agilent Technologies, Santa Clara, CA) was used for instrument control, data acquisition, and ESI–MS/MS parameter optimization (version B.03.01) and for data analysis (version B.04.00).

Prepared samples were stored in the autosampler tray at 5°C. Sample injection volumes ranged from 10–100 µL. Injection volumes within each batch did not vary, but adjustments were made over time as needed based on changes in instrument response (magnitude of chromatographic peak areas). Samples were injected in the following order: calibration standards (ascending concentrations), analyte-free samples with and without IS, QC set 1, approximately half of the validation/study samples, QC set 2, remaining validation/study samples, QC set 3. Between injections, the autosampler needle was washed with methanol/water (1/1, v/v). For the plasma assay only, the analytical system was equilibrated by injecting 7 extra prepared matrix samples at the beginning of each batch. Chromatographic separation was achieved with an Agilent Poroshell 120 EC–C18 column (2.1 x 100 mm, 2.7 µm particle size, Agilent Technologies, Santa Clara, CA) maintained at 40°C and using a gradient mobile phase consisting of 10 mM aqueous ammonium acetate, pH 3.5 (A) and methanol (B) at a flow rate of 0.25 mL/min. Mobile phase was maintained at 3% B for the first 6 min, increased linearly to 35% B over 3 min, maintained at 95% B for 3 min, decreased linearly to 3% B over 0.5 min, and then re-equilibrated at 3% B for 7.5 min, yielding a total run time of 20 min/injection. The MS diverter valve was only directed to the ion source during the anticipated retention time range for analytes and IS.

The mass spectrometer was operated in ESI + Agilent Jet Stream mode with

multiple reaction monitoring (MRM). APAP-sulf and APAP-d3-sulf were monitored in negative ionization mode; all other analytes and APAP-d4 were monitored in positive ionization mode. Ultra-high-purity nitrogen was used for source and collision cell gas. The following settings were applied: 350°C gas temperature, 10 L/min gas flow, 30 psi nebulizer pressure, 350°C sheath gas temperature, 9 L/min sheath gas flow, 3500 V capillary voltage, 500 V nozzle voltage, and 250 V delta EMV. Analyte- and IS-specific MRM transitions, fragmentor voltages, collision energies, and dwell times are provided in Table 2.2. Wide resolution (FWHM approximately 1.2 amu) was applied in both mass analyzers.

Quantitation calculations and acceptance criteria

Throughout method validation and study sample analysis, calibration curves were constructed by plotting the analyte/IS chromatographic peak area ratio against the nominal analyte concentration in each calibration standard. APAP-d4 was used as the IS for APAP, and APAP-d3-sulf was used as the IS for all other analytes. Calibration curves were fit by linear regression for all analytes except APAP-gluc, for which a quadratic regression was used. Weighting of $1/x^2$ was applied to all calibration curves. Back-calculated calibrator and QC concentrations determined by interpolation were required to be within ±20% of nominal concentration. Calibration standards that failed to meet this criterion were excluded from regression, and at least ¾ of the calibrators were required to be included in regression. The lower limit of quantification (LLOQ) was defined as the lowest concentration of analyte with acceptable imprecision (≤20%) and mean accuracy (±20% of nominal concentration). At each QC concentration, at least 2 of the 3 replicates

Table 2.2 Analyte- and IS-specific ESI–MS/MS parameters.

Compound	MS segment	ESI mode	MRM transition (precursor→ product *m/z*)	Fragmentor voltage (V)	Collision energy (V)	Dwell time (ms)	Type[a]
APAP-gluc	2	+	328.1→152.1	100	5	200	quant
APAP-d3-sulf	3	−	233.1→153.1	110	14	200	quant
	3	−	233.1→107.1	110	30	200	qual
APAP-sulf	3	−	230.1→150.1	110	14	200	quant
	3	−	230.1→107.1	110	30	200	qual
APAP-cys	4	+	271.1→140.0	80	22	100	quant
	4	+	271.1→182.0	80	10	100	qual
APAP-d4	4	+	156.1→114.1	80	14	100	quant
APAP	4	+	152.1→110.0	80	14	100	quant
APAP-glut	5	+	457.1→140.0	110	42	100	quant
APAP-NAC	6	+	313.1→208.0	80	14	100	quant
	6	+	313.1→140.0	80	34	100	qual

[a] MRM transition type: quant, quantifier; qual, qualifier.

were required to meet the ±20% accuracy criterion in order for a sample batch to meet acceptance criteria for reporting of quantitative results.

Method validation

The methods were validated by assessment of LLOQ, intra- and inter-day accuracy and imprecision, specificity, recovery and ionization efficiency, matrix effect, stock solution stability, and sample stability.

To identify an appropriate LLOQ for each analyte in each matrix, analyte-free human plasma and urine were fortified with analyte working solutions at several concentrations near the target LLOQ (n = 6 for each concentration). Fortified samples were prepared and analyzed, and each appropriate LLOQ was selected based on the acceptance criteria described above. A LLOQ calibrator was included in each calibration curve, but the LLOQ test replicates were excluded from regression for determinations of accuracy and imprecision.

Accuracy and imprecision were determined from replicate samples of analyte-free human plasma and urine fortified with analytes at the QC concentrations indicated in Table 2.1. Intra-assay accuracy and imprecision at each concentration were determined from 5 replicate samples assayed within the same analytical batch. Inter-assay accuracy and imprecision at each concentration were calculated from a total of 20 replicates assayed over 7 separate analytical batches. Accuracy is expressed as a percent of the nominal concentration and imprecision as percent coefficient of variation (% CV).

Specificity of the methods was assessed by analysis of human plasma and urine from 6 APAP-abstinent individuals. To allow for identification of potential interfering

peaks co-eluting with either analytes or IS, plasma and urine samples were prepared in triplicate according to the usual procedures, and one plasma and urine sample from each individual was prepared similarly but without IS fortification. For samples prepared with IS, the specificity acceptance criterion for each lot was that the mean analyte/IS peak area ratio at the analyte retention time must be <20% of the corresponding peak area ratio from a concurrently assayed LLOQ sample. Additionally, qualification transitions were incorporated for some analytes (APAP-sulf, APAP-cys, and APAP-NAC), and the presence of a qualifier ion peak with a signal-to-noise ratio >3 was required for declaration of a positive result for these analytes. For samples prepared without IS, any peak area at the IS retention time was required to be <5% of the IS peak area in the LLOQ sample in order to meet acceptance criterion.

Recovery and ionization efficiency (suppression/enhancement) were determined at the QC concentrations indicated in Table 2.1. For each biological matrix, one QC set (set A, $n = 5$) was prepared according to the usual procedures. Another QC set (set B, $n = 5$) was prepared similarly but IS was added during the final step of sample preparation. A third QC set (set C, $n = 5$) was prepared with water in place of analyte-free matrix and with IS added during the final step of sample preparation. In the HPLC–ESI–MS/MS injection sequence, each QC set was interspersed so that comparable samples were injected consecutively (i.e., low QC A replicate 1, low QC B replicate 1, low QC C replicate 1, etc.). IS recovery was calculated by dividing each IS peak area from set A by the IS peak area from the corresponding set B sample. Ionization efficiency was calculated by dividing each analyte or IS peak area from set B by the analyte or IS peak area from the corresponding set C sample.

The influence of inter-individual variability in matrix effects on analyte accuracy and imprecision was assessed using analyte-free plasma or urine obtained from 6 individuals. Each lot was fortified with analytes at low and high QC concentrations (QC levels 2 and 4 for plasma, and levels 1 and 3 for urine). The fortified samples were then prepared for analysis.

Stability of analyte stock solutions was assessed by comparison of freshly prepared solutions to solutions that had been stored at −20°C for approximately 6 or 12 months. Solutions were diluted in 0.1% aqueous formic acid to concentrations appropriate for injection on the HPLC–ESI–MS/MS (n = 3 for each comparison), and the test solutions were then analyzed under the usual conditions. Stability was calculated by dividing the mean analyte/IS peak area ratios from test solutions prepared from stored stocks by the mean analyte/IS peak area ratios from test solutions prepared from the fresh stocks.

For plasma stability experiments, analyte concentrations were equivalent to the lowest and highest QC concentrations. Plasma fortification was performed in triplicate in silanized glass tubes by first evaporating appropriate amounts of analyte working solutions to dryness in a TurboVap LV Evaporator (35°C water bath, 10–15 psi air stream) and then reconstituting each sample in 1 mL analyte-free plasma. Because reference standard material is costly and the urine stability samples required relatively high analyte concentrations, a urine sample for stability studies was obtained from a volunteer at the Center for Human Toxicology who was known to have ingested 1 g of APAP approximately 3 h prior. This specimen was serially diluted in analyte-free urine from the same donor to obtain analyte concentrations in the low-to-mid and mid-to-high

regions of the calibration curves. Stability samples were prepared for initial analysis immediately after fortification/collection, and aliquots of matrix (200 μL for plasma; 1 mL for urine) were also subjected to the following conditions: up to 24 h of storage at room temperature, up to 6 months (plasma) or 1 month (urine) of storage at −80°C, and 3 cycles of freezing (at least 12 h storage at −80°C) and thawing (60 min at room temperature). Analyte concentrations determined from stored aliquots were then compared to the concentrations determined from initial analysis. Additionally, stability of prepared samples was assessed following storage in the autosampler (5°C) for 72 h.

Statistical software

All calculations for descriptive statistics were performed in Excel (version 14.0, Microsoft Corp., Redmond, WA).

Results and Discussion

Method development

Table 2.1 provides a summary of the calibrator and QC concentrations used for both the plasma and urine assays. Based on previous knowledge about APAP pharmacokinetics [28], calibration curve ranges were carefully selected to be most appropriate for each biological matrix and analyte. Because cytochrome P450-mediated oxidation accounts for a small portion of APAP metabolism, plasma concentrations of NAPQI-derived metabolites (APAP-glut, APAP-cys, and APAP-NAC) are anticipated to be substantially lower than plasma concentrations of the other analytes in samples collected from typical adult human subjects. Additionally, urinary analyte concentrations

are generally expected to be significantly higher than the respective plasma concentrations. Calibrator concentrations for plasma and urine were also designed to be compatible with a single set of stock and working solutions so that costly metabolite reference standards could be used as economically as possible. As a result, the calibration range for APAP in urine extends to much higher concentrations than typically necessary.

A variety of LC conditions were tested during method development. In addition to the Poroshell 120 EC–C18 column, which was ultimately employed for the assay, a Polaris C18–A column (2.0 x 150 mm, 5 µm particle size, Agilent Technologies, Santa Clara, CA) was considered. Potential aqueous mobile phase solutions included various ammonium acetate buffers, formate buffers, dilute formic acid, dilute acetic acid, and dilute trifluoroacetic acid. Acetonitrile was also explored as a potential organic mobile phase solvent. Additionally, numerous variations in pump flow rate, pump timetable program, and column temperature were tested. Ultimately, the conditions reported in the Materials and Methods section (above) were found to provide optimal chromatographic separation within a reasonable run time. Typical retention times for analytes and IS can be observed in Figures 2.2 and 2.3.

Analyte- and IS-specific ESI–MS/MS parameters are summarized in Table 2.2. Ion source and MS/MS conditions were optimized during direct infusion of individual analyte solutions (10 µg/mL in methanol/water (1/1, v/v)) at 10 µL/min into 0.25 mL/min mobile phase flow with a composition approximately equivalent to that at the time of analyte elution from the HPLC column. MRM transitions for analyte quantification were selected based on the ability to provide acceptable specificity and optimal product ion abundance for maximum sensitivity. For APAP-sulf, APAP-d3-sulf, APAP-cys, and

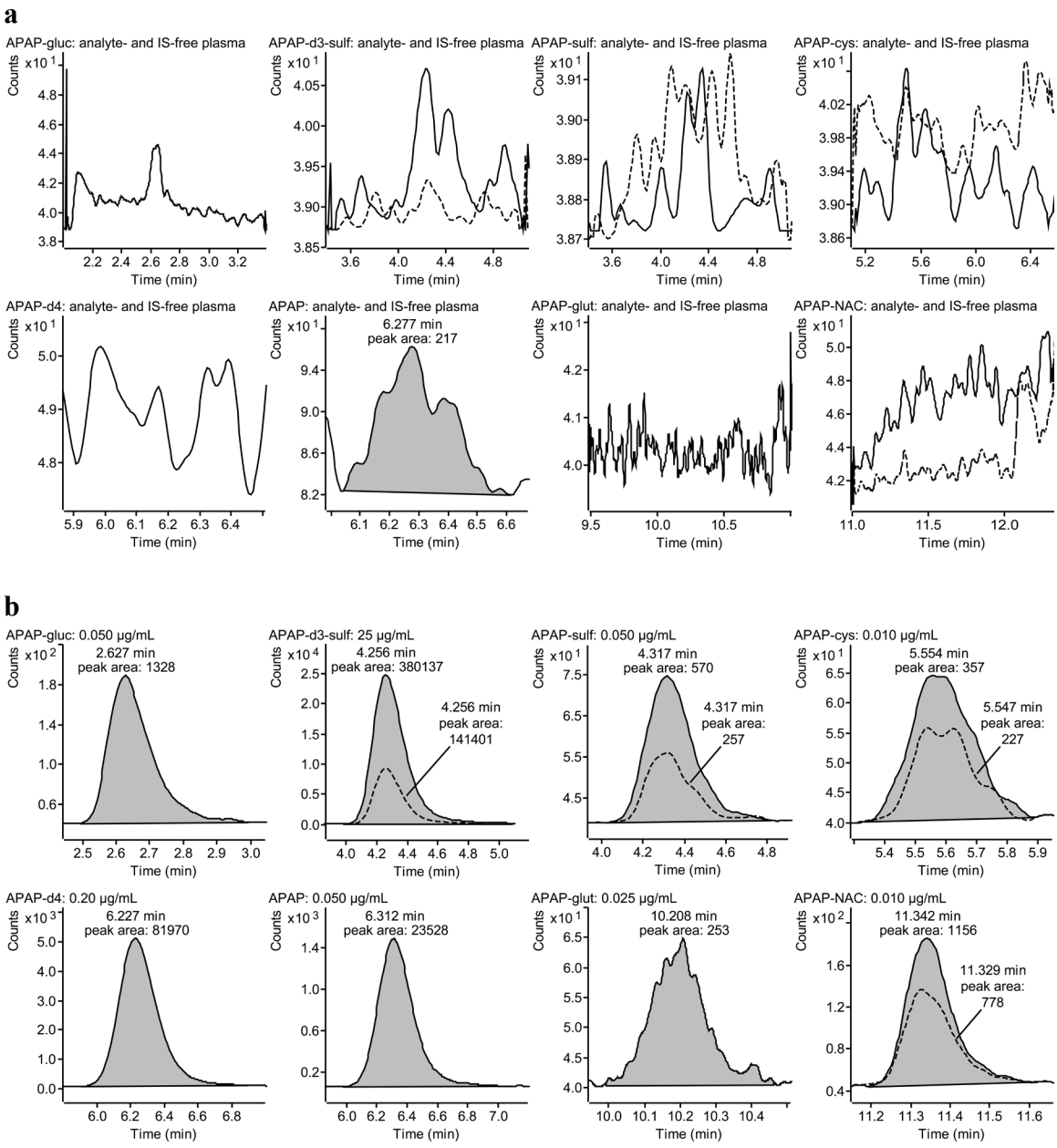

Figure 2.2 Representative MRM chromatograms for determination of APAP and metabolites in human plasma: **a** analyte- and IS-free plasma, **b** plasma fortified with IS and with APAP and metabolites at each LLOQ. Specific precursor→product ion transitions for each analyte and IS are provided in Table 2.2. Solid lines depict MRM traces for quantifier transitions and dashed lines depict MRM traces for qualifier transitions. Nominal concentrations for analytes and IS are provided in the heading of each MRM trace. MRM chromatograms in **b** are derived from three sample injections (the three lowest calibrators).

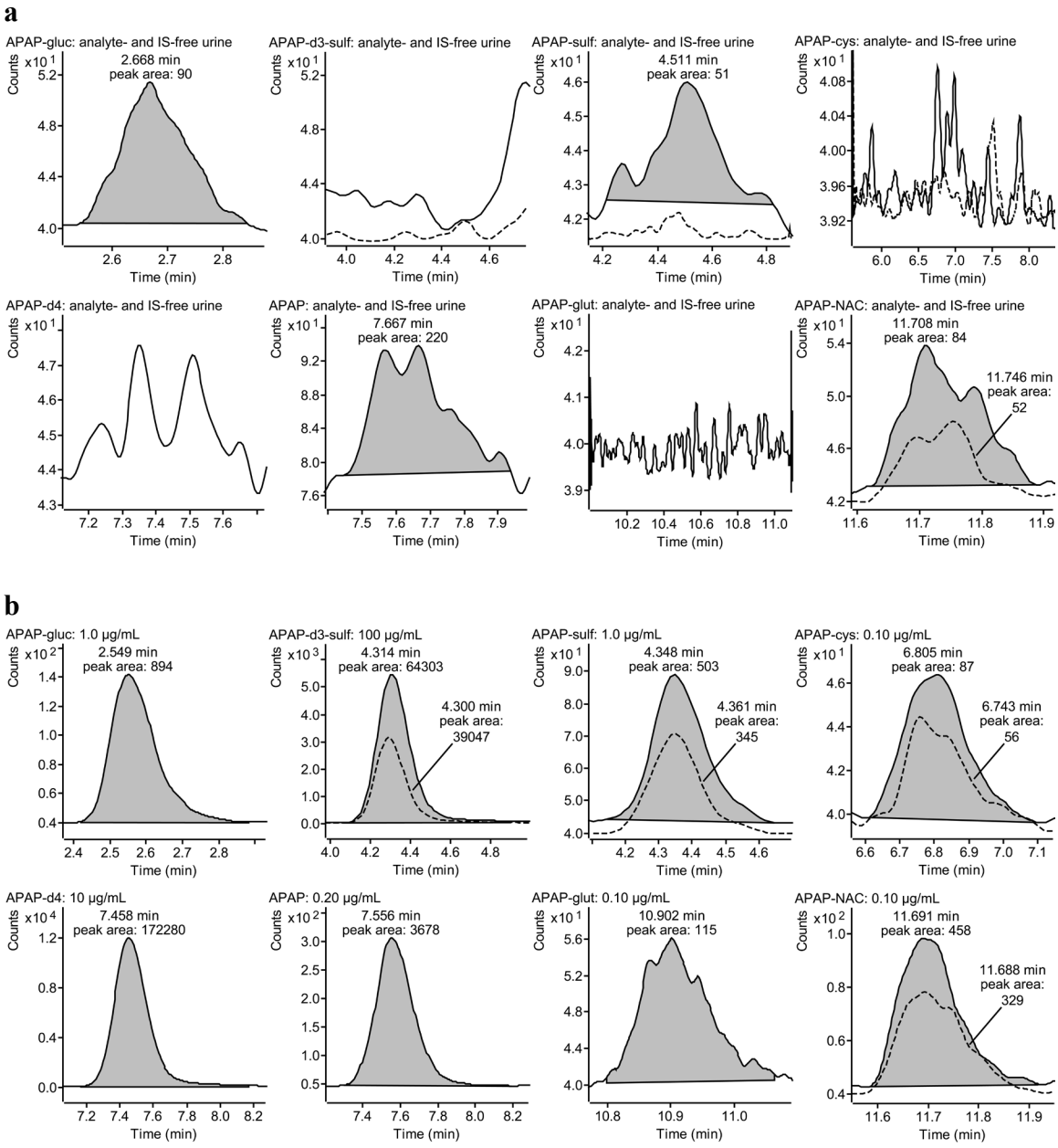

Figure 2.3 Representative MRM chromatograms for determination of APAP and metabolites in human urine: **a** analyte- and IS-free urine, **b** urine fortified with IS and with APAP and metabolites at each LLOQ. Specific precursor→product ion transitions for each analyte and IS are provided in Table 2.2. Solid lines depict MRM traces for quantifier transitions and dashed lines depict MRM traces for qualifier transitions. Nominal concentrations for analytes and IS are provided in the heading of each MRM trace. MRM chromatograms in **b** are derived from two sample injections (the two lowest calibrators).

APAP-NAC, additional qualification transitions were monitored to enhance assay specificity. Samples were required to have a qualifier ion peak with a signal-to-noise ratio >3 in order for a quantifiable analyte concentration to be reported, and this was particularly helpful for samples with concentrations near the LLOQ. Many of these quantifier and qualifier mass transitions have previously been utilized in LC–MS/MS methods for these analytes [22-24, 26, 29, 30].

At the time of initial method development, deuterated analogues of sufficient purity for use as IS (≥95%) were unavailable for some analytes. During preliminary testing, APAP-d4 performed well as an IS for APAP. However, the instrument response was much greater for APAP and APAP-d4 than for the other analytes. This is apparent by examination of the peak areas in Figures 2.2b and 2.3b; even when concentration and molecular weight differences are taken into account, peak areas for APAP are significantly larger than for the other analytes. As a result, APAP-d4 did not perform well as an IS for the other analytes. Both APAP and APAP-d4 showed evidence of ion suppression at the high end of the calibration curve. This self-induced ion suppression was not problematic for quantification of APAP, but it did limit the utility of APAP-d4 as an IS for other analytes. Preliminary testing showed that APAP-d3-sulf performed well as an IS for APAP-sulf and for the remaining analytes. It provided consistent peak areas across the calibration curve ranges and allowed for linear curve fits for all analytes except APAP-gluc, for which a quadratic curve fit was applied. IS working solution concentrations of APAP-d4 and APAP-d3-sulf were selected based on the relative instrument response for each.

Due to the wide variability in the chemical nature of the analytes (i.e., relatively

nonpolar parent drug and several highly polar metabolites), nonspecific sample preparation procedures were expected to be most suitable. Thus, plasma samples were prepared for analysis by protein precipitation, and the relatively high urinary analyte concentrations inspired the testing and eventual implementation of a dilution-only urine sample preparation. As evidenced by the validation results, these simple and efficient preparation procedures performed well.

Method validation

Appropriate LLOQ concentrations were determined based on the predefined acceptance criteria. LLOQ values for the plasma and urine assays are presented in Tables 2.3 and 2.4, respectively, along with intra-assay accuracy and imprecision data for each LLOQ. Representative MRM chromatograms are provided for analyte- and IS-free plasma (Figure 2.2a), plasma LLOQ calibrators fortified with IS (Figure 2.2b), analyte- and IS-free urine (Figure 2.3a), and urine LLOQ calibrators fortified with IS (Figure 2.3b).

Most calibration curves were fit well by linear regression with $1/x^2$ weighting. APAP-gluc, however, required quadratic regression. Also, in plasma, the APAP-NAC curve was linear only up to 1.0 µg/mL. Back-calculation of calibrator and QC concentrations by interpolation consistently yielded values within ±20% of nominal concentration, and coefficients of determination (R^2) for calibration curves were typically ≥0.99. No evidence of chromatographic carryover was observed when analyte-free matrix samples were injected immediately after the highest calibration standards.

Intra- and inter-assay accuracy and imprecision data for each QC concentration

Table 2.3 LLOQ and intra- and inter-assay accuracy and imprecision for determination of APAP and metabolites in human plasma.

Analyte	Nominal concentration (µg/mL)	Intra-assay accuracy and imprecision[a]			Inter-assay accuracy and imprecision (n = 20)		
		Observed concentration (µg/mL)[b]	Mean accuracy (%)	Imprecision (% CV)	Observed concentration (µg/mL)[b]	Mean accuracy (%)	Imprecision (% CV)
APAP	0.050[c]	0.046 ± 0.002	92	5.3	n/a	n/a	n/a
	0.15	0.15 ± 0.01	99	7.1	0.15 ± 0.01	101	7.2
	0.80	0.83 ± 0.01	104	1.4	0.82 ± 0.03	102	4.2
	8.0	7.9 ± 0.5	98	6.3	7.9 ± 0.3	99	4.2
	40	39 ± 4	98	9.1	39 ± 3	98	6.8
APAP-gluc	0.050[c]	0.040 ± 0.006	80	13.9	n/a	n/a	n/a
	0.15	0.14 ± 0.01	92	6.1	0.15 ± 0.02	101	11.5
	0.80	0.81 ± 0.04	102	5.2	0.83 ± 0.08	104	9.2
	8.0	7.2 ± 0.4	91	5.5	7.5 ± 0.5	94	6.5
	40	40 ± 5	100	13.7	40 ± 4	101	8.8
APAP-sulf	0.050[c]	0.050 ± 0.003	100	6.5	n/a	n/a	n/a
	0.15	0.15 ± 0.01	100	6.8	0.15 ± 0.02	101	12.4
	0.80	0.80 ± 0.02	100	2.3	0.79 ± 0.06	99	7.4
	8.0	8.2 ± 0.5	102	5.9	8.0 ± 0.4	100	4.4
	40	43 ± 2	107	5.8	42 ± 2	105	5.2
APAP-glut	0.025[c]	0.028 ± 0.004	111	13.6	n/a	n/a	n/a
	0.080	0.089 ± 0.004	112	4.3	0.086 ± 0.007	107	8.0
	0.80	0.89 ± 0.03	111	3.4	0.87 ± 0.06	108	6.7
	4.0	4.4 ± 0.2	111	5.4	4.3 ± 0.3	107	7.3

Table 2.3 (continued)

Analyte	Nominal concentration (µg/mL)	Intra-assay accuracy and imprecision[a]			Inter-assay accuracy and imprecision (n = 20)		
		Observed concentration (µg/mL)[b]	Mean accuracy (%)	Imprecision (% CV)	Observed concentration (µg/mL)[b]	Mean accuracy (%)	Imprecision (% CV)
APAP-cys	0.010[c]	0.0097 ± 0.0004	97	4.3	n/a	n/a	n/a
	0.015	0.013 ± 0.001	85	8.2	0.013 ± 0.002	90	14.5
	0.080	0.070 ± 0.005	87	6.7	0.074 ± 0.005	93	6.8
	0.80	0.71 ± 0.03	89	4.4	0.74 ± 0.05	92	6.9
	4.0	3.6 ± 0.2	89	6.9	3.7 ± 0.3	93	7.2
APAP-NAC	0.010[c]	0.0082 ± 0.0008	82	9.4	n/a	n/a	n/a
	0.015	0.014 ± 0.002	93	12.3	0.015 ± 0.002	97	11.9
	0.080	0.084 ± 0.004	105	4.9	0.083 ± 0.005	104	6.4
	0.80	0.75 ± 0.05	94	6.1	0.77 ± 0.05	97	6.3

[a] LLOQ n = 6; QC n = 5.

[b] Reported values are mean concentration ± standard deviation.

[c] LLOQ.

n/a, not applicable.

Table 2.4 LLOQ and intra- and inter-assay accuracy and imprecision for determination of APAP and metabolites in human urine.

Analyte	Nominal concentration (µg/mL)	Intra-assay accuracy and imprecision[a]			Inter-assay accuracy and imprecision (n = 20)		
		Observed concentration (µg/mL)[b]	Mean accuracy (%)	Imprecision (% CV)	Observed concentration (µg/mL)[b]	Mean accuracy (%)	Imprecision (% CV)
APAP	0.20[c]	0.20 ± 0.01	98	4.2	n/a	n/a	n/a
	7.5	7.1 ± 0.4	94	5.0	7.5 ± 0.4	100	5.7
	50	53 ± 1	106	1.3	52 ± 2	105	4.1
	500	494 ± 13	99	2.6	496 ± 25	99	5.0
APAP-gluc	1.0[c]	1.02 ± 0.03	102	2.6	n/a	n/a	n/a
	7.5	6.5 ± 0.4	87	5.6	7.4 ± 0.9	99	11.9
	50	49 ± 2	98	3.1	51 ± 3	102	6.5
	500	488 ± 20	98	4.1	517 ± 53	103	10.2
APAP-sulf	1.0[c]	1.0 ± 0.1	103	4.9	n/a	n/a	n/a
	7.5	6.9 ± 0.4	92	5.9	7.9 ± 0.7	106	8.7
	50	50 ± 1	101	1.7	54 ± 3	108	6.4
	500	491 ± 25	98	5.0	554 ± 47	111	8.4
APAP-glut	0.10[c]	0.111 ± 0.004	111	3.2	n/a	n/a	n/a
	0.75	0.69 ± 0.04	92	5.6	0.72 ± 0.07	96	9.3
	5.0	5.1 ± 0.1	101	1.6	4.8 ± 0.3	96	6.7
	50	54 ± 2	107	4.2	53 ± 3	105	6.6

Table 2.4 (continued)

Analyte	Nominal concentration (µg/mL)	Intra-assay accuracy and imprecision[a]			Inter-assay accuracy and imprecision (n = 20)		
		Observed concentration (µg/mL)[b]	Mean accuracy (%)	Imprecision (% CV)	Observed concentration (µg/mL)[b]	Mean accuracy (%)	Imprecision (% CV)
APAP-cys	0.10[c]	0.10 ± 0.01	96	7.4	n/a	n/a	n/a
	0.75	0.67 ± 0.04	89	6.4	0.76 ± 0.09	101	12.2
	5.0	5.0 ± 0.1	100	2.5	5.1 ± 0.4	102	7.9
	50	51 ± 2	102	3.1	53 ± 4	106	8.4
APAP-NAC	0.10[c]	0.114 ± 0.004	114	3.4	n/a	n/a	n/a
	0.75	0.70 ± 0.05	93	7.3	0.69 ± 0.05	92	7.9
	5.0	5.2 ± 0.1	104	2.8	4.8 ± 0.3	96	7.3
	50	54 ± 2	107	3.7	50 ± 4	100	7.9

[a] LLOQ n = 6; QC n = 5.

[b] Reported values are mean concentration ± standard deviation.

[c] LLOQ.

n/a, not applicable.

are summarized in Tables 2.3 and 2.4 for plasma and urine, respectively. The methods were found to be highly accurate and precise. Mean values for intra- and inter-assay accuracy in plasma ranged from 85–112% and 90–108%, respectively. In plasma, intra- and inter-assay imprecision did not exceed 14% and 15%, respectively. Mean values for intra- and inter-assay accuracy in urine ranged from 87–107% and 92–111%, respectively. In urine, intra- and inter-assay imprecision did not exceed 8% and 13%, respectively.

Analysis of human plasma and urine from 6 APAP-abstinent individuals demonstrated that the assays provide requisite specificity. In plasma samples fortified with IS, mean peak area ratios (analyte/IS) for each lot were <5% of the LLOQ peak area ratio for all analytes. Similarly, in plasma samples that were not fortified with IS, peak areas in the IS MRM transitions were <0.1% of the IS peak areas in the LLOQ samples. In urine samples fortified with IS, mean peak area ratios for APAP-cys/IS were slightly greater than 20% in most of the test lots (range: 20–24%); however, these samples did not produce detectable peaks in the APAP-cys qualifier MRM transition. For all other analytes, mean peak area ratios (analyte/IS) for each urine lot were <19% of the LLOQ peak area ratio. In urine samples that were not fortified with IS, peak areas in the IS MRM transitions were <1% of the IS peak areas in the LLOQ samples.

APAP-d4 and APAP-d3-sulf were recovered from plasma at 86 ± 6% and 81 ± 7%, respectively (mean % recovery ± SD, n = 20). These values suggest that small but consistent amounts of IS and, presumably, analytes were lost during the supernatant transfer step that occurred prior to sample evaporation. Results for ionization efficiency and matrix effect experiments for the plasma assay are summarized in Table 2.5. For

APAP and APAP-sulf, mean ionization efficiencies ranged from 87–97%, suggesting insignificant influence of plasma matrix components on analyte ionization. Results for APAP-gluc, APAP-glut, and APAP-NAC were indicative of ion suppression, with mean ionization efficiencies ranging from 32–75%. In contrast, results for APAP-cys suggest that ion enhancement occurred at lower analyte concentrations, with mean ionization efficiencies of 381% and 168% at QC levels 1 and 2, respectively. In spite of these variable ionization efficiencies, results from the matrix effect experiment demonstrate that the influence of plasma matrix components on analyte ionization was relatively consistent across 6 different individuals. With the exception of APAP-glut, mean accuracies ranged from 101–114% and standard deviations did not exceed 6%. Matrix effect results for APAP-glut were less accurate and less precise (Table 2.5); however, APAP-glut is arguably the least important of the analytes in this matrix (see further discussion below), and these results were therefore considered acceptable for this particular analyte.

APAP-d4 and APAP-d3-sulf were recovered from urine at 104 ± 8% and 104 ± 7%, respectively (mean % recovery ± SD, n = 15). As expected for a dilution-only sample preparation, these values are close to 100%. Results for ionization efficiency and matrix effect experiments for the urine assay are summarized in Table 2.6. Across all analytes, mean ionization efficiencies ranged from 94–104%, which suggests that urine matrix components neither suppressed nor enhanced analyte ionization. Results from the matrix effect experiment demonstrate that the analytes could be quantified with acceptable accuracy and imprecision in urine from 6 different individuals. Across all analytes, mean accuracies ranged from 87–115% and standard deviations did not exceed

Table 2.5 Ionization efficiency and matrix effect for determination of APAP and metabolites in human plasma.

Compound	Ionization efficiency (%)[a] (*n* = 5)				Accuracy and imprecision of matrix effect samples (%)[a] (*n* = 6)	
	QC level 1	QC level 2	QC level 3	QC level 4	QC level 2	QC level 4
APAP	96 ± 6	93 ± 3	97 ± 5	97 ± 2	101 ± 3	108 ± 1
APAP-d4	95 ± 10	97 ± 3	96 ± 5	98 ± 6	n/a	n/a
APAP-gluc	32 ± 4	32 ± 1	42 ± 1	51 ± 2	111 ± 6	109 ± 5
APAP-sulf	90 ± 5	87 ± 5	91 ± 7	91 ± 4	107 ± 3	113 ± 3
APAP-d3-sulf	91 ± 16	90 ± 4	84 ± 4	91 ± 5	n/a	n/a
APAP-glut	n/a	61 ± 4	57 ± 2	56 ± 9	132 ± 16	117 ± 15
APAP-cys	381 ± 200	168 ± 29	109 ± 7	101 ± 4	114 ± 4	114 ± 3
APAP-NAC	75 ± 3	73 ± 5	74 ± 3	n/a	104 ± 3	n/a

[a] Reported values are mean % ± standard deviation.

n/a, not applicable.

Table 2.6 Ionization efficiency and matrix effect for determination of APAP and metabolites in human urine.

Compound	Ionization efficiency (%)[a] (n = 5)			Accuracy and imprecision of matrix effect samples (%)[a] (n = 6)	
	QC level 1	QC level 2	QC level 3	QC level 1	QC level 3
APAP	100 ± 5	99 ± 5	99 ± 2	101 ± 4	97 ± 1
APAP-d4	100 ± 6	103 ± 8	103 ± 9	n/a	n/a
APAP-gluc	96 ± 3	94 ± 3	94 ± 3	107 ± 12	99 ± 8
APAP-sulf	101 ± 4	99 ± 4	97 ± 3	112 ± 4	115 ± 2
APAP-d3-sulf	100 ± 7	103 ± 7	102 ± 6	n/a	n/a
APAP-glut	99 ± 4	99 ± 3	99 ± 4	101 ± 5	112 ± 8
APAP-cys	104 ± 5	99 ± 5	99 ± 4	108 ± 5	107 ± 1
APAP-NAC	99 ± 4	98 ± 2	98 ± 4	87 ± 4	91 ± 1

[a] Reported values are mean % ± standard deviation.

n/a, not applicable.

12%.

Analyte stock solutions appeared stable (within ±20% of freshly prepared solution) following 6 months of storage at −20°C. After 12 months of storage at −20°C, APAP-glut stock solution had deteriorated to less than 40% of the values obtained from fresh stock solution; however, significant deterioration was not observed for any of the other analyte stock solutions. Based on these results, it was determined that APAP, APAP-gluc, APAP-sulf, APAP-cys, and APAP-NAC stock solutions could be used up to 1 year after the preparation date, and APAP-glut stock solution could be used up to 6 months after the preparation date.

Results of plasma stability experiments are summarized in Table 2.7. Under all tested storage and handling conditions, APAP-glut quickly deteriorated in human plasma, presumably as a result of hydrolysis by gamma-glutamyl transpeptidase and dipeptidases. APAP-cys is a major hydrolysis product of APAP-glut, and the decline in APAP-glut was accompanied by a concomitant increase in APAP-cys concentrations. For many analytes, such instability would be cause for concern. However, in this case, investigators are often primarily interested in using the sum of APAP-glut, APAP-cys, and APAP-NAC concentrations as a surrogate for the amount of NAPQI that formed. Thus, APAP-glut instability is not a major concern here because the critical information is essentially retained through measurement of APAP-cys. Furthermore, these stability data were derived from fortified APAP-glut concentrations, which are likely far higher than physiologically relevant concentrations. In *in vitro* experiments with human fetal and adult liver homogenates, APAP-glut was rapidly transformed to APAP-cys [21]. Additionally, the dipeptide conjugate APAP-cysteinylglycine was not detected, which

Table 2.7 Stability of APAP and metabolites in human plasma.

Analyte	Nominal concentration (µg/mL)	Stability in plasma (%)[a] (n = 3)			Stability in prepared samples (%)[b] (n = 3)
		24 h at room temperature	6 months at −80°C	3 freeze-thaw cycles	72 h in 5°C autosampler
APAP	0.15	99 ± 8	103 ± 10	102 ± 6	95 ± 5
	40	109 ± 9	102 ± 8	105 ± 9	98 ± 8
APAP-gluc	0.15	105 ± 6	99 ± 13	96 ± 3	101 ± 7
	40	120 ± 11	96 ± 10	97 ± 9	111 ± 4
APAP-sulf	0.15	97 ± 12	103 ± 9	82 ± 8	102 ± 9
	40	112 ± 8	101 ± 8	102 ± 7	98 ± 6
APAP-glut	0.080	0 ± n/a	35 ± 3	15 ± 1	94 ± 4
	4.0	0.16 ± 0.03	46 ± 4	23 ± 2	107 ± 7
APAP-cys	0.015	365 ± 29	127 ± 11	197 ± 31	90 ± 10
	4.0	307 ± 24	123 ± 13	160 ± 17	97 ± 6
APAP-NAC	0.015	94 ± 10	74 ± 16	90 ± 11	102 ± 14
	0.80	106 ± 8	87 ± 10	100 ± 7	98 ± 7

[a] Reported values are mean % of initial observed concentration ± standard deviation. Stability of the analytes in plasma was assessed with fortified samples obtained by reconstitution of evaporated analyte working solutions in analyte- and IS-free plasma.

[b] Reported values are mean % of observed concentration from freshly prepared samples ± standard deviation.

n/a, not applicable.

suggests that hydrolysis of APAP-glut by gamma-glutamyl transpeptidase is the rate-limiting step in the conversion to APAP-cys [21]. The results reported herein also indicate that substantial gamma-glutamyl transpeptidase and dipeptidase activities are present in human plasma. Thus, circulating concentrations of APAP-glut in humans are likely to be quite low. Nevertheless, if a particular research question required differentiation between relative amounts of APAP-glut and APAP-cys, it seems likely that addition of peptidase inhibitors during sample collection would prevent or at least minimize APAP-glut degradation, but such experiments were beyond the scope of this study.

APAP, APAP-gluc, and APAP-sulf were adequately stable in human plasma under all tested storage and handling conditions (Table 2.7). For these analytes, mean concentrations were within ±20% of initial values following storage of fortified human plasma at room temperature for 24 h, at −80°C for 6 months, and after 3 freeze-thaw cycles. These results are in agreement with previous studies where APAP [26, 31-34] and APAP-gluc [26] have been found to be quite stable in human plasma under typical sample handling conditions. The results for stability of APAP-cys in human plasma were obscured due to the degradation of APAP-glut to APAP-cys. However, previous work has shown that APAP-cys was adequately stable in human plasma/serum for up to 24 h at room temperature and through 3 freeze-thaw cycles [26, 29, 30]. APAP-NAC appeared adequately stable in human plasma following 24 h of storage at room temperature and after 3 freeze-thaw cycles, but significant deterioration was evident at QC level 1 after 6 months of storage at −80°C (mean stability: 74% of initial concentration). After only 1 month of storage at −80°C, stability for APAP-NAC at QC levels 1 and 3 was acceptable

at 88 ± 8% and 93 ± 11%, respectively (mean % of initial observed concentration ± SD). All analytes were adequately stable in prepared plasma samples that were stored in the autosampler at 5°C for up to 72 h. Across all analytes and QC concentrations, mean concentrations of postpreparative stability samples were within ±11% of freshly prepared QC samples (Table 2.7). Taken together, the stability experiment results suggest that plasma samples can be handled at room temperature during routine sample preparation and subjected to several freeze-thaw cycles without concern for analyte degradation. Furthermore, plasma samples should ideally be assayed within the first few months after sample collection.

Results of urine stability experiments are summarized in Table 2.8. APAP-glut was not detected in the initial urine stability samples (see further discussion below), but all other analytes were adequately stable in human urine under the tested storage and handling conditions. For these analytes, mean concentrations were within ±19% of initial concentrations following storage of human urine at room temperature for 24 h, at −80°C for 1 month, and after 3 freeze-thaw cycles. Additionally, all analytes were adequately stable in prepared urine samples that were stored in the autosampler at 5°C for up to 72 h. Mean concentrations of postpreparative stability samples were within ±10% of freshly prepared QC samples.

Application to neonatal pharmacokinetic samples

The methods presented in this paper have been successfully applied for determination of APAP and metabolites in the plasma and urine of neonatal clinical study participants receiving therapeutic doses of intravenous APAP. The analysis of samples

Table 2.8 Stability of APAP and metabolites in human urine.

Analyte	Stability in urine (%)[a] (n = 3)				Stability in prepared samples (%)[b] (n = 3–5)	
	Initial concentration (μg/mL)	24 h at room temperature	1 month at −80°C	3 freeze-thaw cycles	Nominal concentration (μg/mL)	72 h in 5°C autosampler
APAP	1.5	103 ± 3	96 ± 7	98 ± 4	7.5	98 ± 1
	15	108 ± 4	81 ± 3	99 ± 1	500	97 ± 8
APAP-gluc	54	100 ± 7	92 ± 3	94 ± 5	7.5	101 ± 9
	489	99 ± 6	82 ± 5	91 ± 7	500	98 ± 11
APAP-sulf	43	98 ± 2	99 ± 4	98 ± 3	7.5	102 ± 3
	416	108 ± 5	86 ± 6	102 ± 1	500	102 ± 8
APAP-glut	<0.10	n/a	n/a	n/a	0.75	106 ± 3
	<0.10	n/a	n/a	n/a	50	103 ± 9
APAP-cys	2.1	98 ± 5	106 ± 14	96 ± 4	0.75	104 ± 7
	21	104 ± 6	90 ± 5	96 ± 4	50	105 ± 12
APAP-NAC	1.4	103 ± 8	99 ± 9	91 ± 5	0.75	110 ± 9
	14	111 ± 6	89 ± 5	96 ± 4	50	106 ± 12

[a] Reported values are mean % of initial observed concentration ± standard deviation. Stability of the analytes in urine was assessed with samples prepared by dilution of a specimen collected from a volunteer approximately 3 h after ingestion of 1 g of APAP.

[b] Reported values are mean % of observed concentration from freshly prepared samples ± standard deviation.

n/a, not applicable.

from this special patient population was greatly facilitated by minimizing the required sample volume (10 µL). Each pharmacokinetic sample consisted of only 200 µL of blood, so most plasma sample volumes were less than 100 µL. Representative MRM chromatograms from the plasma assay show all analytes to be <LLOQ in a predose sample (Figure 2.4a) and APAP, APAP-gluc, APAP-sulf, APAP-cys, and APAP-NAC concentrations that are well above LLOQ in a sample collected from the same clinical study participant approximately 7 h after the first 15 mg/kg dose (Figure 2.4b). Similar representative MRM chromatograms are provided for pre and postdose urine samples in Figure 2.5.

The percentage of postdose plasma and urine samples that were <LLOQ did not exceed 1% for most analytes (Table 2.9). The exception was APAP-glut, which was <LLOQ in nearly all plasma samples and in all of the urine samples. However, this was not unexpected because APAP-glut is thought to be particularly short-lived in humans, perhaps due to relatively high expression of gamma-glutamyl transpeptidase compared to other species [21, 35]. Additionally, results of stability experiments with fortified plasma showed that APAP-glut was rapidly converted to APAP-cys under routine storage and handling conditions (Table 2.7). In spite of these expectations, APAP-glut was included as an analyte in these assays because it is a critical intermediate in APAP metabolism, and the ability to quantitate APAP-glut makes the assays readily adaptable to other matrices where concentrations are anticipated to be quantifiable, such as rodent plasma, bile, and tissue [20, 22, 36].

The majority of the samples did not require dilution in order to fall within the upper limit of quantification (ULOQ) (Table 2.9). APAP-NAC in plasma had the highest

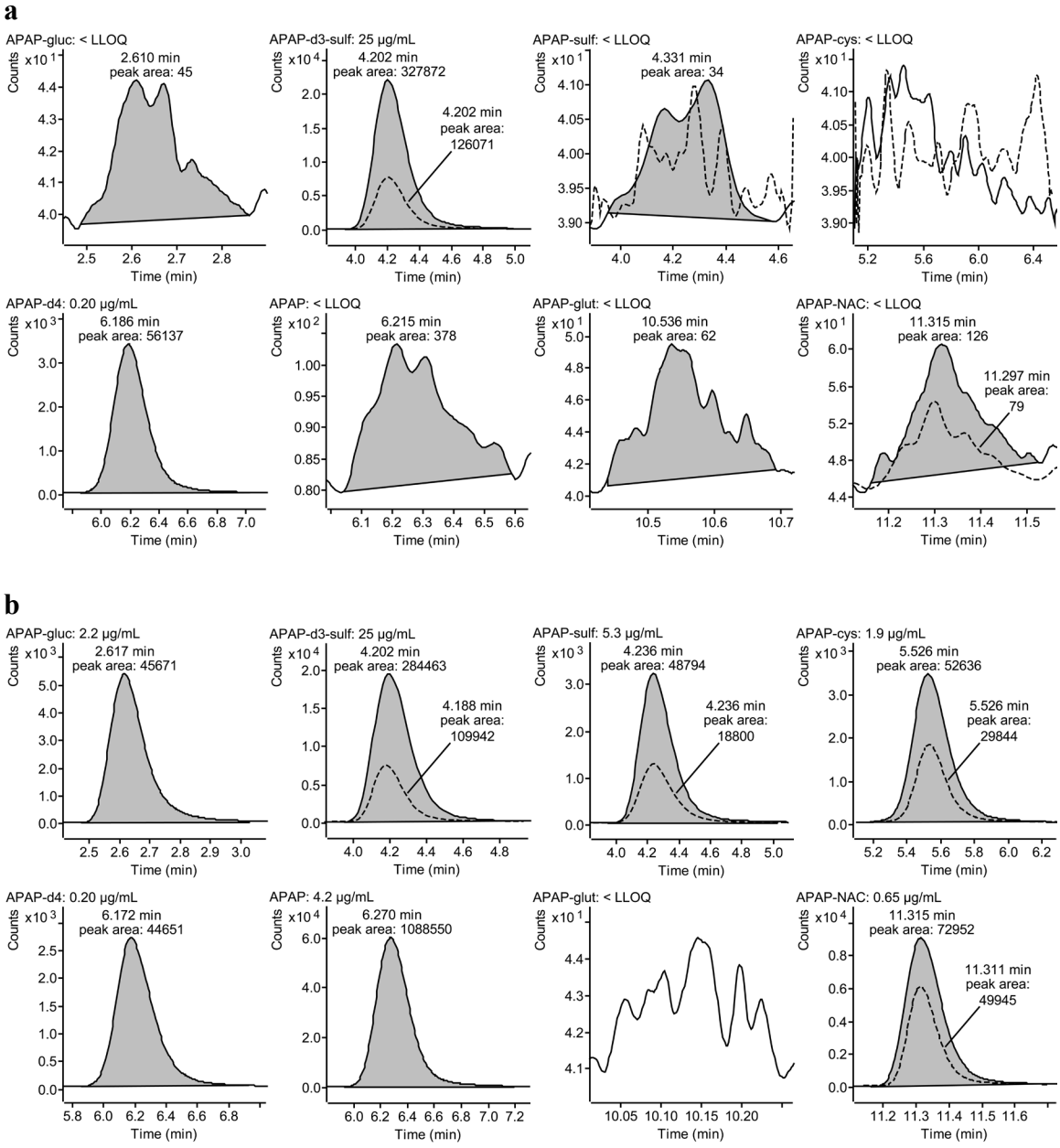

Figure 2.4 Representative MRM chromatograms for determination of APAP and metabolites in human plasma: **a** predose plasma sample from a clinical study participant, **b** a plasma sample collected from the same clinical study participant approximately 7 h after the first 15 mg/kg dose. Specific precursor→product ion transitions for each analyte and IS are provided in Table 2.2. Solid lines depict MRM traces for quantifier transitions and dashed lines depict MRM traces for qualifier transitions. All analytes in **a** were determined to be <LLOQ. Interpolated analyte concentrations in **b** are provided in the MRM trace headings.

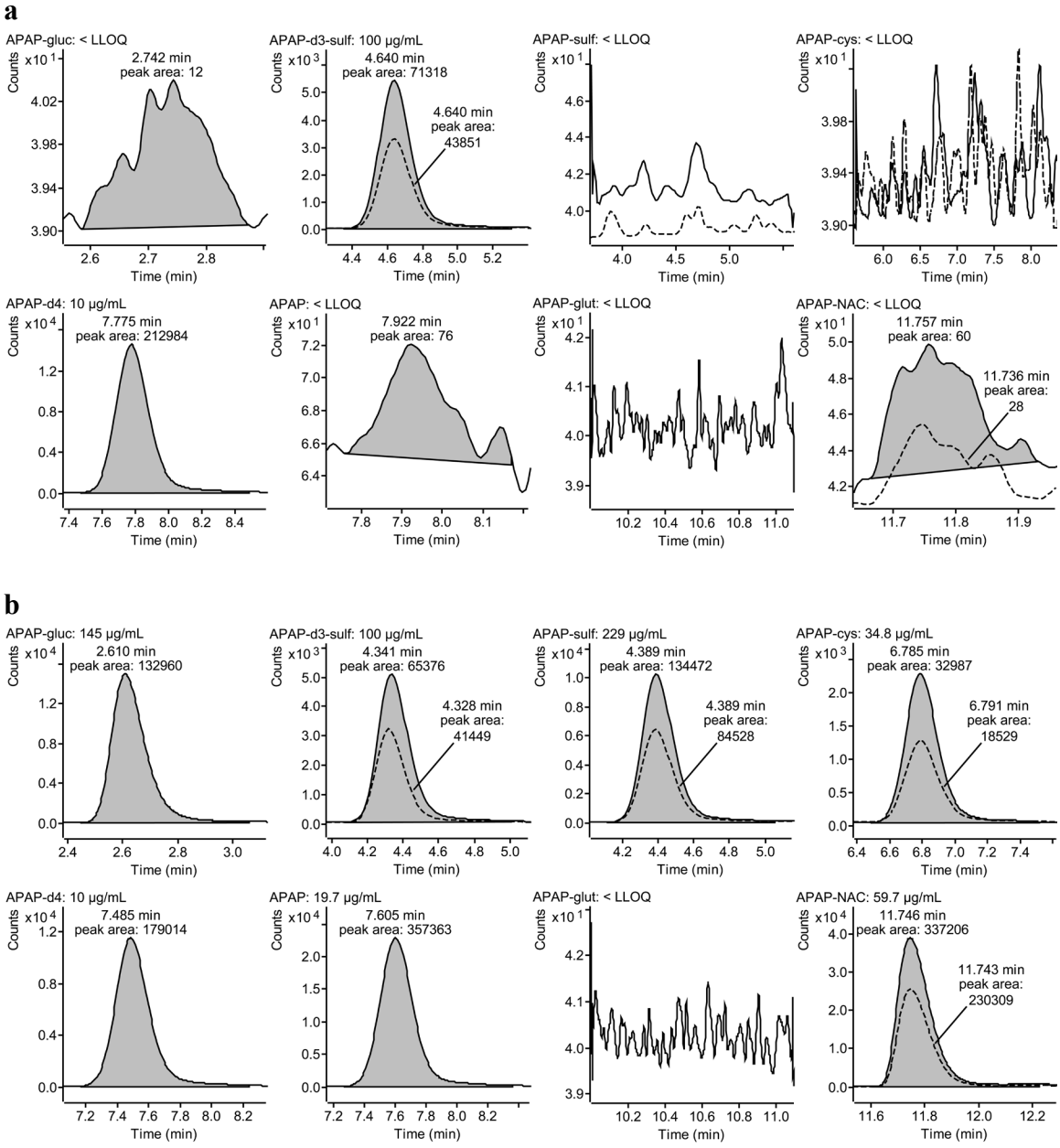

Figure 2.5 Representative MRM chromatograms for determination of APAP and metabolites in human urine: **a** predose urine sample from a clinical study participant, **b** a 4-h urine sample collected from the same clinical study participant approximately 1 h after the fourth 15 mg/kg dose. Specific precursor→product ion transitions for each analyte and IS are provided in Table 2.2. Solid lines depict MRM traces for quantifier transitions and dashed lines depict MRM traces for qualifier transitions. All analytes in **a** were determined to be <LLOQ. Interpolated analyte concentrations in **b** are provided in the MRM trace headings.

Table 2.9 Assay suitability for analysis of neonatal pharmacokinetic samples.

Analyte	Samples < LLOQ (%)		Undiluted samples > ULOQ (%)	
	Plasma[a]	Urine[b]	Plasma[a]	Urine[b]
APAP	0	1	0	0
APAP-gluc	0	1	0	0
APAP-sulf	0	1	9	3
APAP-glut	97	100	0	0
APAP-cys	0	1	8	5
APAP-NAC	1	1	34	11

[a] n = 267 postdose samples.

[b] n = 387 postdose samples.

percentage of samples requiring dilution (34%), which was largely a consequence of the fact that the upper range of the APAP-NAC plasma curve was limited in order to maintain a linear fit. Those samples with analyte concentrations above the ULOQ required only minor dilution (no more than 10 fold), and they could easily be anticipated prior to being assayed based on patient dosing schedule and pharmacokinetic sample collection time.

Conclusion

A novel HPLC–ESI–MS/MS procedure for simultaneous quantification of APAP and five APAP metabolites in small volumes (10 μL) of human plasma and urine was developed and successfully validated. The utility, sensitivity, and suitability of the assays were demonstrated by analysis of samples from a pharmacokinetic study of intravenous APAP in neonates. The reported methods were found to be sensitive, specific, accurate, precise, and efficient. These new methods will serve as powerful tools for researchers studying APAP pharmacokinetics and APAP-induced hepatotoxicity.

References

[1] D.W. Kaufman, J.P. Kelly, L. Rosenberg, T.E. Anderson, A.A. Mitchell, Recent patterns of medication use in the ambulatory adult population of the United States: the Slone survey, JAMA 287 (2002) 337.

[2] R. Paulose-Ram, R. Hirsch, C. Dillon, K. Losonczy, M. Cooper, Y. Ostchega, Prescription and non-prescription analgesic use among the US adult population: results from the third National Health and Nutrition Examination Survey (NHANES III), Pharmacoepidemiol. Drug Saf. 12 (2003) 315.

[3] R. Paulose-Ram, R. Hirsch, C. Dillon, Q. Gu, Frequent monthly use of selected non-prescription and prescription non-narcotic analgesics among U.S. adults, Pharmacoepidemiol. Drug Saf. 14 (2005) 257.

[4] L. Vernacchio, J.P. Kelly, D.W. Kaufman, A.A. Mitchell, Medication use among children <12 years of age in the United States: results from the Slone Survey, Pediatrics 124 (2009) 446.

[5] R.C. Dart, E. Bailey, Does therapeutic use of acetaminophen cause acute liver failure? Pharmacotherapy 27 (2007) 1219.

[6] A.M. Larson, Acetaminophen hepatotoxicity, Clin. Liver Dis. 11 (2007) 525, vi.

[7] G.G. Graham, M.J. Davies, R.O. Day, A. Mohamudally, K.F. Scott, The modern pharmacology of paracetamol: therapeutic actions, mechanism of action, metabolism, toxicity and recent pharmacological findings, Inflammopharmacol. 21 (2013) 201.

[8] E.M. Boyd, G.M. Bereczky, Liver necrosis from paracetamol, Br. J. Pharmacol. Chemother. 26 (1966) 606.

[9] D.G. Davidson, W.N. Eastham, Acute liver necrosis following overdose of paracetamol, Br. Med. J. 2 (1966) 497.

[10] J.S. Thomson, L.F. Prescott, Liver damage and impaired glucose tolerance after paracetamol overdosage, Br. Med. J. 2 (1966) 506.

[11] B. McJunkin, K.W. Barwick, W.C. Little, J.B. Winfield, Fatal massive hepatic necrosis following acetaminophen overdose, JAMA 236 (1976) 1874.

[12] A.M. Larson, J. Polson, R.J. Fontana, T.J. Davern, E. Lalani, L.S. Hynan, J.S. Reisch, F.V. Schiodt, G. Ostapowicz, A.O. Shakil, W.M. Lee, Acetaminophen-induced acute liver failure: results of a United States multicenter, prospective study, Hepatology 42 (2005) 1364.

[13] H. Jaeschke, M.R. McGill, A. Ramachandran, Oxidant stress, mitochondria, and cell death mechanisms in drug-induced liver injury: lessons learned from acetaminophen hepatotoxicity, Drug Metab. Rev. 44 (2012) 88.

[14] M.J. Tunon, M. Alvarez, J.M. Culebras, J. Gonzalez-Gallego, An overview of animal models for investigating the pathogenesis and therapeutic strategies in acute hepatic failure, World J. Gastroenterol. 15 (2009) 3086.

[15] B. Fromenty, Bridging the gap between old and new concepts in drug-induced liver injury, Clin. Res. Hepatol. Gastroenterol. 37 (2013) 6.

[16] J.A. Hinson, D.W. Roberts, L.P. James, Mechanisms of acetaminophen-induced liver necrosis, Handb. Exp. Pharmacol. DOI 10.1007/978-3-642-00663-0_12 (2010) 369.

[17] H. Jaeschke, Acetaminophen: dose-dependent drug hepatotoxicity and acute liver failure in patients, Dig. Dis. 33 (2015) 464.

[18] M.R. McGill, H. Jaeschke, Metabolism and disposition of acetaminophen: recent advances in relation to hepatotoxicity and diagnosis, Pharm. Res. 30 (2013) 2174.

[19] L.P. James, P.R. Mayeux, J.A. Hinson, Acetaminophen-induced hepatotoxicity, Drug Metab. Dispos. 31 (2003) 1499.

[20] Z. Gregus, C. Madhu, C.D. Klaassen, Species variation in toxication and detoxication of acetaminophen in vivo: a comparative study of biliary and urinary excretion of acetaminophen metabolites, J. Pharmacol. Exp. Ther. 244 (1988) 91.

[21] P. Moldeus, C. von Bahr, A. Rane, Metabolism of a glutathione conjugate in human fetal and adult tissues, Dev. Pharmacol. Ther. 1 (1980) 83.

[22] J.H. An, H.J. Lee, B.H. Jung, Quantitative analysis of acetaminophen and its six metabolites in rat plasma using liquid chromatography/tandem mass spectrometry, Biomed. Chromatogr. 26 (2012) 1596.

[23] T. Gicquel, J. Aubert, S. Lepage, B. Fromenty, I. Morel, Quantitative analysis of acetaminophen and its primary metabolites in small plasma volumes by liquid chromatography-tandem mass spectrometry, J. Anal. Toxicol. 37 (2013) 110.

[24] A.K. Hewavitharana, S. Lee, P.A. Dawson, D. Markovich, P.N. Shaw, Development of an HPLC-MS/MS method for the selective determination of paracetamol metabolites in mouse urine, Anal. Biochem. 374 (2008) 106.

[25] Q.Y. Tan, R.H. Zhu, H.D. Li, F. Wang, M. Yan, L.B. Dai, Simultaneous quantitative determination of paracetamol and its glucuronide conjugate in human plasma and urine by liquid chromatography coupled to electrospray tandem mass spectrometry: application to a clinical pharmacokinetic study, J. Chromatogr. B Analyt. Technol. Biomed. Life Sci. 893-894 (2012) 162.

[26] D. Tonoli, E. Varesio, G. Hopfgartner, Quantification of acetaminophen and two of its metabolites in human plasma by ultra-high performance liquid chromatography-low and high resolution tandem mass spectrometry, J. Chromatogr. B Analyt. Technol. Biomed. Life Sci. 904 (2012) 42.

[27] C. Bylda, R. Thiele, U. Kobold, D.A. Volmer, Simultaneous quantification of acetaminophen and structurally related compounds in human serum and plasma, Drug Test. Anal. 6 (2014) 451.

[28] L.F. Prescott, Kinetics and metabolism of paracetamol and phenacetin, Br. J. Clin. Pharmacol. 10 Suppl 2 (1980) 291S.

[29] T. Hairin, A.R. Marzilawati, E.M.H. Didi, S. Mahadeva, Y.K. Lee, N. Abd. Rahman, A.M. Mustafa, Z. Chik, Quantitative LC/MS/MS analysis of acetaminophen-cysteine adducts (APAP-CYS) and its application in acetaminophen overdose patients, Anal. Methods 5 (2013) 1955.

[30] S.F. Cook, A.D. King, Y. Chang, G.J. Murray, H.R. Norris, R.C. Dart, J.L. Green, S.C. Curry, D.E. Rollins, D.G. Wilkins, Quantification of a biomarker of acetaminophen protein adducts in human serum by high-performance liquid chromatography-electrospray ionization-tandem mass spectrometry: Clinical and animal model applications, J. Chromatogr. B Analyt. Technol. Biomed. Life Sci. 985 (2015) 131.

[31] C. Celma, J.A. Allue, J. Prunonosa, C. Peraire, R. Obach, Simultaneous determination of paracetamol and chlorpheniramine in human plasma by liquid chromatography-tandem mass spectrometry, J. Chromatogr. A 870 (2000) 77.

[32] H. Li, C. Zhang, J. Wang, Y. Jiang, J.P. Fawcett, J. Gu, Simultaneous quantitation of paracetamol, caffeine, pseudoephedrine, chlorpheniramine and cloperastine in human plasma by liquid chromatography-tandem mass spectrometry, J. Pharm. Biomed. Anal. 51 (2010) 716.

[33] H.G. Lou, H. Yuan, Z.R. Ruan, B. Jiang, Simultaneous determination of paracetamol, pseudoephedrine, dextrophan and chlorpheniramine in human plasma by liquid chromatography-tandem mass spectrometry, J. Chromatogr. B Analyt. Technol. Biomed. Life Sci. 878 (2010) 682.

[34] R.R. Taylor, K.L. Hoffman, B. Schniedewind, C. Clavijo, J.L. Galinkin, U. Christians, Comparison of the quantification of acetaminophen in plasma, cerebrospinal fluid and dried blood spots using high-performance liquid chromatography-tandem mass spectrometry, J. Pharm. Biomed. Anal. 83 (2013) 1.

[35] C.P. Siegers, W. Loeser, J. Gieselmann, D. Oltmanns, Biliary and renal excretion of paracetamol in man, Pharmacology 29 (1984) 301.

[36] L.J. Fischer, M.D. Green, A.W. Harman, Levels of acetaminophen and its metabolites in mouse tissues after a toxic dose, J. Pharmacol. Exp. Ther. 219 (1981) 281.

CHAPTER 3

POPULATION PHARMACOKINETICS OF INTRAVENOUS PARACETAMOL (ACETAMINOPHEN) IN PRETERM AND TERM NEONATES: MODEL DEVELOPMENT AND EXTERNAL EVALUATION

Clinical Pharmacokinetics (2015) Epub Jul 24. Population Pharmacokinetics of Intravenous Paracetamol (Acetaminophen) in Preterm and Term Neonates: Model Development and External Evaluation. S. F. Cook, J. K. Roberts, S. Samiee-Zafarghandy, C. Stockmann, A. D. King, N. Deutsch, E. F. Williams, K. Allegaert, D. G. Wilkins, C. M. T. Sherwin, J. N. van den Anker. Reprinted with kind permission from Springer Science and Business Media.

Clin Pharmacokinet
DOI 10.1007/s40262-015-0301-3

ORIGINAL RESEARCH ARTICLE

Population Pharmacokinetics of Intravenous Paracetamol (Acetaminophen) in Preterm and Term Neonates: Model Development and External Evaluation

Sarah F. Cook[1] · Jessica K. Roberts[2] · Samira Samiee-Zafarghandy[3,4] · Chris Stockmann[2,5] · Amber D. King[1] · Nina Deutsch[6] · Elaine F. Williams[3] · Karel Allegaert[7,8] · Diana G. Wilkins[1,9] · Catherine M. T. Sherwin[2] · John N. van den Anker[3,10,11,12]

Abstract

Objectives The aims of this study were to develop a population pharmacokinetic model for intravenous paracetamol in preterm and term neonates and to assess the generalizability of the model by testing its predictive performance in an external dataset.

Methods Nonlinear mixed-effects models were constructed from paracetamol concentration–time data in NONMEM 7.2. Potential covariates included body weight, gestational age, postnatal age, postmenstrual age, sex, race, total bilirubin, and estimated glomerular filtration rate. An external dataset was used to test the predictive performance of the model through calculation of bias, precision, and normalized prediction distribution errors.

Results The model-building dataset included 260 observations from 35 neonates with a mean gestational age of 33.6 weeks [standard deviation (SD) 6.6]. Data were well-described by a one-compartment model with first-order elimination. Weight predicted paracetamol clearance and volume of distribution, which were estimated as 0.348 L/h (5.5 % relative standard error; 30.8 % coefficient of variation) and 2.46 L (3.5 % relative standard error; 14.3 % coefficient of variation), respectively, at the mean subject weight of 2.30 kg. An external evaluation was performed on an independent dataset that included 436 observations from 60 neonates with a mean gestational age of 35.6 weeks (SD 4.3). The median prediction error was 10.1 % [95 % confidence interval (CI) 6.1–14.3] and the median absolute prediction error was 25.3 % (95 % CI 23.1–28.1).

Conclusions Weight predicted intravenous paracetamol pharmacokinetics in neonates ranging from extreme

✉ Catherine M. T. Sherwin
catherine.sherwin@hsc.utah.edu

[1] Center for Human Toxicology, Department of Pharmacology and Toxicology, University of Utah, Salt Lake City, UT, USA

[2] Division of Clinical Pharmacology, Department of Pediatrics, University of Utah School of Medicine, 295 Chipeta Way, Salt Lake City, UT 84108, USA

[3] Division of Clinical Pharmacology, Children's National Health System, Washington, DC, USA

[4] Division of Neonatology, Department of Pediatrics, McMaster University, Hamilton, ON, Canada

[5] Department of Pharmacology and Toxicology, University of Utah, Salt Lake City, UT, USA

[6] Division of Anesthesiology, Sedation, and Perioperative Medicine, Children's National Health System, Washington, DC, USA

[7] Neonatal Intensive Care Unit, University Hospitals Leuven, Leuven, Belgium

[8] Department of Development and Regeneration, KU Leuven, Leuven, Belgium

[9] Division of Medical Laboratory Sciences, Department of Pathology, University of Utah School of Medicine, Salt Lake City, UT, USA

[10] Departments of Pediatrics, Integrative Systems Biology, Pharmacology and Physiology, George Washington University School of Medicine and Health Sciences, Washington, DC, USA

[11] Intensive Care and Department of Pediatric Surgery, Erasmus Medical Center-Sophia Children's Hospital, Rotterdam, The Netherlands

[12] Department of Paediatric Pharmacology, University Children's Hospital Basel, Basel, Switzerland

Published online: 23 July 2015

preterm to full-term gestational status. External evaluation suggested that these findings should be generalizable to other similar patient populations.

Key Points

In neonates ranging from extreme preterm to full-term gestational status, body weight is the principal predictor of intravenous paracetamol pharmacokinetics.

A parsimonious regimen based only on equivalent per kilogram doses may be sufficient to accommodate maturational changes in paracetamol pharmacokinetics, even for extremely preterm neonates; however, additional studies are needed to ensure that such a simplified dosing regimen does not increase the risk of paracetamol-induced hepatotoxicity in any neonatal subpopulations.

1 Introduction

Inadequate management of neonatal pain is associated with poor short- and long-term neurodevelopmental outcomes [1]. In neonates and infants, mild to moderate pain is commonly treated with paracetamol (*N*-acetyl-*p*-aminophenol, acetaminophen) [2, 3]. Although paracetamol has been widely used for nearly a century, intravenous formulations only became available recently [4], with regulatory approval for use in patients aged 2 years or older occurring as late as 2010 in the case of the US [5]. Intravenous paracetamol has rapidly gained favor for applications in which enteral delivery is not possible, such as postoperative pain relief [4], and several recent studies have reported on the pharmacokinetics of intravenous paracetamol in neonates [6–8]. However, there is still a lack of consensus regarding optimal dosing guidelines [3, 6, 9–11] and, in many cases, administration of intravenous paracetamol to neonates is limited to off-label use [3]. Furthermore, pharmacokinetic data from extremely preterm neonates (<28 weeks' gestation) remain scarce [3, 6, 8].

Appropriate dose selection for neonates is complicated by developmental changes that occur during early life [12]. Paracetamol is primarily eliminated by hepatic metabolism; therefore, measures of hepatic maturation and function are critical for explanation of between-subject variability (BSV) in paracetamol pharmacokinetics [6–8, 13, 14]. Population pharmacokinetic modeling is a powerful tool for analyzing sparse neonatal data because the approach simultaneously utilizes information from all subjects to characterize the study population, BSV, and influential patient characteristics (covariates) [15, 16]. Unfortunately, neonatal population pharmacokinetic studies are frequently limited by small numbers of subjects. Ideally, the external generalizability of population pharmacokinetic models should be evaluated with independent data that were not used in model development; however, due to a paucity of neonatal studies, this is rarely possible [15–18].

The aims of this study were to develop a population pharmacokinetic model for intravenous paracetamol in preterm and term neonates, and to assess generalizability of the model by testing its predictive performance when applied to an external dataset.

2 Methods

2.1 Study 1: Model-Building Dataset

2.1.1 Ethics Approval and Study Registration

This was a prospective, single-center, open-label study of the pharmacokinetics of intravenous paracetamol in neonates. The study was approved by the Institutional Review Board at the Children's National Health System (Washington, DC, USA) and was carried out in concordance with International Conference on Harmonisation (ICH) Guidelines for Good Clinical Practice [19]. The study was registered at ClinicalTrials.gov (NCT01328808) [20].

2.1.2 Study Population

Patients <28 days postnatal age with an indwelling arterial line and a clinical indication for intravenous analgesia who were admitted to intensive care units at the Children's National Health System (Washington, DC, USA) were considered for inclusion. Exclusion criteria were severe asphyxia, grade III or IV intraventricular hemorrhage, major congenital malformations, neurological disorders, receipt of neuromuscular blockers, and hepatic or renal failure, including systemic hypoperfusion.

2.1.3 Dosing and Sampling Schedule

Intravenous paracetamol (Ofirmev, 10 mg/mL; Mallinckrodt Pharmaceuticals, Dublin, Ireland) was administered by 30-min infusions at 15 mg/kg/dose. The dosing schedule was based on gestational age. Neonates <28 weeks' gestation received five doses at 12-h intervals; neonates ≥28 weeks' gestation received seven doses at 8-h intervals. Blood samples (0.2 mL) were obtained from arterial lines at approximately 0, 1, 2, 4, 6, 8, 12, and 24 h after the first

and last paracetamol doses. Patients were randomly assigned to one of two sampling schedules, each consisting of 9–10 collection times. Blood was collected in sodium heparin Vacutainer tubes (BD, Franklin Lakes, NJ, USA) and centrifuged for 10–15 min at 1500×*g* at 4 °C. Plasma was transferred to cryovials and stored at −70 °F. Study samples were shipped on dry ice to the Center for Human Toxicology at the University of Utah, and stored at −80 °C prior to analysis.

2.1.4 Analytical Method

Paracetamol plasma concentrations were determined using high-performance liquid chromatography–tandem mass spectrometry (HPLC–MS/MS). Plasma samples (10 µL) were fortified with paracetamol-*d4* internal standard (Toronto Research Chemicals, Toronto, ON, Canada) and prepared using protein precipitation with acetonitrile (600 µL). Sample supernatants were evaporated to dryness and reconstituted in 0.1 % aqueous formic acid (400 µL). Reconstituted samples were injected (100 µL) onto an Agilent 1260 Infinity HPLC system interfaced with an Agilent 6460 triple-quadrupole mass spectrometer (Agilent Technologies, Santa Clara, CA, USA). The autosampler was maintained at 5 °C, and the autosampler needle was washed with methanol/water (1/1, v/v) between injections. Chromatographic separation was achieved with an Agilent Poroshell 120 EC-C18 column (2.1 × 100 mm, 2.7 µm particle size; Agilent Technologies, Santa Clara, CA, USA) maintained at 40 °C using a gradient mobile phase consisting of 10 mM aqueous ammonium acetate, pH 3.5 (A) and methanol (B) at a flow rate of 0.25 mL/min. Mobile phase was maintained at 3 % B for 6 min, increased linearly to 35 % B over 3 min, maintained at 95 % B for 3 min, decreased linearly to 3 % B over 0.5 min, and re-equilibrated at 3 % B for 7.5 min. The mass spectrometer was operated in positive electrospray ionization + Agilent Jet Stream mode with multiple reaction monitoring (MRM). The following settings were applied: 350 °C gas temperature, 10 L/min gas flow, 30 psi nebulizer pressure, 350 °C sheath gas temperature, 9 L/min sheath gas flow, 3500 V capillary voltage, 500 V nozzle voltage, 250 V delta EMV, 80 V fragmentor voltage, 14 V collision energy, and 100 ms dwell time. MRM transitions for paracetamol and paracetamol-*d4* were 152.1 → 110.0 and 156.1 → 114.1 (precursor → product *m*/*z*), respectively.

The lower limit of quantification (LLOQ) was 0.05 mg/L [mean accuracy 92 %, coefficient of variation (CV) 5.3 %, $n = 6$], and the calibration curve maintained linearity up to 50 mg/L ($1/x^2$ weighting). Triplicate sets of quality control samples at concentrations of 0.15, 0.80, 8.0, and 40 mg/L accompanied each study sample batch. At these concentrations, mean intra-assay ($n = 5$) and inter-assay ($n = 20$) accuracy ranged from 98 to 104 %, and intra- and inter-assay imprecision was <10 % CV.

2.2 Study 2: External Evaluation Dataset

2.2.1 Ethics Approval and Study Registration

Data for external model evaluation were obtained from a previously published, prospective, single-center, open-label study on the pharmacokinetics of intravenous paracetamol in neonates (PARANEO) [6]. The study was approved by the Ethics Committee at University Hospitals Leuven (Leuven, Belgium) and was carried out in concordance with ICH Guidelines for Good Clinical Practice [19]. The study was registered at ClinicalTrials.gov (NCT00969176) [21] and with the European Clinical Trials Database (EUdraCT) (2009-011243-39).

2.2.2 Study Population

Patients ≤28 days postnatal age with a clinical indication for intravenous paracetamol who were admitted to the Neonatal Intensive Care Unit at University Hospitals Leuven (Leuven, Belgium) were considered for inclusion. Exclusion criteria were recent receipt of paracetamol (<48 h) or clinical contraindication for paracetamol administration (i.e. hepatic failure).

2.2.3 Dosing and Sampling Schedule

Intravenous paracetamol (10 mg/mL; Sintetica SA, Mendrisio, Switzerland) was administered by 15-min infusions with a loading dose of 20 mg/kg, followed by up to seven maintenance doses at 6-h intervals. Each maintenance dose consisted of 5.0, 7.5, or 10.0 mg/kg, respectively, for neonates with postmenstrual ages <32, 32–36, or >36 weeks. Samples were obtained from an arterial line over the 48 h following paracetamol loading doses. The sampling schedule focused on the periods shortly after each loading dose (<2 h; peak concentrations) and just before maintenance doses (5–6 h after the previous dose; trough concentrations). Blood was centrifuged, and plasma samples were stored at −20 °C until analysis.

2.2.4 Analytical Method

Paracetamol plasma concentrations were determined using HPLC coupled with ultraviolet detection. Details of the analytical method have been previously reported [22]. The LLOQ was 0.08 mg/L (<20 % CV), and intra- and interday imprecision was <15 % CV.

2.3 Pharmacometric Model Development

The paracetamol pharmacokinetic model was developed in NONMEM (nonlinear mixed-effects modeling) 7.2 interfaced with PDx-Pop 5.0 (ICON Development Solutions, Ellicott City, MD, USA) using the first-order conditional estimation with interaction method. Processing and visualization of NONMEM output were performed in R 3.0.1 (CRAN.R-project.org). Throughout model development, standard diagnostic plots were generated to evaluate model fit, including observed concentrations versus population- and individual-predicted concentrations, conditional weighted residuals versus time and population-predicted concentrations, and histograms of individual random effects. Models were also compared based on the precision of parameter estimates (parametric standard errors) and condition number [23]. Hierarchical models were compared using the objective function value (OFV). Non-hierarchical models were compared using the Bayesian Information Criterion (BIC) [24].

Based on visual data inspection and a review of the literature, one- and two-compartment structural models were considered. Models were parameterized with clearance and volume terms. Structural models also incorporated the rate and duration of intravenous paracetamol infusion for each dose. Random effects were classified as either between-subject variability (BSV) or residual unexplained variability (RUV). Individual pharmacokinetic parameters were assumed to be log-normally distributed, and BSV was modeled with an exponential function (Eq. 1):

$$\theta_i = \theta_{\text{pop}} \times e^{\eta_i} \quad (1)$$

where θ_i is the individual model-predicted pharmacokinetic parameter (e.g. clearance), θ_{pop} is the population mean for the pharmacokinetic parameter θ, and η_i is the between-subject random effect on θ for the ith individual; η_i is normally distributed with a mean of zero and a variance of ω^2. Additive, proportional, and combined additive and proportional functions were tested for incorporation of RUV [25].

Potential covariates included current body weight, current body length, current body mass index (BMI), gestational age, postnatal age, postmenstrual age, total bilirubin, estimated glomerular filtration rate (GFR), sex, race (White/Caucasian or Black/African American), ethnicity, and indication (surgical or procedural). Laboratory samples were obtained within 24 h prior to the first paracetamol dose or during the pharmacokinetic sample collection period. Estimated GFR was calculated using the updated Schwartz formula (Eq. 2) [26]:

$$\text{eGFR} = 0.413 \times \left(\frac{\text{length}}{\text{Scr}}\right) \quad (2)$$

where eGFR is estimated GFR (mL/min/1.73 m^2), length is body length (cm), and Scr is serum creatinine (mg/dL, modified kinetic Jaffe method). Serum creatinine concentrations obtained at ≤3 days postnatal age were considered to reflect maternal renal function and were excluded from analysis. Continuous covariates were normalized to population mean values and were tested for inclusion in linear, power, and exponential functional forms [27]. Categorical covariates were tested for inclusion using additive shift models. Potential covariates were tested using stepwise forward selection followed by stepwise backward elimination. Changes in OFV were considered significant at $p < 0.05$ (Chi-square distribution, 1 *df*, $\Delta\text{OFV} > 3.84$) during forward selection, and $p < 0.01$ ($\Delta\text{OFV} > 6.63$) during backward elimination [28].

2.4 Internal Model Evaluation

Stability of the final covariate model was evaluated by nonparametric bootstrap [29]. PDx-Pop was used to generate 1000 bootstrap datasets by random sampling with replacement from the original model-building dataset. Additionally, normalized prediction distribution errors (NPDEs) based on 1000 simulations were calculated in NONMEM, and plots were generated for the NPDE distribution and NPDEs versus time, population-predicted concentrations, and influential covariates [30]. Finally, numerical and visual predictive checks were performed to compare observed paracetamol concentrations with concentrations obtained from model-based simulations of 1000 datasets [31]. Predictive checks were performed using Perl-speaks-NONMEM 4.2.0 (PsN, http://psn.sourceforge.net) interfaced with Pirana 2.9.0 (http://pirana-software.com) [32]. Visual predictive check data were prediction corrected [33] and binned based on observation counts.

2.5 External Model Evaluation

An external dataset (Study 2) was used to assess the generalizability of the final covariate model [6]. Predictive performance was assessed as suggested by Sheiner and Beal [34] to quantify bias and precision. Confidence intervals for central tendency measures of bias and precision were obtained via bootstrap techniques (n = 2000). Additionally, external evaluation procedures based on NPDEs and numerical and visual predictive checks were performed as described in Sect. 2.4.

3 Results

Key information from Studies 1 and 2 is summarized in Table 1. The model-building dataset (Study 1) consisted of 267 observations from 35 patients (median 8; range 3–11 concentrations/patient). Of these 267 paracetamol concentrations, one measurement was less than the assay LLOQ and was excluded from the analysis. Six measurements (2 %) were implausible (e.g. peak concentrations observed at trough collection times) and were also excluded. Thus, 260 paracetamol concentrations were used for the development and internal evaluation of the population pharmacokinetic model. The external dataset (Study 2) consisted of 436 paracetamol concentrations from 60 patients (median 7; range 2–11 concentrations/patient). The proportion of patients who received intravenous paracetamol for postoperative analgesia versus a medical condition was similar in the two studies; however, the types of surgery and specific medical indications were more diverse in Study 2. The two studies also had similar proportions of preterm and full-term neonates but the percentage of extremely preterm neonates in Study 1 was more than three times that in Study 2 (29 vs. 8 %).

Table 1 Study information for the model-building and external evaluation datasets

	Study 1, model-building dataset	Study 2, external dataset (PARANEO) [6]
NCT identifier	01328808	00969176
Study description	Phase II/III, multiple-dose study of intravenous paracetamol	Phase II/III, multiple-dose study of intravenous paracetamol
Study drug	Ofirmev (10 mg/mL)	Paracetamol Sintetica (10 mg/mL)
Sampling route	Arterial	Arterial
Analytical method	HPLC–MS/MS	HPLC–UV
Subjects	35 neonates	60 neonates
Samples (*n*)	260	436
N per subject [median (range)]	8 (3–11)	7 (2–11)
Primary indication for intravenous paracetamol [*n* (%)]		
Postoperative analgesia	19 (54)	33 (55)
Cardiac surgery	19 (54)	15 (25)
Thoracic surgery	0 (0)	11 (18)
Abdominal surgery	0 (0)	6 (10)
Other	0 (0)	1 (2)
Medical conditions	16 (46)	27 (45)
Alprostadil administration	0 (0)	8 (13)
Procedural/respiratory	16 (46)	8 (13)
Traumatic pain	0 (0)	5 (8)
Fever	0 (0)	3 (5)
Other	0 (0)	3 (5)
Gestational status [*n* (%)]		
Extreme preterm (<28 weeks' GA)	10 (29)	5 (8)
Preterm (<37 weeks' GA)	17 (49)	28 (47)
Full-term (37–42 weeks' GA)	18 (51)	32 (53)
Current body weight[a] (kg) by gestational age subgroup [median (range)]		
Extreme preterm (<28 weeks' GA)	0.69 (0.55–1.30)	0.90 (0.61–1.41)
Preterm (<37 weeks' GA)	0.96 (0.46–2.80)	2.08 (0.61–3.66)
Full-term (37–42 weeks' GA)	3.16 (2.70–4.20)	3.22 (1.80–4.30)
Postnatal age[a] (days) by gestational age subgroup [median (range)]		
Extreme preterm (<28 weeks' GA)	10 (1–26)	17 (6–24)
Preterm (<37 weeks' GA)	9 (1–26)	6 (1–27)
Full-term (37–42 weeks' GA)	6 (2–12)	2 (1–10)

GA gestational age, *HPLC* high-performance liquid chromatography, *MS/MS* tandem mass spectrometry, *NCT* National Clinical Trial, *PARANEO* Paracetamol in Neonates, *UV* ultraviolet detection

[a] On the day of the first paracetamol dose

Table 2 Subject demographics for continuous covariates tested in the model-building dataset

Characteristic	*N*	Mean	SD	CV	Median	Range
Current body weight[a] (kg)	35	2.30	1.22	0.530	2.80	0.46–4.20
Current body length[a] (cm)	34	43.4	9.15	0.211	47.5	25.0–56.0
BMI (kg/m^2)	34	11.1	2.91	0.263	12.0	6.04–16.7
Gestational age (weeks)	35	33.6	6.57	0.196	37	23–41
Postnatal age[a] (days)	35	7.49	5.73	0.766	6	1–26
Postmenstrual age[a] (weeks)	35	34.6	6.28	0.181	37.6	23.1–41.6
Total bilirubin (mg/dL)	22	6.65	4.88	0.734	4.8	0.9–17.5
Serum creatinine[b] (mg/dL)	30	0.707	0.242	0.342	0.7	0.3–1.1
Estimated GFR[c] (mL/min/1.73 m^2)	29	30.1	16.6	0.551	24.1	12.6–70.9

BMI body mass index, *CV* coefficient of variation, *GFR* glomerular filtration rate, *SD* standard deviation

[a] On the day of the first paracetamol dose

[b] Serum creatinine concentrations obtained at ≤3 days postnatal age were considered to reflect maternal renal function and were excluded from the analysis

[c] Estimated GFR was calculated using the updated Schwartz formula (Eq. 2) [26]

Demographic characteristics of the model-building study population are summarized in Tables 2 and 3 for continuous and categorical variables, respectively. The median gestational age was 37 weeks (range 23–41), and most study subjects (66 %) received the first paracetamol dose within 1 week after birth. Median body weight at the time of the first paracetamol dose was 2.80 kg (range 0.46–4.20). Body length was missing from one patient record, which precluded calculation of BMI and estimated GFR for that subject. Total bilirubin measurements were not obtained within the requisite timeframe for 13 subjects. Additionally, two subjects did not have serum creatinine measurements obtained within the requisite timeframe, and three subjects had serum creatinine measurements that were excluded because they were considered to reflect maternal renal function (postnatal age ≤3 days).

Table 3 Subject demographics for categorical covariates tested in the model-building dataset

Characteristic	*N* (%)
Sex	
Male	20 (57)
Female	15 (43)
Race	
White/Caucasian	16 (46)
Black/African American	14 (40)
American Indian/Alaska Native	1 (3)
Asian	1 (3)
Declined to respond	3 (9)
Ethnicity	
Non-Hispanic	24 (69)
Hispanic	8 (23)
Declined to respond	3 (9)

The model-building dataset was best described by a one-compartment structural model with first-order elimination. A two-compartment model had a higher BIC than a comparable one-compartment model (847.6 vs. 841.7) and provided no visual improvement in standard diagnostic plots relative to a one-compartment model. Additionally, condition numbers of 14 and 161,905 were obtained, respectively, for comparable one- and two-compartment models, which suggested that the two-compartment model was an over-parameterized representation of the data [23]. When additive, proportional, and combined additive and proportional error functions were tested for characterization of RUV, the proportional function produced the lowest OFV and was selected for inclusion in the model (Eq. 3):

$$Y_{ij} = Y_{\mathrm{m}ij} + Y_{\mathrm{m}ij} \times \varepsilon_{ij} \quad (3)$$

where Y_{ij} is the observed paracetamol concentration for the ith individual at time j, $Y_{\mathrm{m}ij}$ is the model-predicted paracetamol concentration, and ε_{ij} is a normally distributed random error with a mean of zero and a variance of σ^2.

During testing of potential covariates, subjects with missing information for a covariate undergoing evaluation were excluded from both the base and covariate models being tested. Current body weight was found to have a strong influence on paracetamol pharmacokinetics. Current body length and BMI were also tested as markers of body size, but their performance was inferior to that of weight. Postnatal age was identified as a significant covariate on clearance during the forward selection process but it failed to meet the criterion for inclusion as a covariate during backward elimination. Additionally, the final forward selection step showed that total bilirubin was a significant covariate on paracetamol clearance and volume of distribution: decreases in OFV ranged from 4.2 to 7.3, depending on the pharmacokinetic parameter and

functional form of the covariate. However, total bilirubin was not included in the model due to the fact that these laboratory values were unavailable for 37 % of the study subjects. None of the other potential covariates met the criterion for inclusion at the final forward selection step. Based on OFV, a power function of mean-centered weight best described the relationship between weight and paracetamol pharmacokinetic parameters (Eq. 4):

$$\theta_i = \theta_{\text{pop}} \times \left(\frac{WT_i}{2.30}\right)^{\theta_{\text{cov}}} \times e^{\eta_i} \quad (4)$$

where θ_i is the individual model-predicted pharmacokinetic parameter (e.g. clearance) for an individual with current body weight of WT_i (kg), θ_{pop} is the population mean for the pharmacokinetic parameter θ when current body weight is equal to the mean current body weight of the study population, 2.30 is the mean current body weight of the study population (kg), θ_{cov} is the covariate effect, and η_i is the between-subject random effect for the ith individual on the pharmacokinetic parameter θ. In the final backward elimination step, removal of weight on clearance and volume of distribution increased the OFV by 65.5 and 81.8, respectively. The θ_{cov} exponent in Eq. 4 was first estimated to be 1.07 and 0.892 for clearance and volume of distribution, respectively. To simplify the final model equations, these values were rounded and fixed at 1.1 and 0.9, which caused a trivial change in OFV (increase of 0.2).

Parameter estimates derived from the final covariate model are provided in Table 4. Overall, model parameters were estimated with reasonably good precision, and bootstrap estimates agreed well with those obtained from the final covariate model. Only one of the 1000 bootstrap datasets (0.1 %) failed to minimize during parameter estimation. Standard diagnostic plots are also provided to illustrate the fit of the final covariate model. Plots of observed versus population- and individual-predicted paracetamol concentrations are provided in Fig. 1, and conditional weighted residuals versus time and population-predicted paracetamol concentrations are shown in Fig. 2.

Simulation-based visualizations of model appropriateness were generated with NPDEs and a visual predictive check. The mean NPDE from the model-building dataset was 0.0485, and the variance was 0.935. These values were not significantly different from the expected mean of 0 (Wilcoxon signed-rank test, $p = 0.231$) and variance of 1 (Fisher variance test, $p = 0.476$) (Fig. 3a). Additionally, there were no visible trends in NPDEs when plotted against time since previous dose (Fig. 3c), population-predicted paracetamol concentration (Fig. 3e), and current body weight (Fig. 3g). The visual predictive check demonstrated good agreement between observed paracetamol concentrations and model-based simulations (Fig. 4a), and a numerical predictive check determined that 92.7 % of the observations fell within the simulation-based 90 % prediction interval.

Key subject characteristics for the external dataset are summarized in Tables 1 and 5. Compared with the model-building dataset, the external dataset had a lower proportion of extremely preterm neonates and tended toward younger postnatal ages. Additionally, whereas the model-building dataset was obtained from a US-based study with fairly even representation of White/Caucasian and Black/African American races, the external dataset was derived from a Belgian study with predominantly White/Caucasian subjects [6].

Bias (prediction error) and precision (absolute prediction error) were quantitated by applying the final covariate model to the external dataset. Population-predicted concentrations from the model tended to be slightly higher than observed values (Table 6). The mean NPDE from the external dataset

Table 4 Parameter estimates for the final covariate model

Parameter	Model fit		Bootstrap 95 % CI[a]	
	Estimated value (%RSE)	BSV (ω^2), as % CV (% RSE)	Estimated value	BSV (ω^2), as % CV
CL (L/h)[b]	0.348 (5.5)	30.8 (19.9)	0.311–0.387	23.9–36.2
Effect of weight[c]	1.1 fixed		1.1 fixed	
V_d (L)[b]	2.46 (3.5)	14.3 (51.2)	2.29–2.64	0.1–19.9
Effect of weight[c]	0.9 fixed		0.9 fixed	
Proportional residual unexplained variability (σ^2)	0.0576 (20.8)		0.0373–0.0844	

BSV between-subject variability, *CI* confidence interval, *CL* total body clearance, *% CV* percent coefficient of variation, *% RSE* percent relative standard error, V_d volume of distribution

[a] Bootstrap success rate was 99.9 % ($n = 1000$)

[b] At the mean current body weight of the study population (2.30 kg)

[c] Exponent on mean-centered weight, i.e. the covariate effect (θ_{cov}) in Eq. 4

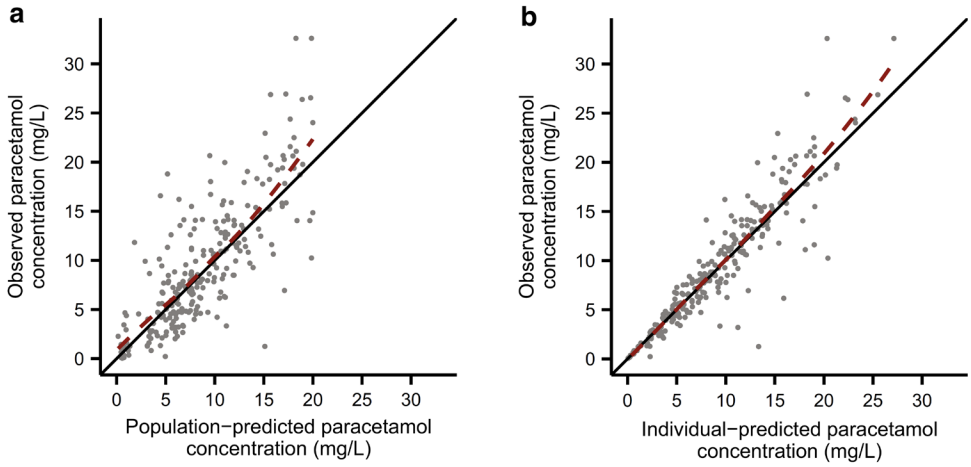

Fig. 1 Diagnostic plots for the final covariate model. Observed versus **a** population-predicted and **b** individual-predicted paracetamol plasma concentrations. The *solid black lines* depict the lines of identity ($y = x$), and the *dashed red lines* depict the LOESS fits of the data

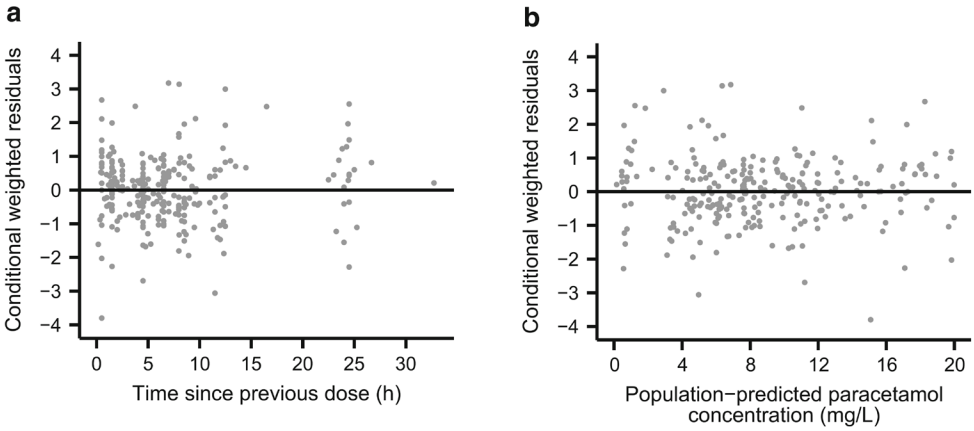

Fig. 2 Diagnostic plots for the final covariate model. Conditional weighted residuals of paracetamol plasma concentrations versus **a** time since previous dose and **b** population-predicted paracetamol concentrations. The *solid black lines* depict $y = 0$

was −0.00772, which was not significantly different from the expected mean of 0 (Wilcoxon signed-rank test, $p = 0.178$), but the NPDE variance from the external dataset was 0.516, which was lower than the expected variance of 1 (Fisher variance test, $p = 2.09 \times 10^{-18}$). Thus, the final covariate model overpredicted the amount of variability in the external dataset (Fig. 3b). However, the NPDE showed no bias when plotted against time since previous dose (Fig. 3d), population-predicted paracetamol concentration (Fig. 3f), and current body weight (Fig. 3h). Additionally, a visual predictive check demonstrated reasonably good agreement between paracetamol concentration observations from the external dataset and model-based simulations (Fig. 4b). Finally, the numerical predictive check determined that 95.9 % of the observations fell within the 90 % prediction interval, which also indicated that the model overestimated the amount of variability in the external dataset.

4 Discussion

Previous neonatal studies of intravenous paracetamol and propacetamol, a prodrug that is rapidly hydrolyzed by plasma esterases to form paracetamol, have used one- [22, 35, 36] and two-compartment [6, 8] models. In the present

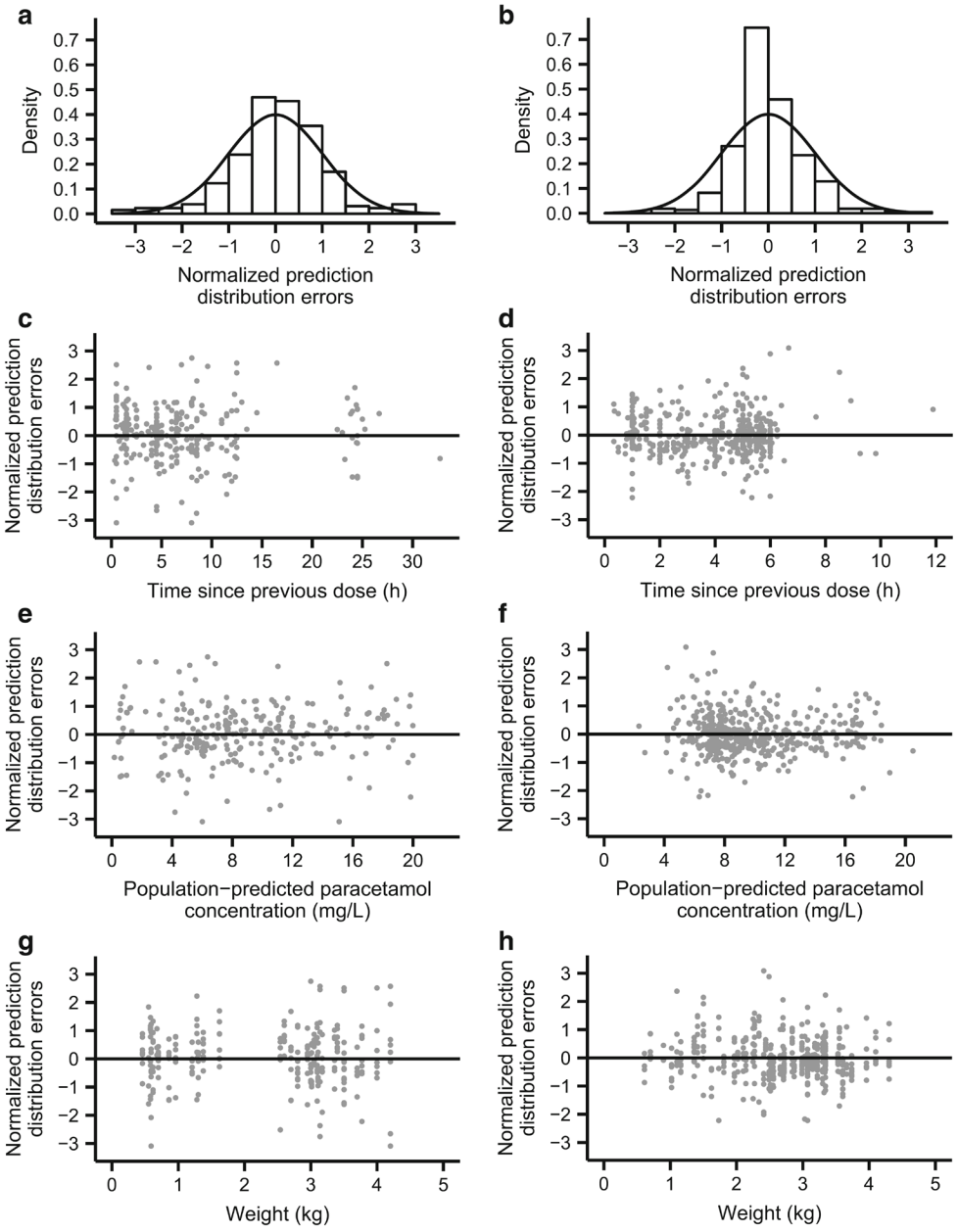

Fig. 3 NPDEs of paracetamol plasma concentrations from the model-building dataset (**a**, **c**, **e**, **g**) and the external evaluation dataset (**b**, **d**, **f**, **h**). Density histograms of NPDEs (**a**, **b**) with overlaid *solid black curves* depicting standard normal distributions for comparison. NPDEs versus time since previous dose (**c**, **d**), population-predicted paracetamol concentration (**e**, **f**), and current body weight (**g**, **h**). *NPDEs* normalized prediction distribution errors

study, the model-building dataset was best described by a one-compartment model. At the mean current body weight of the study population, the final covariate model gave parameter estimates of 0.151 L/h/kg (0.348 L/h/2.30 kg) and 1.07 L/kg (2.46 L/2.30 kg) for clearance and volume of distribution, respectively. Clearance estimates from earlier

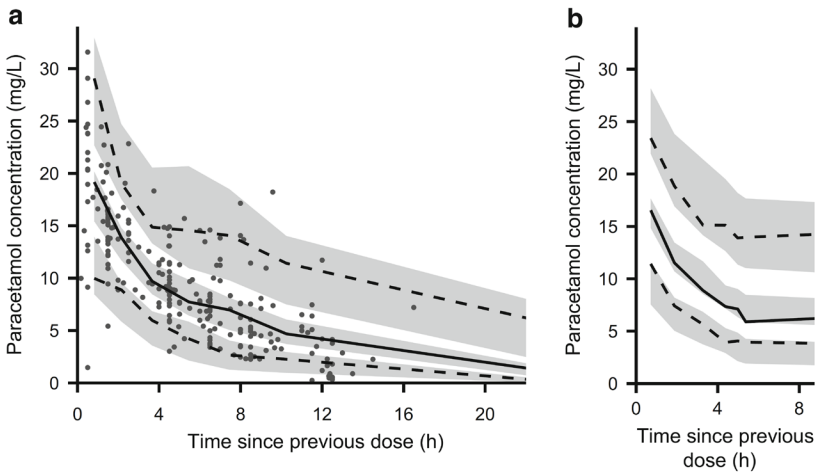

Fig. 4 Visual predictive checks of the final covariate model for **a** the model-building dataset and **b** the external evaluation dataset. The *solid black lines* depict the observed 50th percentiles, and the *dashed black lines* depict the observed 5th and 95th percentiles. The *shaded gray regions* depict the 95 % confidence intervals surrounding the predicted 5th, 50th, and 95th percentiles. Individual observations are depicted as *gray dots*. Individual observations were omitted from **b** because the density of points would obscure the percentile lines and prediction intervals

Table 5 Key subject demographics from the external evaluation dataset

Characteristic	*N*	Mean	SD	CV	Median	Range
Current body weight (kg)	60	2.62	0.894	0.341	2.71	0.61–4.30
Gestational age (weeks)	60	35.6	4.34	0.122	37	24–41
Postnatal age (days)	60	6.08	6.85	1.126	3	1–27
Postmenstrual age (weeks)	60	36.5	3.89	0.106	37.4	26.4–42.0

CV coefficient of variation, *SD* standard deviation

Table 6 Predictive performance of the final covariate model when applied to the external dataset

	Concentration (mg/L)		Percentage of observed concentration	
	Median	95 % CI	Median	95 % CI
Prediction error	0.911	0.495–1.33	10.1	6.13–14.3
Absolute prediction error	2.22	2.07–2.35	25.3	23.1–28.1

CI confidence interval

neonatal studies ranged from 0.090–0.21 L/h/kg, depending in part on gestational, postmenstrual, or postconceptional age [6, 8, 22, 35, 36]. Previously reported volume of distribution estimates were slightly lower than those observed here, with values ranging from 0.56–0.76 L/kg [8, 35].

To compare the neonatal pharmacokinetic parameter estimates from the present study with adult values, estimates can be extrapolated to a standard 70 kg adult using allometric scaling. If allometric exponents of 0.75 and 1 are applied to the clearance and volume of distribution terms, respectively [37], this yields values of 4.51 L/h/70 kg for clearance and 74.9 L/70 kg for volume of distribution. These values are consistent with allometrically standardized neonatal estimates from prior studies of both intravenous [6, 22, 36] and enteral [13, 38] paracetamol. In neonates, paracetamol clearance values are approximately one-quarter to one-third of typical adult values [39], and the relatively low neonatal clearance can be attributed to incomplete maturation of hepatic drug metabolism pathways [14, 40–42].

Current body weight was the only covariate that met criteria for inclusion in the final model. Previous population pharmacokinetic studies found weight, as a correlate of body size, was the major covariate influencing intravenous paracetamol pharmacokinetics in neonates [6, 22, 36]. Postmenstrual age [6, 36], postconceptional age [22], and unconjugated bilirubin [6, 36] have also been shown to have minor effects on neonatal clearance of intravenous paracetamol but these characteristics were not identified as significant covariates in the present study. The current study was expected to have reasonably good power to detect an effect of postmenstrual age on clearance because

it had a good representation of extreme preterm, preterm, and full-term neonates (Table 1) and was obtained from subjects with a fairly wide range of postmenstrual ages (23.1–41.6 weeks). Given that prior studies in neonates have found only minor increases in paracetamol clearance with increasing postmenstrual or postconceptional age, the failure to identify postmenstrual age as a significant covariate was not surprising. Indeed, maturation of paracetamol clearance appears to be fairly slow up until a postmenstrual age of 40 weeks and then occurs more rapidly during the first year of life [42]; therefore, the ability of this study to detect any age-related covariate effects was likely limited by the fact that the postnatal age of most study subjects (66 %) did not exceed 7 days.

During forward covariate selection, total bilirubin was inversely correlated with clearance, which agrees with previous findings that high unconjugated bilirubin was associated with reduced clearance [6, 36]. Physiologically, these observations can be attributed to the fact that both paracetamol and bilirubin undergo substantial clearance via glucuronidation, and concentrations of paracetamol and unconjugated or total bilirubin are therefore expected to be correlated. Because the association between total bilirubin and paracetamol pharmacokinetic parameters was fairly weak, and these laboratory values were unavailable for 37 % of the study subjects, it was decided that omission of this covariate from the final model was preferable to the data imputation that would be required if the covariate was retained.

Perhaps the most comprehensive study to date on the pharmacokinetics of intravenous paracetamol in neonates is the pooled analysis performed by Allegaert et al. [6]. A subset of that pooled data was used to externally evaluate the final covariate model reported herein. This external dataset from the PARANEO trial was selected because the study design and subject demographics were relatively consistent with those of the study from which the model-building dataset was obtained. The final covariate model demonstrated acceptable bias and precision when applied to the external dataset (Table 6). The most substantial difference between model predictions and external data observations was an overestimation of variability, which was particularly evident in the NPDEs and numerical and visual predictive checks. This discrepancy could be attributable to differences in patient demographics, study design or execution, or analytical drug quantification. However, given the gestational age distributions from the two studies, larger variability might be expected in the model-building dataset, based on the higher proportion of extremely preterm subjects. Overall, the external evaluation indicated that the final covariate model performed adequately despite notable study differences in the proportion of extremely preterm neonates, postnatal age, racial composition, and geographic location.

One major strength of the present study was the inclusion of a large number of extremely preterm neonates. Additionally, the final covariate model was successfully evaluated against a dataset obtained from a similar, independent clinical trial—a validation procedure that is rarely performed in neonatal clinical research. This study demonstrated that the pharmacokinetics of intravenous paracetamol can be predicted using body weight in neonates ranging from extreme preterm to full-term gestational status. This finding reinforces previous work that supported the use of a simplified neonatal dosing regimen in which maturational changes in paracetamol pharmacokinetics could be accommodated using only equivalent per kilogram dosing, without requiring different doses or dosing intervals dependent on gestational or postmenstrual age [6]. The results of the present study suggest that extension of such a parsimonious dosing regimen to extremely preterm neonates may be valid; however, these findings should be interpreted with caution based on the limitations outlined below.

Although the number and proportion of extremely preterm neonates in this study was substantially higher than in previous reports, the sample size was still relatively small, as is often the case for neonatal trials. Additionally, BSV in the final covariate model remained fairly large, particularly for clearance (30.8 % CV), and it is possible that other unmeasured factors could be incorporated as covariates to further reduce the unexplained BSV. Another important limitation is related to hepatotoxicity, the principal safety concern that accompanies use of the drug. Paracetamol-induced hepatotoxicity is not associated with exposure to the parent drug *per se* but rather depends on the amount of exposure to a relatively minor toxic metabolite, *N*-acetyl-*p*-benzoquinone imine (NAPQI) [43]. In humans, cytochrome P450 (CYP) 2E1 is predominantly responsible for the conversion of paracetamol to NAPQI [43]. Hepatic expression of CYP2E1 increases during the neonatal period, approaching adult values by approximately 90 days postnatal age [44]. Additionally, glucuronidation accounts for the majority of paracetamol clearance in adults, but glucuronidation capacity is immature in neonates [14, 45]. Thus, maturational changes in hepatotoxicity risk may not be reflected in the pharmacokinetics of the parent drug, and the pharmacokinetics of paracetamol metabolites should be studied to address this safety concern more thoroughly. Finally, although this study provides critical information regarding the pharmacokinetics of intravenous paracetamol in neonates, it should be noted that pharmacodynamic data for paracetamol are still quite limited in this patient population [46]. Further studies are needed to determine appropriate pharmacodynamic targets, which may vary by indication (e.g. analgesia, antipyresis, or patent ductus arteriosus closure) [47, 48].

5 Conclusions

A one-compartment model successfully characterized the pharmacokinetics of intravenous paracetamol in preterm and term neonates. Clearance and volume of distribution increased with body weight, and weight was the principal predictor of intravenous paracetamol pharmacokinetics in extremely preterm to full-term neonates. An external evaluation supported the generalizability of the final covariate model to other similar patient populations.

Acknowledgments The authors would like to thank Syamala Mankala of the Division of Clinical Pharmacology at the Children's National Health System (Washington, DC, USA) for administrative support.

Compliance with Ethical Standards

Funding This work was supported by National Institutes of Health grants from the Eunice Kennedy Shriver National Institute of Child Health and Human Development (R01HD060543, to John N. van den Anker) and the National Center for Advancing Translational Sciences (UL1TR000075, to the Children's National Health System), and by a contract for analytical laboratory services from McNeil Consumer Healthcare (Division of McNEIL-PPC, Inc., Fort Washington, PA, USA, to Diana G. Wilkins). Karel Allegaert was supported by a Fundamental Clinical Investigatorship (1800214N) from the Fund for Scientific Research—Flanders (FWO-Vlaanderen, Belgium). Sarah F. Cook received stipend support from the Howard Hughes Medical Institute (Med into Grad Initiative); Sarah F. Cook and Chris Stockmann were supported by pre-doctoral fellowships from the American Foundation for Pharmaceutical Education; and Jessica K. Roberts was supported by a Pharmacotherapy Subspecialty Award from the Primary Children's Hospital Foundation (Salt Lake City, UT, USA).

Conflicts of interest Sarah Cook, Jessica Roberts, Samira Samiee-Zafarghandy, Chris Stockmann, Amber King, Nina Deutsch, Elaine Williams, Karel Allegaert, Diana Wilkins, Catherine Sherwin, and John van den Anker have no potential conflicts of interest to declare.

Ethical approval All human studies were approved by the appropriate Ethics Committees and were carried out in concordance with ICH Guidelines for Good Clinical Practice [19]. Informed consent was obtained prior to study inclusion.

References

1. Hall RW, Anand KJ. Pain management in newborns. Clin Perinatol. 2014;41(4):895–924.
2. Allegaert K, Tibboel D, van den Anker J. Pharmacological treatment of neonatal pain: in search of a new equipoise. Semin Fetal Neonatal Med. 2013;18(1):42–7.
3. Pacifici GM, Allegaert K. Clinical pharmacology of paracetamol in neonates: a review. Curr Ther Res Clin Exp. 2015;77:24–30.
4. Duggan ST, Scott LJ. Intravenous paracetamol (acetaminophen). Drugs. 2009;69(1):101–13.
5. US FDA. Drug approval package: Ofirmev (acetaminophen) injection, 10 mg/mL. Available at: http://www.accessdata.fda.gov/drugsatfda_docs/nda/2010/022450_ofirmev_toc.cfm. Accessed 24 Mar 2015.
6. Allegaert K, Palmer GM, Anderson BJ. The pharmacokinetics of intravenous paracetamol in neonates: size matters most. Arch Dis Child. 2011;96(6):575–80.
7. Zuppa AF, Hammer GB, Barrett JS, Kenney BF, Kassir N, Mouksassi S, et al. Safety and population pharmacokinetic analysis of intravenous acetaminophen in neonates, infants, children, and adolescents with pain or fever. J Pediatr Pharmacol Ther. 2011;16(4):246–61.
8. van Ganzewinkel C, Derijks L, Anand KJ, van Lingen RA, Neef C, Kramer BW, et al. Multiple intravenous doses of paracetamol result in a predictable pharmacokinetic profile in very preterm infants. Acta Paediatr. 2014;103(6):612–7.
9. Allegaert K, Murat I, Anderson BJ. Not all intravenous paracetamol formulations are created equal. Paediatr Anaesth. 2007;17(8):811–2.
10. Bartocci M, Lundeberg S. Intravenous paracetamol: the 'Stockholm protocol' for postoperative analgesia of term and preterm neonates. Paediatr Anaesth. 2007;17(11):1120–1.
11. van den Anker JN, Tibboel D. Pain relief in neonates: when to use intravenous paracetamol. Arch Dis Child. 2011;96(6):573–4.
12. Kearns GL, Abdel-Rahman SM, Alander SW, Blowey DL, Leeder JS, Kauffman RE. Developmental pharmacology: drug disposition, action, and therapy in infants and children. N Engl J Med. 2003;349(12):1157–67.
13. Anderson BJ, van Lingen RA, Hansen TG, Lin YC, Holford NH. Acetaminophen developmental pharmacokinetics in premature neonates and infants: a pooled population analysis. Anesthesiology. 2002;96(6):1336–45.
14. Allegaert K, Vanhaesebrouck S, Verbesselt R, van den Anker JN. In vivo glucuronidation activity of drugs in neonates: extensive interindividual variability despite their young age. Ther Drug Monit. 2009;31(4):411–5.
15. De Cock RF, Piana C, Krekels EH, Danhof M, Allegaert K, Knibbe CA. The role of population PK-PD modelling in paediatric clinical research. Eur J Clin Pharmacol. 2011;67(Suppl 1):5–16.
16. Knibbe CA, Danhof M. Individualized dosing regimens in children based on population PKPD modelling: are we ready for it? Int J Pharm. 2011;415(1–2):9–14.
17. Tod M, Jullien V, Pons G. Facilitation of drug evaluation in children by population methods and modelling. Clin Pharmacokinet. 2008;47(4):231–43.
18. Krekels EH, van Hasselt JG, Tibboel D, Danhof M, Knibbe CA. Systematic evaluation of the descriptive and predictive performance of paediatric morphine population models. Pharm Res. 2011;28(4):797–811.
19. The International Conference on Harmonisation of Technical Requirements for Registration of Pharmaceuticals for Human Use (ICH). Available at: http://www.ich.org/. Accessed 15 Apr 2015.
20. van den Anker J. Metabolism and toxicity of acetaminophen. Available at: https://clinicaltrials.gov/show/NCT01328808. Acce ssed 1 Mar 2015.
21. Universitaire Ziekenhuizen Leuven. Pharmacokinetics, -dynamics and safety of intravenous paracetamol in neonates (PARANEO). Available at: https://clinicaltrials.gov/show/NCT00969176. Accessed 1 Mar 2015.
22. Allegaert K, Anderson BJ, Naulaers G, de Hoon J, Verbesselt R, Debeer A, et al. Intravenous paracetamol (propacetamol) pharmacokinetics in term and preterm neonates. Eur J Clin Pharmacol. 2004;60(3):191–7.
23. Bonate PL. Pharmacokinetic-pharmacodynamic modeling and simulation. New York: Springer Science+Business Media, Inc.; 2006.
24. Ludden TM, Beal SL, Sheiner LB. Comparison of the akaike information criterion, the Schwarz criterion and the *F* test as

guides to model selection. J Pharmacokinet Biopharm. 1994;22 (5):431–45.
25. Mould DR, Upton RN. Basic concepts in population modeling, simulation, and model-based drug development—part 2: introduction to pharmacokinetic modeling methods. CPT Pharmacomet Syst Pharmacol. 2013;2(4):e38.
26. Schwartz GJ, Munoz A, Schneider MF, Mak RH, Kaskel F, Warady BA, et al. New equations to estimate GFR in children with CKD. J Am Soc Nephrol. 2009;20(3):629–37.
27. McLeay SC, Morrish GA, Kirkpatrick CM, Green B. The relationship between drug clearance and body size: systematic review and meta-analysis of the literature published from 2000 to 2007. Clin Pharmacokinet. 2012;51(5):319–30.
28. Owen JS, Fiedler-Kelly J. Introduction to population pharmacokinetic/pharmacodynamic analysis with nonlinear mixed effects models. London: Wiley; 2014.
29. Ette EI. Stability and performance of a population pharmacokinetic model. J Clin Pharmacol. 1997;37(6):486–95.
30. Brendel K, Comets E, Laffont C, Mentre F. Evaluation of different tests based on observations for external model evaluation of population analyses. J Pharmacokinet Pharmacodyn. 2010;37 (1):49–65.
31. Karlsson MO, Savic RM. Diagnosing model diagnostics. Clin Pharmacol Ther. 2007;82(1):17–20.
32. Keizer RJ, Karlsson MO, Hooker A. Modeling and simulation workbench for NONMEM: tutorial on Pirana, PsN, and Xpose. CPT Pharmacometrics Syst Pharmacol. 2013;2:e50.
33. Bergstrand M, Hooker AC, Wallin JE, Karlsson MO. Prediction-corrected visual predictive checks for diagnosing nonlinear mixed-effects models. AAPS J. 2011;13(2):143–51.
34. Sheiner LB, Beal SL. Some suggestions for measuring predictive performance. J Pharmacokinet Biopharm. 1981;9(4):503–12.
35. Allegaert K, Van der Marel CD, Debeer A, Pluim MA, Van Lingen RA, Vanhole C, et al. Pharmacokinetics of single dose intravenous propacetamol in neonates: effect of gestational age. Arch Dis Childhood Fetal Neonatal Ed. 2004;89(1):F25–8.
36. Palmer GM, Atkins M, Anderson BJ, Smith KR, Culnane TJ, McNally CM, et al. I.V. acetaminophen pharmacokinetics in neonates after multiple doses. Br J Anaesth. 2008;101(4):523–30.
37. Anderson BJ, Holford NH. Mechanism-based concepts of size and maturity in pharmacokinetics. Ann Rev Pharmacol Toxicol. 2008;48:303–32.
38. Anderson BJ, Woollard GA, Holford NH. A model for size and age changes in the pharmacokinetics of paracetamol in neonates, infants and children. Br J Clin Pharmacol. 2000;50(2):125–34.
39. Allegaert K, Olkkola KT, Owens KH, Van de Velde M, de Maat MM, Anderson BJ. Covariates of intravenous paracetamol pharmacokinetics in adults. BMC Anesthesiol. 2014;14:77.
40. Levy G, Khanna NN, Soda DM, Tsuzuki O, Stern L. Pharmacokinetics of acetaminophen in the human neonate: formation of acetaminophen glucuronide and sulfate in relation to plasma bilirubin concentration and D-glucaric acid excretion. Pediatrics. 1975;55(6):818–25.
41. Miller RP, Roberts RJ, Fischer LJ. Acetaminophen elimination kinetics in neonates, children, and adults. Clin Pharmacol Ther. 1976;19(3):284–94.
42. Anderson BJ, Holford NH. Mechanistic basis of using body size and maturation to predict clearance in humans. Drug Metab Pharmacokinet. 2009;24(1):25–36.
43. McGill MR, Jaeschke H. Metabolism and disposition of acetaminophen: recent advances in relation to hepatotoxicity and diagnosis. Pharm Res. 2013;30(9):2174–87.
44. Johnsrud EK, Koukouritaki SB, Divakaran K, Brunengraber LL, Hines RN, McCarver DG. Human hepatic CYP2E1 expression during development. J Pharmacol Exp Ther. 2003;307(1):402–7.
45. Krekels EH, Danhof M, Tibboel D, Knibbe CA. Ontogeny of hepatic glucuronidation; methods and results. Curr Drug Metab. 2012;13(6):728–43.
46. Allegaert K, Naulaers G, Vanhaesebrouck S, Anderson BJ. The paracetamol concentration-effect relation in neonates. Paediatr Anaesth. 2013;23(1):45–50.
47. Gibb IA, Anderson BJ. Paracetamol (acetaminophen) pharmacodynamics: interpreting the plasma concentration. Arch Dis Child. 2008;93(3):241–7.
48. Ohlsson A, Shah PS. Paracetamol (acetaminophen) for patent ductus arteriosus in preterm or low-birth-weight infants. Cochrane Database Syst Rev. 2015;3:CD010061.

CHAPTER 4

DEVELOPMENT OF A PARENT–METABOLITE POPULATION PHARMACOKINETIC MODEL FOR INTRAVENOUS PARACETAMOL (ACETAMINOPHEN) IN PRETERM AND TERM NEONATES

Abstract

This study aimed to model the population pharmacokinetics of intravenous paracetamol and its major metabolites in neonates and to identify influential patient characteristics, especially those affecting the formation clearance ($CL_{formation}$) of oxidative pathway metabolites. Neonates with a clinical indication for intravenous analgesia received five 15 mg/kg doses of paracetamol at 12-h intervals (<28 weeks' gestation) or seven 15 mg/kg doses at 8-h intervals (≥28 weeks' gestation). Plasma and urine were sampled throughout the 72-h study period. Concentration–time data for paracetamol, paracetamol-glucuronide, paracetamol-sulfate, and the combined oxidative pathway metabolites (paracetamol-cysteine and paracetamol-*N*-acetylcysteine) were simultaneously modeled in NONMEM 7.2. The model incorporated 259 plasma and 350 urine samples from 35 neonates with mean gestational age of 33.6 weeks (standard deviation 6.6). $CL_{formation}$ for all metabolites increased with weight; $CL_{formation}$ for glucuronidation and oxidation also increased with postnatal age. At the mean weight (2.3 kg) and postnatal age (7.5 days), $CL_{formation}$ estimates (bootstrap 95% confidence interval; between-subject variability) were 0.049 L/h (0.038–0.062; 62%) for glucuronidation, 0.21 L/h (0.17–0.24; 33%) for sulfation, and 0.058 L/h (0.044–0.078; 72%) for oxidation. Expression of individual oxidation $CL_{formation}$ as a fraction of total individual paracetamol clearance showed that, on average, fractional oxidation $CL_{formation}$ increased <15% when plotted against weight or postnatal age. The parent–metabolite model successfully characterized the pharmacokinetics of intravenous paracetamol and its metabolites in neonates. Maturational changes in the fraction of paracetamol undergoing oxidation were small relative to between-subject variability.

Introduction

Paracetamol (*N*-acetyl-*p*-aminophenol, acetaminophen) is commonly used to manage mild to moderate pain in neonates [1, 2]. Intravenous formulations of the drug have only become available recently but have rapidly been adopted into clinical practice for applications in which enteral delivery is unsuitable, such as postoperative analgesia [3]. Several neonatal studies have characterized the pharmacokinetics of intravenous paracetamol [4-7].

Paracetamol primarily undergoes hepatic elimination, so markers of hepatic maturation and function are critical for explaining between-subject variability in paracetamol pharmacokinetics [4-6, 8, 9]. Metabolism also plays a key role in paracetamol-induced hepatotoxicity, which is a principal safety concern associated with use of the drug [10, 11]. The nontoxic products of glucuronidation and sulfation are efficiently excreted in urine, but paracetamol also undergoes oxidation by cytochrome P450 (CYP) enzymes, predominantly CYP2E1, to form the reactive intermediate *N*-acetyl-*p*-benzoquinone imine (NAPQI). This electrophile can be detoxified by conjugation with glutathione, and rapid, subsequent metabolism of paracetamol-glutathione produces paracetamol-cysteine and paracetamol-*N*-acetylcysteine. However, sufficiently high doses of paracetamol will saturate the glutathione detoxification pathway. Excess NAPQI binds covalently to hepatic proteins, and toxicity is thought to result from a combination of the inactivation of critical hepatic proteins and oxidative stress [12, 13].

Susceptibility to paracetamol-induced hepatotoxicity is likely influenced by maturational changes in the metabolic pathways described above. Previous studies have

shown that body weight is the principal predictor of intravenous paracetamol pharmacokinetics in extremely preterm to full-term neonates [4, 7]. These findings support implementation of a parsimonious neonatal dosing regimen based solely on equivalent per-kilogram dosing, without a requirement for different doses or dosing intervals dependent upon gestational or postmenstrual age [4]; however, these studies only utilized pharmacokinetic data for parent drug, which may not reflect maturational differences in the pharmacokinetics of hepatotoxicity-associated metabolites. Unfortunately, neonatal pharmacokinetic data for paracetamol metabolites remain scarce across all routes of administration, and previous studies that have incorporated metabolite data focused only on glucuronide and sulfate conjugates [6, 14-18].

The aim of this study was to develop a parent–metabolite population pharmacokinetic model for intravenous paracetamol in neonates to (i) estimate pharmacokinetic parameters for all major metabolic pathways of paracetamol, (ii) quantify between-subject variability in metabolite pharmacokinetics, and (iii) identify patient characteristics (covariates) that influence metabolite pharmacokinetic parameters, with a particular focus on formation clearance of the oxidative pathway metabolites (paracetamol-cysteine and paracetamol-*N*-acetylcysteine).

Methods

Study design and population

This was a prospective, single-center, open-label study of the pharmacokinetics of intravenous paracetamol in neonates. The study was approved by the Institutional Review Board at Children's National Health System (Washington, DC) and was conducted in

accordance with good clinical practice. Written informed consent was obtained from a parent or legal guardian prior to study inclusion. The study was registered at ClinicalTrials.gov (NCT01328808).

Patients <28 days' postnatal age with an indwelling arterial line and a clinical indication for intravenous analgesia who were admitted to intensive care units at Children's National Health System were considered for inclusion. Exclusion criteria were severe asphyxia, grade III or IV intraventricular hemorrhage, major congenital malformations, neurological disorders, receipt of neuromuscular blockers, and hepatic or renal failure, including systemic hypoperfusion. Intravenous paracetamol (Ofirmev, 10 mg/mL, Mallinckrodt Pharmaceuticals, Dublin, Ireland) was administered by 30-min infusions at 15 mg/kg/dose. Neonates <28 weeks' gestation received 5 doses at 12-h intervals; neonates ≥28 weeks' gestation received 7 doses at 8-h intervals.

Sampling procedure and analytical methods

Blood samples (0.2 mL) were obtained from arterial lines at approximately 0, 1, 2, 4, 6, 8, 12, and 24 h after the first and final paracetamol doses. Patients were randomly assigned to one of two blood sampling schedules, each consisting of 9–10 collection times. Blood was collected in sodium heparin Vacutainer tubes (BD, Franklin Lakes, NJ) and centrifuged for 10–15 min at 1500 x *g* at 4°C. Plasma was transferred to cryovials and stored at −70°C. Urine samples were collected via indwelling catheter (postoperative patients) or from gel-free study diapers (procedural patients; Cuddle Buns Preemie diapers, Small Beginnings Inc., Hesperia, CA) at 3-4-h intervals over the 24 h following the first and final paracetamol doses. Urine sample volumes were recorded, and 3-5-mL

aliquots were reserved and stored at −70°C. Study samples were shipped on dry ice to the Center for Human Toxicology at the University of Utah and stored at −80°C prior to analysis.

Plasma and urinary concentrations of paracetamol, paracetamol-glucuronide, paracetamol-sulfate, paracetamol-cysteine, and paracetamol-*N*-acetylcysteine were determined by high-performance liquid chromatography–electrospray ionization–tandem mass spectrometry according to the methods reported in Chapter 2. Mean intra- and inter-assay accuracy ranged from 85–111%, and intra- and inter-assay imprecision did not exceed 15% coefficient of variation (CV). In plasma, the lower limit of quantification (LLOQ) was 0.05 mg/L for paracetamol, paracetamol-glucuronide, and paracetamol-sulfate, and 0.01 mg/L for paracetamol-cysteine and paracetamol-*N*-acetylcysteine. In urine, the LLOQ was 0.2 mg/L for paracetamol, 1 mg/L for paracetamol-glucuronide and paracetamol-sulfate, and 0.1 mg/L for paracetamol-cysteine and paracetamol-*N*-acetylcysteine.

Base model development

All concentrations were expressed in paracetamol equivalents (mg/L) via conversion based on molecular weights. Following conversion to paracetamol equivalents, paracetamol-cysteine and paracetamol-*N*-acetylcysteine concentrations for each sample were summed to approximate the total concentration of metabolites derived from CYP-mediated oxidation. The parent–metabolite pharmacokinetic model was developed using NONMEM 7.2 (nonlinear mixed effects modeling, ICON Development Solutions, Hanover, MD) interfaced with PsN 4.4.0 (Perl-speaks-NONMEM,

psn.sourceforge.net) and Pirana 2.9.0 (pirana-software.com). Urinary concentrations and urine sample volumes were included as NONMEM data items so that the software program could scale appropriately to urinary amounts [19]. Population parameters were estimated using the first-order conditional estimation with interaction method and the ADVAN6 subroutine. The number of significant digits required for convergence (NSIG), predicted values (TOL), and the objective function (SIGL) was set, respectively, to 2, 6, and 6 [20]. Processing and visualization of NONMEM output were performed in R 3.2.1 (CRAN.R-project.org). Throughout model development, standard diagnostic plots were generated to evaluate model fit, including observations versus population predictions, observations versus individual predictions, conditional weighted residuals versus time, and conditional weighted residuals versus population predictions. During covariate analysis, nested models were compared using the objective function value (OFV). At all other stages of development, model discrimination was based on the Akaike Information Criterion (AIC) [21].

A schematic representation of the base structure for the parent–metabolite pharmacokinetic model is shown in Figure 4.1. The structural model incorporated the rate and duration of the intravenous paracetamol infusion. Paracetamol, paracetamol-glucuronide, paracetamol-sulfate, and the combined oxidative pathway metabolites (paracetamol-cysteine and paracetamol-*N*-acetylcysteine) were each modeled with a single plasma compartment and subsequent urinary compartment. Similar structural models have been employed to describe the pharmacokinetics of intravenous paracetamol and its metabolites in adult surgical patients [22] and in women during the peripartum period [23]. One-compartment distribution of paracetamol was considered appropriate

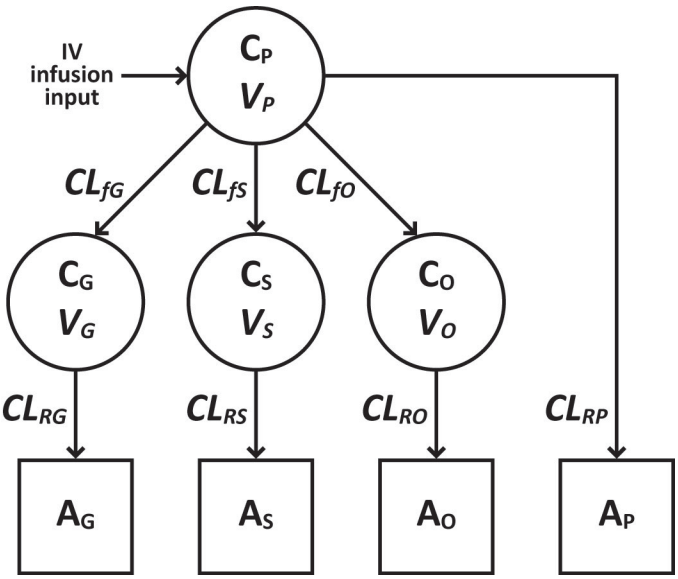

Figure 4.1 Schematic representation of the structural pharmacokinetic model for paracetamol and its metabolites in plasma (circles) and urine (squares). Abbreviations: C_P, C_G, C_S, and C_O represent, respectively, plasma concentrations of paracetamol, paracetamol-glucuronide, paracetamol-sulfate, and the combined oxidative pathway metabolites (paracetamol-cysteine and paracetamol-*N*-acetylcysteine); A_P, A_G, A_S, and A_O represent, respectively, urinary amounts of unchanged paracetamol, paracetamol-glucuronide, paracetamol-sulfate, and the oxidative pathway metabolites; V_P, V_G, V_S, and V_O represent, respectively, volumes of distribution for paracetamol, paracetamol-glucuronide, paracetamol-sulfate, and the oxidative pathway metabolites; CL_{fG}, CL_{fS}, and CL_{fO} represent, respectively, formation (hepatic) clearances for paracetamol-glucuronide, paracetamol-sulfate, and the oxidative pathway metabolites; CL_{RP}, CL_{RG}, CL_{RS}, and CL_{RO} represent, respectively, renal clearances for unchanged paracetamol, paracetamol-glucuronide, paracetamol-sulfate, and the oxidative pathway metabolites. All formation and renal clearances were modeled as first-order processes.

based on previous work with parent drug data from the same dataset [7]. The model structure required the assumption that the pathways illustrated in Figure 4.1 account for all elimination of paracetamol and its metabolites. All formation (hepatic) and renal clearances were modeled as first-order processes. Reith et al. modeled the Michaelis-Menten kinetics of paracetamol glucuronidation, sulfation, and oxidation in healthy adults undergoing third molar dental extraction and found evidence of slight saturation occurring for sulfation and oxidation at a dose of 90 mg/kg [24]; thus, an assumption of first-order kinetics does not seem unreasonable given the doses administered in the present study. In total, the model was defined by 8 differential equations and 11 pharmacokinetic parameters.

Random effects were classified as between-subject variability (BSV) or residual unexplained variability (RUV). Individual pharmacokinetic parameters were assumed to be log-normally distributed, and BSV was modeled exponentially (Equation 4.1):

$$P_i = \theta_{pop} \times e^{\eta_i} \tag{4.1}$$

where P_i is the individual pharmacokinetic parameter, θ_{pop} is the population mean for P, η_i is the between-subject random effect on P for individual i, and η_i is normally distributed with a mean of 0 and a variance of ω^2. Additive, proportional, and combined additive and proportional functions were tested for incorporation of RUV [25].

Covariate analysis

Potential covariates included current body weight, postnatal age, postmenstrual age, indication (postoperative or procedural), sex, race (Caucasian or African American), ethnicity, occasion (first or second), urine flow rate, and estimated glomerular filtration rate (GFR). The first and second occasions were defined, respectively, as ≤ and >42 h after the first paracetamol dose. Average flow rate for each urine sample was calculated by dividing the sample volume (mL) by the time elapsed during sample collection (h). Estimated GFR was calculated from body length and serum creatinine (modified kinetic Jaffe method) using the updated Schwartz formula [26]. Laboratory samples were obtained within 24 h prior to the first paracetamol dose or during the pharmacokinetic sample collection period. Serum creatinine concentrations obtained at ≤3 days' postnatal age were considered to reflect maternal renal function and were excluded from analysis. During covariate analysis, subjects with missing information for a covariate undergoing evaluation were excluded from both the base and covariate models being tested.

Due to the large number of potential covariate–pharmacokinetic parameter combinations, only the most physiologically relevant covariate–parameter pairs were considered. Categorical covariates were considered for inclusion using proportional shift models (Equation 4.2):

$$P_i = \left(\theta_{pop} + \theta_{pop} \times \theta_{cov} \times COV_i\right) \times e^{\eta_i} \quad (4.2)$$

where P_i is the individual pharmacokinetic parameter, θ_{pop} is the population mean for P when the categorical indicator variable COV_i is 0, θ_{cov} is the proportional change in θ_{pop}

when COV_i is 1, and η_i is the between-subject random effect on P for individual i.

Current body weight, postnatal age, postmenstrual age, indication, and sex were tested on all pharmacokinetic parameters. For these covariates, continuous variables were normalized to population mean values and tested for inclusion in a power function (Equation 4.3):

$$P_i = \theta_{pop} \times \left(\frac{COV_i}{COV_{mean}}\right)^{\theta_{cov}} \times e^{\eta_i} \quad (4.3)$$

where P_i is the individual pharmacokinetic parameter for an individual with covariate value COV_i, θ_{pop} is the population mean for P when COV_i equals the mean covariate value COV_{mean}, θ_{cov} is the covariate effect, and η_i is the between-subject random effect on P for individual i. Given the potential for genetically mediated differences in paracetamol metabolism [27, 28], race and ethnicity were tested on all metabolite formation clearances (Equation 4.2). Additionally, occasion was tested on all metabolite formation clearances (Equation 4.2) because previous work has suggested that upregulation of paracetamol glucuronidation occurs with repeated administration in adults [29, 30] and in neonates [17, 31]. Finally, urine flow rate and estimated GFR were tested on all renal clearances. Based on a previous pharmacokinetic model of paracetamol, paracetamol-glucuronide, and paracetamol-sulfate in infants, an exponential function was used for incorporation of urine flow rate [32] (Equation 4.4):

$$P_{ij} = \theta_{pop} \times e^{\theta_{cov} \times (UFLOW_{ij} - UFLOW_{med})} \times e^{\eta_i} \quad (4.4)$$

where P_{ij} is the pharmacokinetic parameter for individual i at time j with urine flow rate $UFLOW_{ij}$, θ_{pop} is the population mean for P when $UFLOW_{ij}$ equals the median urine flow rate $UFLOW_{med}$ (6.5 mL/h), θ_{cov} is the covariate effect, and η_i is the between-subject random effect on P for individual i. Estimated GFR was tested in a mean-centered power function (Equation 4.3).

Potential covariates were tested using a modified stepwise forward selection procedure followed by stepwise backward elimination. Changes in OFV were considered significant at $p < 0.05$ (χ^2 distribution, 1 degree of freedom, ΔOFV > 3.84) during forward selection and $p < 0.01$ (ΔOFV > 6.63) during backward elimination [33]. Additionally, covariates were required to provide at least 5% reduction in BSV or RUV in order to be added to or retained in the model. The modified forward selection was conducted in a series of rounds. In round 1, weight was tested on all pharmacokinetic parameters and subsequently included on all parameters for which selection criteria were met. In round 2, the remaining covariate–parameter pairs of interest were tested. Round 3 consisted of standard stepwise forward selection using only those covariate–parameter pairs that met selection criteria in round 2. Rounds 2 and 3 were repeated until none of the remaining covariate–parameter pairs met the selection criteria, at which point standard stepwise backward elimination was performed.

Model refinement

Following covariate analysis, the model was refined by testing the validity of the default assumption that random effects exhibit no covariance. The extent of covariance in BSV terms was assessed by estimating off-diagonal elements of the Ω matrix. Covariance

in RUV terms was evaluated by estimating off-diagonal elements of the Σ matrix, which required utilization of the NONMEM L2 data item for designation of multivariate observations [19]. Finally, all covariates included in the model were tested by backward elimination to ensure that covariate criteria were still met after model refinement.

Model evaluation

A nonparametric bootstrap was performed to assess the stability of the final model and to quantify uncertainty in parameter estimates [34]. Bootstrap datasets (n = 200) were generated in PsN by random sampling with replacement from the original dataset. Additionally, normalized prediction distribution errors (NPDE) based on 1000 simulations were calculated in NONMEM, and plots were generated for NPDE distributions and for NPDE versus time, population predictions, and influential covariates [35].

Results

Patients and pharmacokinetic observations

Demographic characteristics of the 35 study subjects are summarized in Table 4.1. Most patients (66%) received the first paracetamol dose within 1 week after birth. Concentrations of paracetamol, paracetamol-glucuronide, paracetamol-sulfate, and oxidative pathway metabolites were available from 266 plasma samples and 352 urine samples. Six plasma samples (2%) had implausible drug concentrations (e.g., peak concentrations observed at trough collection times) and were excluded from analysis. One additional plasma sample (<1%) and 2 urine samples (<1%) were excluded because

Table 4.1 Demographic characteristics of neonates who received intravenous paracetamol.

Characteristic	*n* (%)	Mean ± SD (range)
Gestational age (weeks)	35 (100)	33.6 ± 6.57 (23–41)
Postnatal age[a] (days)	35 (100)	7.49 ± 5.73 (1–26)
Postmenstrual age[a] (weeks)	35 (100)	34.6 ± 6.28 (23.1–41.6)
Current body weight[a] (kg)	35 (100)	2.30 ± 1.22 (0.46–4.20)
Current body length[a] (cm)	34 (97)	43.4 ± 9.15 (25.0–56.0)
Current body weight[a] (kg) by gestational age		
Extreme preterm, <28 weeks' GA	10 (29)	0.81 ± 0.27 (0.55–1.30)
Preterm, <37 weeks' GA (includes <28 weeks' GA)	17 (49)	1.22 ± 0.76 (0.46–2.80)
Full-term, 37–42 weeks' GA	18 (51)	3.32 ± 0.39 (2.70–4.20)
Serum creatinine[b] (mg/dL)	30 (86)	0.707 ± 0.242 (0.3–1.1)
Estimated GFR[c] (mL/min/1.73 m^2)	29 (83)	30.1 ± 16.6 (12.6–70.9)
Primary indication for intravenous paracetamol		
Postoperative analgesia (cardiac surgery)	19 (54)	-
Procedural analgesia	16 (46)	-
Sex		
Male	20 (57)	-
Female	15 (43)	-
Race		
Caucasian	16 (46)	-
African American	14 (40)	-
American Indian/Alaska Native	1 (3)	-
Asian	1 (3)	-
Declined to respond	3 (9)	-
Ethnicity		
Non-Hispanic	24 (69)	-
Hispanic	8 (23)	-
Declined to respond	3 (9)	-

[a] On the day of the first paracetamol dose.

[b] Serum creatinine concentrations obtained at ≤3 days' postnatal age were considered to reflect maternal renal function and were excluded from analysis.

[c] Estimated GFR was calculated using the updated Schwartz formula [26].

GA, gestational age; GFR, glomerular filtration rate; SD, standard deviation.

all analytes were <LLOQ. Three plasma samples (1%) had paracetamol-*N*-acetylcysteine concentrations <LLOQ, and 2 urine samples (<1%) had one analyte <LLOQ (paracetamol or paracetamol-glucuronide); values of LLOQ÷2 were used in these instances [36]. Thus, 259 plasma samples (median: 8; range: 3–11 samples/patient) and 350 urine samples (median: 11; range: 2–16 samples/patient) were used to develop the population pharmacokinetic model. These samples provided a total of 1036 plasma concentrations and 1400 urinary concentrations. Figure 4.2 shows observed paracetamol and metabolite plasma concentrations over time following the first and final paracetamol doses.

Population pharmacokinetic model development

When additive, proportional, and combined additive and proportional error functions were tested for characterization of RUV, the combined function provided the lowest AIC and was selected for inclusion in the model.

Based on covariate selection criteria, weight was incorporated into the final model on all pharmacokinetic parameters, postnatal age was included on formation clearances of paracetamol-glucuronide and oxidative pathway metabolites, urine flow rate was included on all renal clearances, and indication was included on renal clearance of unchanged paracetamol. Final estimates for covariate effects are provided in Table 4.2, along with estimates for pharmacokinetic parameters, BSV, and RUV. Current body weight had a strong influence on all pharmacokinetic parameters. When weight was included on each parameter during round 1 of the modified forward selection process, decreases in OFV ranged from 11.5–86.4 and reductions in BSV ranged from 13–74%

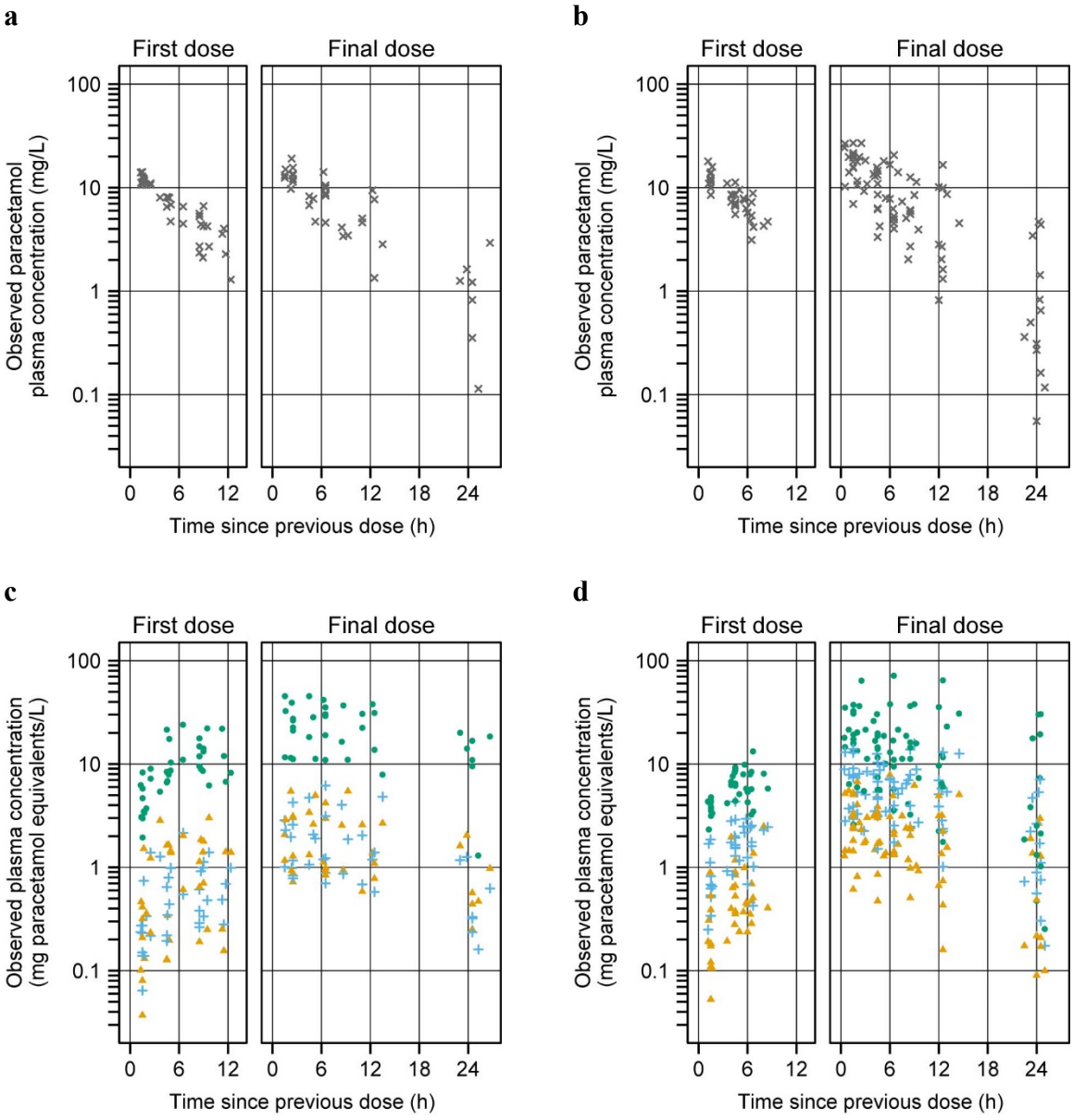

Figure 4.2 Observed plasma concentrations versus time for neonates who received 5 doses at 12-h intervals (**a** and **c**, 15 mg/kg/dose) and for neonates who received 7 doses at 8-h intervals (**b** and **d**, 15 mg/kg/dose). **a** and **b** show paracetamol concentrations (gray *x* marks); **c** and **d** show concentrations of paracetamol-glucuronide (blue plus signs), paracetamol-sulfate (green circles), and the combined oxidative pathway metabolites (paracetamol-cysteine and paracetamol-*N*-acetylcysteine, orange triangles).

Table 4.2 Parameter estimates for the final model of paracetamol and its metabolites in neonates.

Parameter	Model fit		Bootstrap median (95% CI)[a]	
	Estimate[b]	**BSV (ω^2), as % CV**	**Estimate[b]**	**BSV (ω^2), as % CV**
CL_{fG} (L/h)	0.049	62	0.049 (0.038–0.062)	60 (45–77)
Effect of weight[c]	2.0	-	2.0 (1.7–2.5)	-
Effect of PNA[c]	0.37	-	0.40 (0.097–0.79)	-
CL_{fS} (L/h)	0.21	33	0.21 (0.17–0.24)	32 (24–39)
Effect of weight[c]	0.90	-	0.89 (0.71–1.1)	-
CL_{fO} (L/h)	0.058	72	0.056 (0.044–0.078)	69 (55–85)
Effect of weight[c]	1.7	-	1.8 (1.4–2.1)	-
Effect of PNA[c]	0.69	-	0.67 (0.25–1.0)	-
V_P (L)	2.7	11	2.7 (2.6–3.2)	12 (7.7–23)
Effect of weight[c]	0.90	-	0.90 (0.83–1.0)	-
V_G (L)	1.2	48	1.2 (0.91–1.4)	47 (30–65)
Effect of weight[c]	1.1	-	1.1 (0.73–1.3)	-
V_S (L)	0.98	36	0.97 (0.77–1.2)	36 (23–50)
Effect of weight[c]	1.2	-	1.2 (0.88–1.4)	-
V_O (L)	3.0	67	2.9 (2.1–4.6)	62 (23–110)
Effect of weight[c]	1.5	-	1.5 (1.3–1.9)	-
CL_{RP} (L/h)	0.016	30	0.016 (0.012–0.024)	30 (18–43)
Effect of weight[c]	0.64	-	0.62 (0.37–1.0)	-
Effect of urine flow rate[d]	0.060	-	0.059 (0.044–0.080)	-
Effect of postoperative indication[e]	−0.57	-	−0.57 (−0.76 – −0.34)	-

Table 4.2 (continued)

Parameter	Model fit		Bootstrap median (95% CI)[a]	
	Estimate[b]	**BSV (ω^2), as % CV**	**Estimate[b]**	**BSV (ω^2), as % CV**
CL_{RG} (L/h)	0.10	37	0.10 (0.079–0.12)	37 (21–47)
Effect of weight[c]	1.1	-	1.1 (0.76–1.3)	-
Effect of urine flow rate[d]	0.015	-	0.016 (0.0020–0.029)	-
CL_{RS} (L/h)	0.12	54	0.12 (0.085–0.14)	54 (38–70)
Effect of weight[c]	1.4	-	1.4 (0.99–1.7)	-
Effect of urine flow rate[d]	0.015	-	0.016 (0.0027–0.031)	-
CL_{RO} (L/h)	0.17	43	0.18 (0.14–0.21)	44 (26–62)
Effect of weight[c]	1.3	-	1.3 (1.1–1.6)	-
Effect of urine flow rate[d]	0.032	-	0.032 (0.015–0.042)	-
Proportional residual unexplained variability (σ^2), as % CV				
Plasma				
Paracetamol	27	-	26 (21–32)	-
Paracetamol-glucuronide	27	-	27 (23–33)	-
Paracetamol-sulfate	23	-	24 (17–30)	-
Oxidative pathway metabolites	35	-	34 (27–43)	-
Urine				
Paracetamol	49	-	49 (42–55)	-
Paracetamol-glucuronide	68	-	68 (59–76)	-
Paracetamol-sulfate	70	-	69 (60–77)	-
Oxidative pathway metabolites	61	-	62 (53–70)	-

Table 4.2 (continued)

Parameter	Model fit		Bootstrap median (95% CI)[a]	
	Estimate[b]	BSV (ω^2), as % CV	Estimate[b]	BSV (ω^2), as % CV
Additive residual unexplained variability (σ^2), as SD				
Plasma (mg/L)				
Paracetamol-sulfate	1.1	-	1.1 (0.028–2.0)	-
Urine (mg/L)				
Paracetamol	1.3	-	1.2 (0.029–1.8)	-
Paracetamol-sulfate	14	-	14 (0.16–35)	-

[a] Bootstrap success rate was 77% (n = 153 out of 200).

[b] Pharmacokinetic parameter estimates are typical values for patients with a procedural indication at the mean current body weight (2.3 kg), mean PNA (7.5 days), and median urine flow rate (6.5 mL/h).

[c] Exponent on mean-centered weight or mean-centered PNA, i.e., the covariate effect (θ_{cov}) in Equation 4.3.

[d] Coefficient on median-centered urine flow rate in the exponential covariate function, i.e., the covariate effect (θ_{cov}) in Equation 4.4.

[e] Proportional change in CL_{RP} for patients with a postoperative indication, i.e., the covariate effect (θ_{cov}) in Equation 4.2.

BSV, between-subject variability; CI, confidence interval; % CV, percent coefficient of variation; PNA, postnatal age; SD, standard deviation; CL_{fG}, CL_{fS}, and CL_{fO} represent, respectively, formation (hepatic) clearances for paracetamol-glucuronide, paracetamol-sulfate, and the oxidative pathway metabolites; V_P, V_G, V_S, and V_O represent, respectively, volumes of distribution for paracetamol, paracetamol-glucuronide, paracetamol-sulfate, and the oxidative pathway metabolites; CL_{RP}, CL_{RG}, CL_{RS}, and CL_{RO} represent, respectively, renal clearances for unchanged paracetamol, paracetamol-glucuronide, paracetamol-sulfate, and the oxidative pathway metabolites.

CV. Urine flow rate was also a highly significant covariate for all renal clearances. In the final model, removal of urine flow rate from each renal clearance produced increases in OFV ranging from 34.0–200.3. Effects of postnatal age and indication were more modest than those of weight and urine flow rate. When postnatal age and indication were excluded from the final model, increases in OFV ranged from 10.0–20.5 and increases in BSV ranged from 5–15% CV.

Incorporation of covariance estimates for all BSV terms (i.e., a full Ω matrix) improved the model fit compared to the default condition of no covariance (i.e., a diagonal Ω matrix). Utilization of a full-covariance structure ensured that critical covariance terms would be included, and any ill effects from unnecessary covariance terms were expected to be minimal [37].

Given the physiological basis for the parent–metabolite structural model, it was anticipated that covariance of some parameters would be strong. Correlations in BSV for renal metabolite clearances were particularly high, with correlation coefficients ranging from 0.73–0.97. Attempting to estimate a correlation near 1 tends to cause numerical instabilities and can hinder model convergence. To avoid such problems, correlations in BSV for renal metabolite clearances were fixed to 1 using a previously reported approach [38]. Renal clearance of paracetamol-glucuronide was described according to the usual exponential form (Equation 4.1). To fix the correlation between random effects for renal clearance of paracetamol-glucuronide and paracetamol-sulfate to 1, renal clearance of paracetamol-sulfate was described as follows (Equation 4.5):

$$CL_{RS,i} = \theta_{pop,CL_{RS}} \times e^{\left(\theta_{scale,CL_{RS}} \times \eta_{i,CL_{RG}}\right)} \quad (4.5)$$

where $CL_{RS,i}$ is the individual renal clearance of paracetamol-sulfate, $\theta_{pop,CLRS}$ is the population mean for renal clearance of paracetamol-sulfate, $\theta_{scale,CLRS}$ is a scale parameter between the variance of CL_{RG} and the variance of CL_{RS} (Equation 4.6), and $\eta_{i,CLRG}$ is the between-subject random effect on renal clearance of paracetamol-glucuronide for individual *i*. Variance for renal clearance of paracetamol-sulfate could then be determined as follows (Equation 4.6):

$$Var(CL_{RS}) = \theta^2_{scale,CL_{RS}} \times Var\left(\eta_{i,CL_{RG}}\right) \quad (4.6)$$

The same approach was used to fix the correlation between random effects for renal clearance of paracetamol-glucuronide and the oxidative pathway metabolites to 1. Model fit suffered slightly when these correlations were fixed, as indicated by a 13.7 increase in AIC. However, this worsening of model fit was considered acceptable in exchange for enhanced model stability and a considerable reduction in the number of model parameters (19 fewer parameters). Final estimates for correlation in BSV are provided in Table 4.3.

When covariance estimates on RUV terms from multivariate observations were incorporated into the model, the AIC decreased by 1520.4, indicating a substantial improvement in model fit compared to the default condition of no covariance. Once the covariance terms were included, most additive RUV variance estimates approached 0 and could be excluded from the model without compromising model fit. Additive RUV components were retained only for plasma paracetamol-sulfate, urinary paracetamol-sulfate, and urinary paracetamol because the model fit worsened significantly when those

Table 4.3 Correlation in between-subject variability for the final model of paracetamol and its metabolites in neonates.[a]

Parameter	CL_{fG}	CL_{fS}	CL_{fO}	V_P	V_G	V_S	V_O	CL_{RP}
CL_{fS}	0.37 (0.036–0.69)	-	-	-	-	-	-	-
CL_{fO}	0.49 (0.16–0.80)	0.054 (−0.33–0.54)	-	-	-	-	-	-
V_P	0.35 (−0.15–0.65)	−0.20 (−0.59–0.36)	0.18 (−0.38–0.67)	-	-	-	-	-
V_G	0.60 (0.14–0.83)	0.032 (−0.30–0.50)	0.42 (−0.0083–0.75)	0.43 (−0.50–0.75)	-	-	-	-
V_S	0.19 (−0.35–0.77)	0.64 (0.10–0.83)	−0.10 (−0.50–0.45)	0.28 (−0.51–0.57)	0.13 (−0.31–0.63)	-	-	-
V_O	−0.10 (−0.42–0.59)	−0.40 (−0.72–0.37)	0.44 (−0.24–0.75)	0.53 (−0.37–0.85)	0.15 (−0.14–0.57)	−0.14 (−0.47–0.44)	-	-
CL_{RP}	0.041 (−0.46–0.51)	−0.033 (−0.41–0.49)	−0.14 (−0.51–0.43)	0.20 (−0.44–0.72)	−0.036 (−0.59–0.42)	−0.0082 (−0.55–0.60)	−0.11 (−0.65–0.59)	-
CL_{RG}, CL_{RS}, CL_{RO}[b]	0.52 (0.29–0.73)	0.73 (0.35–0.91)	0.28 (−0.37–0.68)	0.22 (−0.25–0.57)	0.23 (−0.16–0.57)	0.46 (−0.065–0.71)	−0.30 (−0.72–0.55)	0.33 (−0.068–0.74)

[a] Data are presented as: correlation point estimate from the final model fit (bootstrap 95% confidence interval). Bootstrap success rate was 77% (n = 153 out of 200).

[b] Correlations in BSV for CL_{RG}, CL_{RS}, and CL_{RO} were observed to be high and were fixed to 1.

CL_{fG}, CL_{fS}, and CL_{fO} represent, respectively, formation (hepatic) clearances for paracetamol-glucuronide, paracetamol-sulfate, and the oxidative pathway metabolites; V_P, V_G, V_S, and V_O represent, respectively, volumes of distribution for paracetamol, paracetamol-glucuronide, paracetamol-sulfate, and the oxidative pathway metabolites; CL_{RP}, CL_{RG}, CL_{RS}, and CL_{RO} represent, respectively, renal clearances for unchanged paracetamol, paracetamol-glucuronide, paracetamol-sulfate, and the oxidative pathway metabolites.

terms were removed. The correlation between additive RUV for urinary paracetamol and paracetamol-sulfate was particularly high, with a correlation coefficient estimated at 1.0; therefore, this correlation was fixed to 1 using the approach shown in Equations 4.5 and 4.6 to stabilize the model. Final estimates for correlation in proportional RUV are provided in Table 4.4.

Model evaluation

Standard diagnostic plots of observations versus population predictions and observations versus individual predictions are provided in Figure 4.3 to illustrate the final model fit. Bootstrap summary statistics for pharmacokinetic parameters, covariate effects, BSV, and RUV are provided in Table 4.2 alongside corresponding point estimates. Median bootstrap estimates were very similar to point estimates from the final model fit, and bootstrap 95% confidence intervals demonstrated reasonably good precision for most parameters. Point estimates and bootstrap-derived 95% confidence intervals are provided in Tables 4.3 and 4.4 for correlations in BSV and RUV, respectively. Many BSV correlations were estimated with poor precision (Table 4.3); however, this was not unexpected given the use of a full Ω matrix. In contrast, correlations in RUV were generally estimated with greater precision than those for BSV, and none of the 95% confidence intervals crossed 0 (Table 4.4).

Out of 200 bootstrap runs, 153 (77%) minimized successfully, and all others failed due to rounding errors. Bootstrap summary statistics were derived only from successful runs; however, parameter estimates from successful and unsuccessful runs were largely in good agreement. For instance, when median bootstrap estimates from

Table 4.4 Correlation in proportional residual unexplained variability for the final model of paracetamol and its metabolites in neonates.[a]

	Plasma compartments			Urine compartments		
	Paracetamol	Paracetamol-glucuronide	Paracetamol-sulfate	Paracetamol	Paracetamol-glucuronide	Paracetamol-sulfate
Paracetamol-glucuronide	0.38 (0.19–0.54)	-	-	0.58 (0.43–0.72)	-	-
Paracetamol-sulfate	0.56 (0.31–0.72)	0.84 (0.55–0.98)	-	0.51 (0.37–0.72)	0.94 (0.92–0.98)	-
Oxidative pathway metabolites	0.29 (0.10–0.50)	0.57 (0.30–0.76)	0.59 (0.28–0.88)	0.55 (0.39–0.70)	0.90 (0.87–0.93)	0.92 (0.89–0.96)

[a] Data are presented as: correlation point estimate from the final model fit (bootstrap 95% confidence interval). Bootstrap success rate was 77% (n = 153 out of 200).

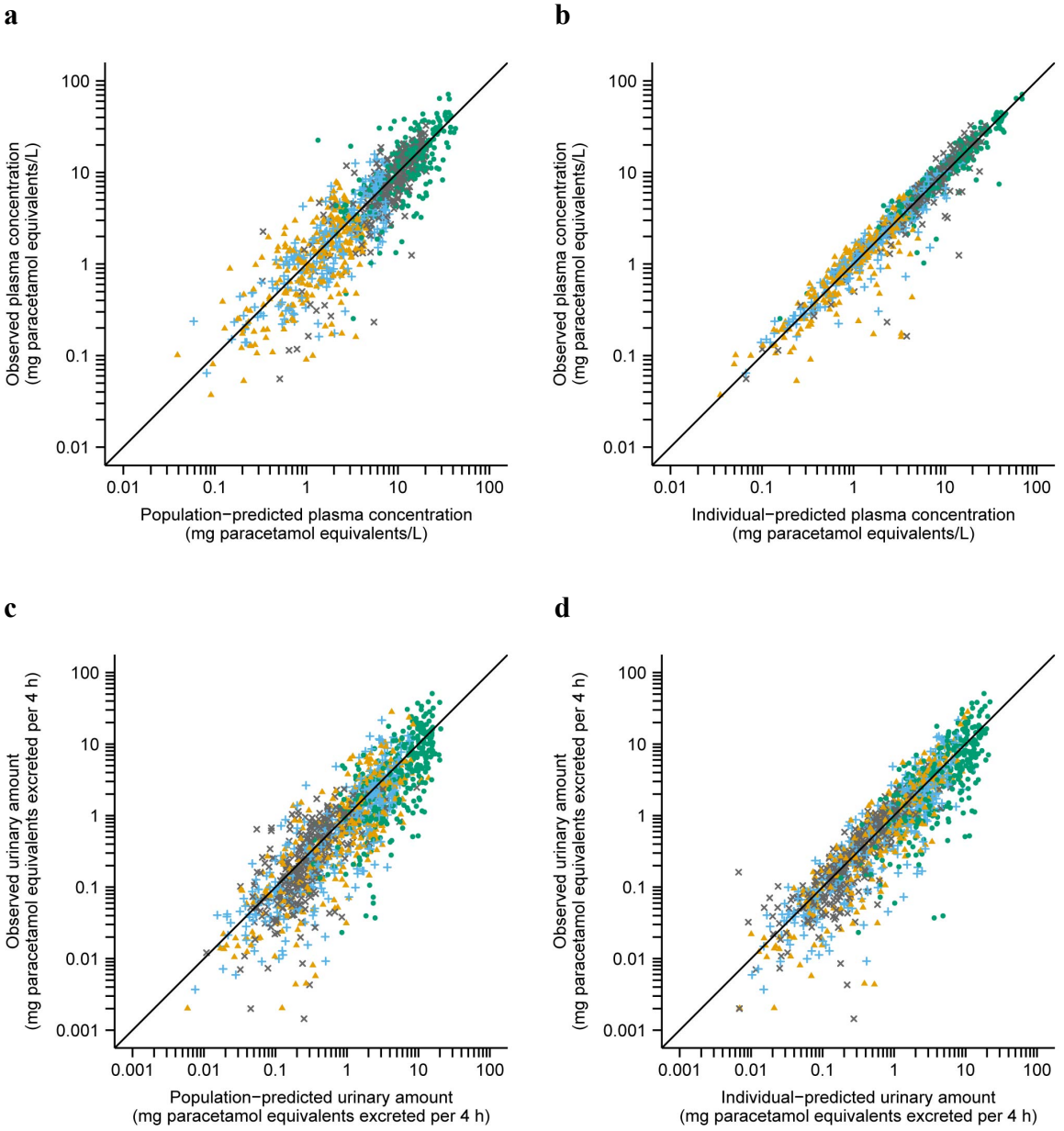

Figure 4.3 Diagnostic plots of observations versus predictions for the final model. Observed versus **a** population-predicted and **b** individual-predicted plasma concentrations, and observed versus **c** population-predicted and **d** individual-predicted urinary amounts for paracetamol (gray *x* marks), paracetamol-glucuronide (blue plus signs), paracetamol-sulfate (green circles), and the combined oxidative pathway metabolites (paracetamol-cysteine and paracetamol-*N*-acetylcysteine, orange triangles). The solid black lines depict the lines of identity (y = x).

successful and unsuccessful runs were compared, most of the parameters listed in Tables 4.2 and 4.4 exhibited less than 5% difference (n = 55 out of 63 parameters, 87%), and all parameters in Tables 4.2 and 4.4 differed by less than 15%. Discrepancies between successful and unsuccessful runs were more evident for between-subject covariance terms (Table 4.3): in a comparison of median bootstrap estimates, most of these parameters differed by greater than 15% (n = 25 out of 36 parameters, 69%). It is plausible that rounding errors would tend to occur on unnecessary, poorly estimated between-subject covariance terms, thus generating larger discrepancies between successful and unsuccessful runs for those parameters.

Simulation-based visualizations of model appropriateness were generated with NPDE, which are expected to have a mean of 0 and a variance of 1. NPDE distributions for plasma compartments showed reasonably good agreement with the expected standard normal distribution (Figure 4.4a), but urinary NPDE distributions exhibited greater deviation from expected values (Figure 4.4b). Importantly, there were no strong trends in NPDE when plotted against time since first dose (Figure 4.4c–d), population predictions (Figure 4.4e–f), or influential covariates (Figure 4.4g–j).

Finally, in order to explore maturational trends in the fraction of paracetamol eliminated by the four routes shown in Figure 4.1, individual clearance estimates for each pathway were expressed as fractions of total individual paracetamol clearance and plotted against influential covariates (Figure 4.5).

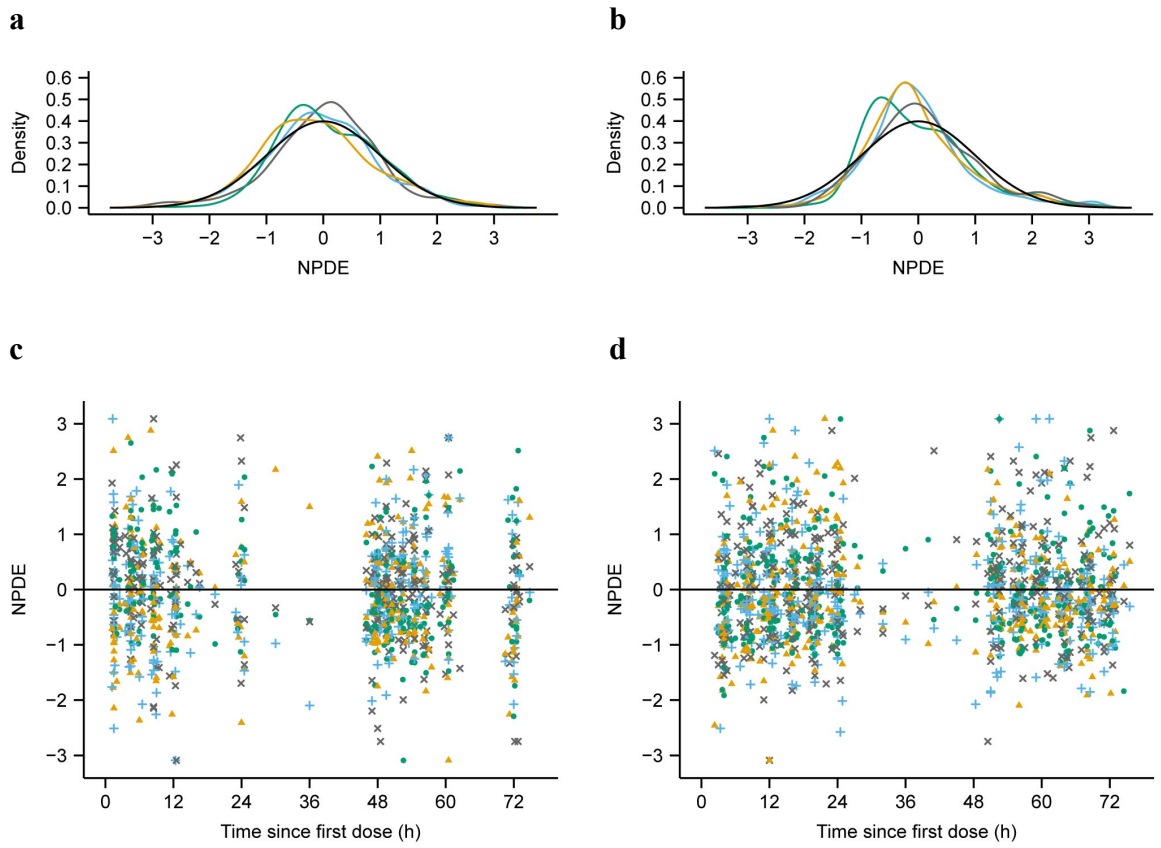

Figure 4.4 Plots of normalized prediction distribution errors (NPDE) for evaluation of the final model. NPDE for plasma concentrations (**a**, **c**, **e**, **g**, **i**) and urinary amounts (**b**, **d**, **f**, **h**, **j**) of paracetamol (gray *x* marks), paracetamol-glucuronide (blue plus signs), paracetamol-sulfate (green circles), and the combined oxidative pathway metabolites (paracetamol-cysteine and paracetamol-*N*-acetylcysteine, orange triangles). **a** and **b** show density histograms of NPDE for paracetamol (gray), paracetamol-glucuronide (blue), paracetamol-sulfate (green), and the oxidative pathway metabolites (orange) with overlaid black curves depicting standard normal distributions for comparison. NPDE are shown versus time (**c** [plasma] and **d** [urine]), population-predicted plasma concentration (**e**), population-predicted urinary amount (**f**), current body weight (**g** [plasma] and **h** [urine]), postnatal age (**i**), and urine flow rate (**j**). The solid black lines in **c**–**j** depict y = 0.

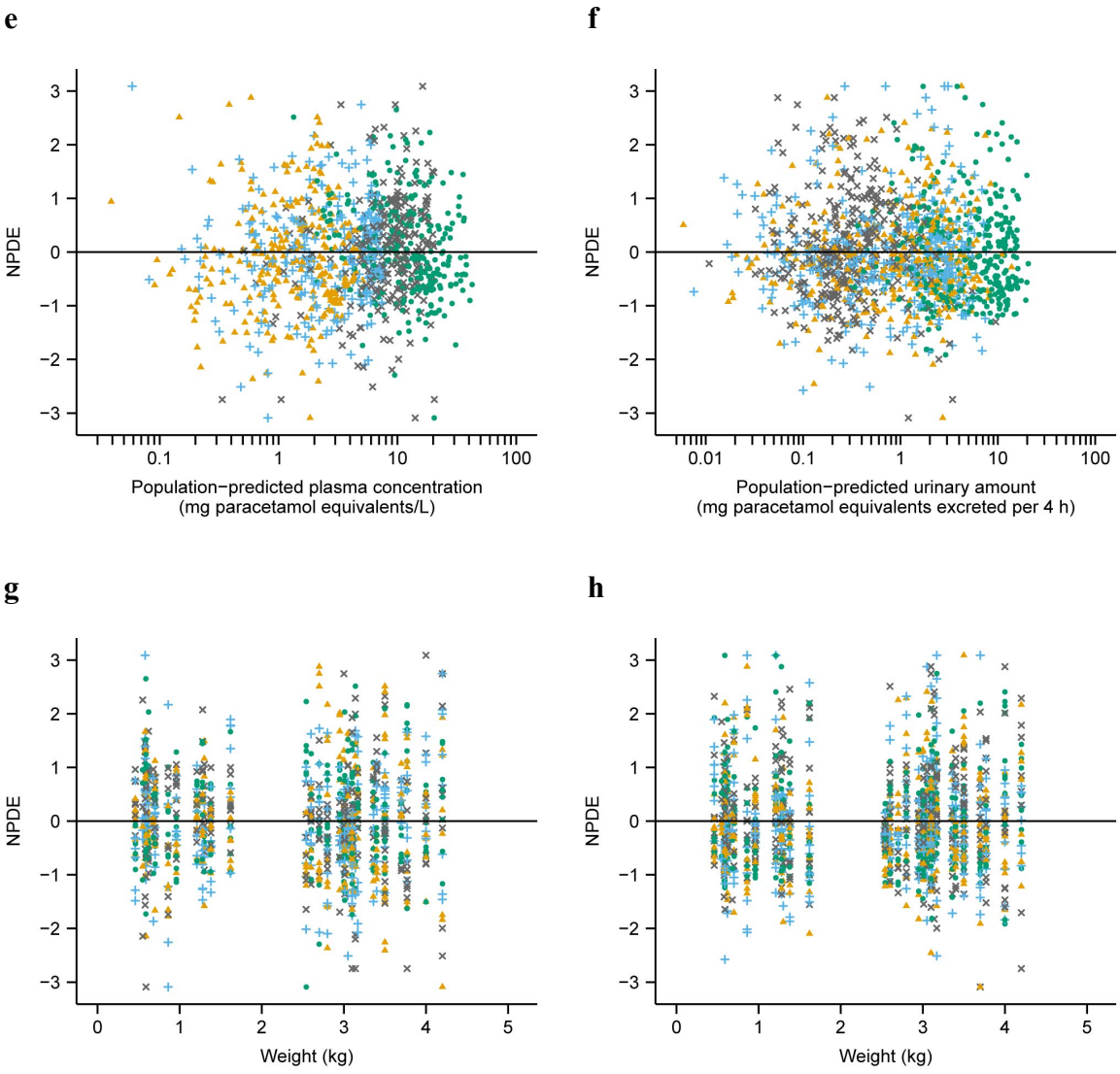

Figure 4.4 (continued)

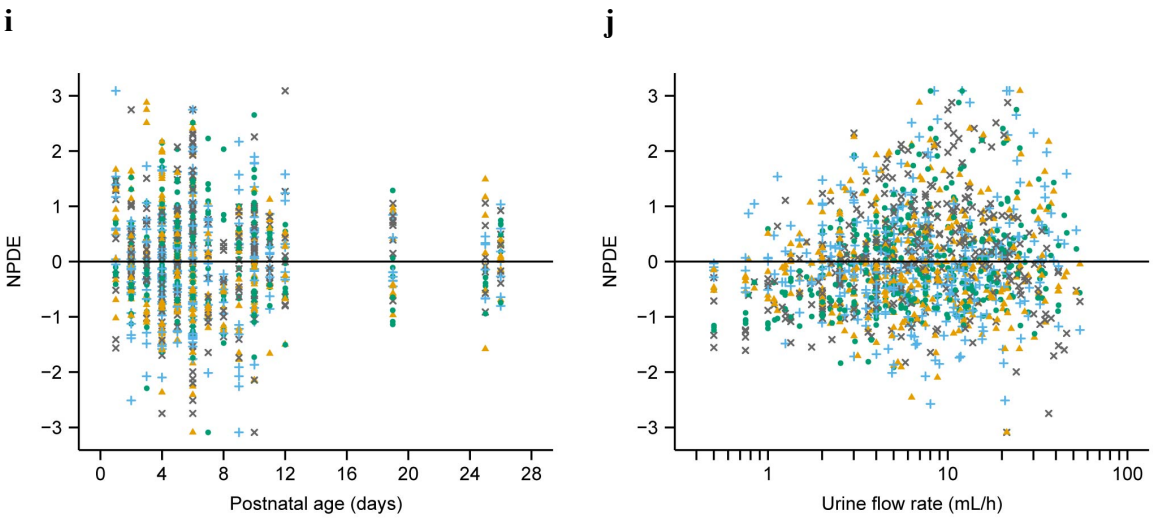

Figure 4.4 (continued)

a

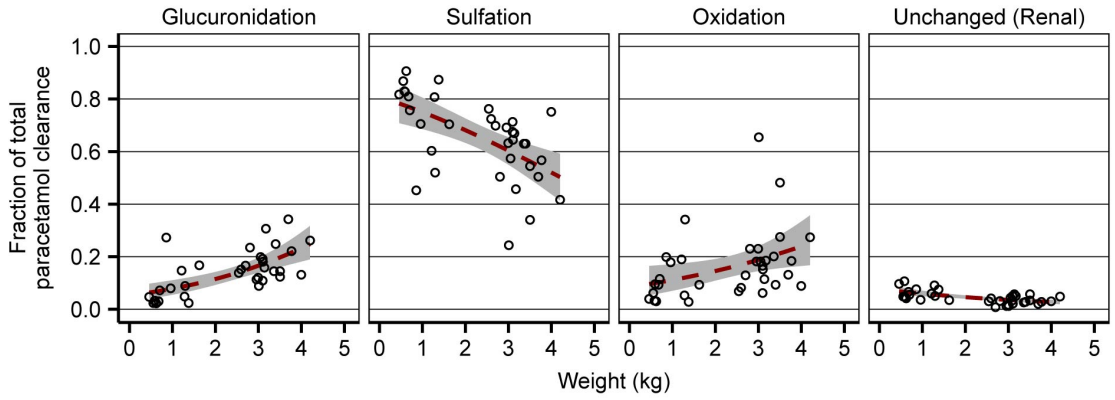

b

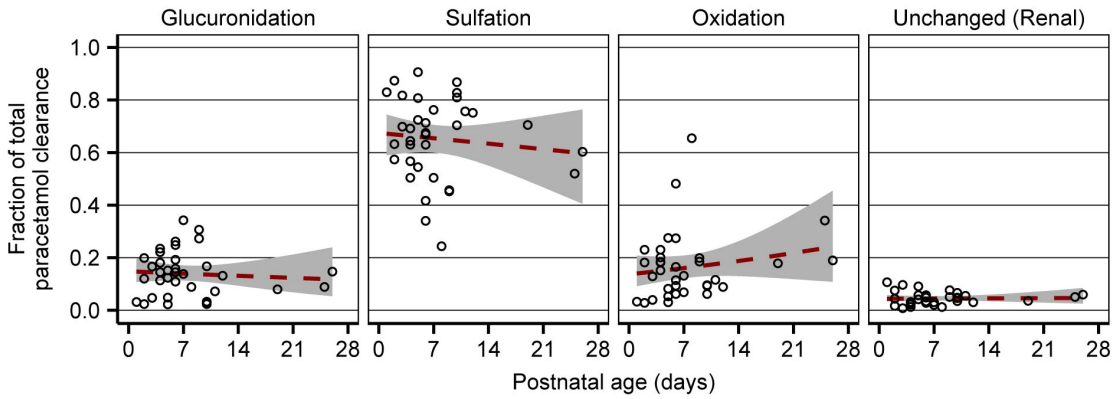

Figure 4.5 Fraction of total paracetamol clearance accounted for by glucuronidation, sulfation, oxidation, and renal clearance of unchanged parent drug. Fractional clearances for each subject (open black circles) are shown versus **a** current body weight and **b** postnatal age. The dashed red lines depict quasibinomial fits of the data, and the shaded gray regions depict 95% confidence intervals surrounding the regression curves. Fractional clearances were calculated from individual formation (hepatic) clearance estimates for paracetamol-glucuronide, paracetamol-sulfate, and the combined oxidative pathway metabolites (paracetamol-cysteine and paracetamol-*N*-acetylcysteine) and from the median individual estimates for renal clearance of unchanged paracetamol.

Discussion

This is the first neonatal study to describe the pharmacokinetics of paracetamol and its metabolites derived from glucuronidation, sulfation, and oxidation. In neonates, sulfation of paracetamol predominates, and the present observations on the relative elimination of paracetamol by glucuronidation, sulfation, or renal elimination of unchanged parent drug agree well with those from prior neonatal pharmacokinetic studies [6, 14-18]. One notable strength of the reported model was incorporation of both plasma and urinary concentrations of paracetamol and metabolites. Such observations made the model structurally identifiable with respect to metabolite volumes of distribution and renal clearances, thus allowing each of these parameters to be estimated. Volumes of distribution for paracetamol-glucuronide and paracetamol-sulfate were approximately 40% of parent drug volume of distribution. This trend is logical given the increased hydrophilicity of these metabolites relative to parent drug, and it is consistent with previous estimates for paracetamol-glucuronide and paracetamol-sulfate volumes of distribution obtained from anephric patients [39]. All three renal metabolite clearances were fairly similar (0.10–0.17 L/h), in agreement with a prior study that found little variation between the same parameters in adult surgical patients [22].

A primary objective of this study was to explore maturational changes in pharmacokinetics of the oxidative pathway metabolites, which serve as markers for the toxic metabolite NAPQI. Weight and postnatal age were identified as covariates that significantly influenced formation clearance of the oxidative pathway metabolites. When weight was incorporated into the model, the OFV decreased by 50.3, and a reduction in BSV of 55% CV was observed. Inclusion of postnatal age was accompanied by an

additional OFV decrease of 20.5 and BSV reduction of 9% CV. Both weight and postnatal age were also significant covariates on formation clearance of paracetamol-glucuronide. Collectively, these observations are consistent with previous evidence that hepatic CYP2E1 expression and UDP-glucuronosyltransferase expression and activity begin during gestation and increase rapidly during the first weeks of life [40, 41].

In extremely preterm to full-term neonates, total clearance of intravenous paracetamol is primarily influenced by body weight [4, 7, 42, 43], and the present findings expand upon prior knowledge by showing that clearances for all four paracetamol elimination routes were significantly affected by weight. Although the fractional clearance by glucuronidation appears relatively constant when plotted against postnatal age (Figure 4.5b), the fact that postnatal age was identified as a significant covariate on formation clearance of paracetamol-glucuronide is consistent with the anticipated marked increase in UDP-glucuronosyltransferase activity during early life [41]. On average, the fraction of drug undergoing oxidation increased slightly (<15%) with increasing weight or postnatal age, but these trends were small relative to BSV (Figure 4.5). Intravenous paracetamol has often been administered more conservatively to less mature neonates (e.g., at wider dosing intervals or in lower per-kilogram doses), but recent analyses of parent drug pharmacokinetics support utilization of a parsimonious regimen based only on equivalent per-kilogram dosing [4, 7]. The present findings indicate that such a dosing regimen also appears suitable with respect to the pharmacokinetics of hepatotoxicity-associated metabolites.

Results from covariate analysis also corroborated a previous infant model in which renal clearances of paracetamol, paracetamol-glucuronide, and paracetamol-sulfate

increased with urine flow rate [32]. In the current study, a similar influence of urine flow rate on renal clearance was also observed for the oxidative pathway metabolites. Additionally, renal clearance of unchanged paracetamol differed significantly between patients with postoperative and procedural indications. However, this finding should be interpreted cautiously. Key patient characteristics were distributed unevenly across the two groups: compared to postoperative patients, procedural patients tended to weigh less and have lower gestational ages and higher postnatal ages. Urine collection procedures also differed between postoperative and procedural patients (catheter and diaper, respectively). Furthermore, even if this covariate reflects a true physiological effect, it is unlikely to be clinically significant given the low fractional clearance of unchanged drug.

The large BSV observed for most pharmacokinetic parameters highlights the importance of continued caution in administration of paracetamol to neonates. BSV was particularly high for glucuronidation and oxidation (62–72% CV), as might be expected based on the rapid development of these processes during early life [40, 41]. Future studies should incorporate additional patient information, such as genetic data, that could further reduce BSV. Urinary RUV also remained fairly high in the final model (Table 4.2), which was not surprising given that urine sampling introduces more opportunities for error than plasma sampling (e.g., longer collection period and requirement for records of sample start time, end time, and volume). These urine-specific aspects of sample collection might also have contributed to the relatively high correlations in urinary RUV (Table 4.4).

Interpretation of these findings is subject to several limitations. First, despite good representation of extremely preterm, preterm, and full-term neonates, the sample size was

still relatively small. Second, the model relies on the assumption that all elimination of paracetamol and its metabolites occurs via the pathways illustrated in Figure 4.1, but small fractions of paracetamol and its metabolites are known to undergo biliary excretion in humans [44, 45]. The model structure also fails to account for NAPQI that covalently binds proteins to form paracetamol protein adducts. This fraction of NAPQI is expected to be small relative to the amount conjugated to glutathione; nevertheless, future studies could explore this point more thoroughly by testing for covariate effects on the pharmacokinetics of circulating paracetamol protein adducts. Finally, although this study contributes critical information regarding the pharmacokinetics of paracetamol metabolites in neonates, pharmacodynamic data for paracetamol in this patient population are still lacking [46]. Further studies are needed for identification of appropriate pharmacodynamic targets for various indications (e.g., analgesia, antipyresis, or patent ductus arteriosus closure) [47, 48].

Conclusion

The reported parent–metabolite model successfully characterized the pharmacokinetics of intravenous paracetamol and its metabolites in preterm and term neonates. Formation clearance of oxidative pathway metabolites increased with body weight and postnatal age; however, maturational increases in the fraction of drug undergoing oxidation were small relative to between-subject variability.

References

[1] K. Allegaert, D. Tibboel, J. van den Anker, Pharmacological treatment of neonatal pain: in search of a new equipoise, Semin. Fetal Neonatal Med. 18

(2013) 42.

[2] G.M. Pacifici, K. Allegaert, Clinical pharmacology of paracetamol in neonates: a review, Curr. Ther. Res. Clin. Exp. 77 (2015) 24.

[3] S.T. Duggan, L.J. Scott, Intravenous paracetamol (acetaminophen), Drugs 69 (2009) 101.

[4] K. Allegaert, G.M. Palmer, B.J. Anderson, The pharmacokinetics of intravenous paracetamol in neonates: size matters most, Arch. Dis. Child. 96 (2011) 575.

[5] A.F. Zuppa, G.B. Hammer, J.S. Barrett, B.F. Kenney, N. Kassir, S. Mouksassi, M.A. Royal, Safety and population pharmacokinetic analysis of intravenous acetaminophen in neonates, infants, children, and adolescents with pain or fever, J. Pediatr. Pharmacol. Ther. 16 (2011) 246.

[6] C. van Ganzewinkel, L. Derijks, K.J. Anand, R.A. van Lingen, C. Neef, B.W. Kramer, P. Andriessen, Multiple intravenous doses of paracetamol result in a predictable pharmacokinetic profile in very preterm infants, Acta Paediatr. 103 (2014) 612.

[7] S.F. Cook, J.K. Roberts, S. Samiee-Zafarghandy, C. Stockmann, A.D. King, N. Deutsch, E.F. Williams, K. Allegaert, D.G. Wilkins, C.M. Sherwin, J.N. van den Anker, Population pharmacokinetics of intravenous paracetamol (acetaminophen) in preterm and term neonates: model development and external evaluation, Clin. Pharmacokinet. DOI 10.1007/s40262-015-0301-3 (2015).

[8] B.J. Anderson, R.A. van Lingen, T.G. Hansen, Y.C. Lin, N.H. Holford, Acetaminophen developmental pharmacokinetics in premature neonates and infants: a pooled population analysis, Anesthesiology 96 (2002) 1336.

[9] K. Allegaert, S. Vanhaesebrouck, R. Verbesselt, J.N. van den Anker, In vivo glucuronidation activity of drugs in neonates: extensive interindividual variability despite their young age, Ther. Drug Monit. 31 (2009) 411.

[10] M.R. McGill, H. Jaeschke, Metabolism and disposition of acetaminophen: recent advances in relation to hepatotoxicity and diagnosis, Pharm. Res. 30 (2013) 2174.

[11] L.P. James, P.R. Mayeux, J.A. Hinson, Acetaminophen-induced hepatotoxicity, Drug Metab. Dispos. 31 (2003) 1499.

[12] H. Jaeschke, M.R. McGill, A. Ramachandran, Oxidant stress, mitochondria, and cell death mechanisms in drug-induced liver injury: lessons learned from acetaminophen hepatotoxicity, Drug Metab. Rev. 44 (2012) 88.

[13] J.A. Hinson, D.W. Roberts, L.P. James, Mechanisms of acetaminophen-induced liver necrosis, Handb. Exp. Pharmacol. DOI 10.1007/978-3-642-00663-0_12 (2010) 369.

[14] G. Levy, N.N. Khanna, D.M. Soda, O. Tsuzuki, L. Stern, Pharmacokinetics of acetaminophen in the human neonate: formation of acetaminophen glucuronide and sulfate in relation to plasma bilirubin concentration and D-glucaric acid excretion, Pediatrics 55 (1975) 818.

[15] R.P. Miller, R.J. Roberts, L.J. Fischer, Acetaminophen elimination kinetics in neonates, children, and adults, Clin. Pharmacol. Ther. 19 (1976) 284.

[16] R.A. van Lingen, J.T. Deinum, J.M. Quak, A.J. Kuizenga, J.G. van Dam, K.J. Anand, D. Tibboel, A. Okken, Pharmacokinetics and metabolism of rectally administered paracetamol in preterm neonates, Arch. Dis. Child. Fetal Neonatal Ed. 80 (1999) F59.

[17] K. Allegaert, J. de Hoon, R. Verbesselt, C. Vanhole, H. Devlieger, D. Tibboel, Intra- and interindividual variability of glucuronidation of paracetamol during repeated administration of propacetamol in neonates, Acta Paediatr. 94 (2005) 1273.

[18] E.H. Krekels, S. van Ham, K. Allegaert, J. de Hoon, D. Tibboel, M. Danhof, C.A. Knibbe, Developmental changes rather than repeated administration drive paracetamol glucuronidation in neonates and infants, Eur. J. Clin. Pharmacol. DOI 10.1007/s00228-015-1887-y (2015).

[19] A.J. Boeckmann, L.B. Sheiner, S.L. Beal, NONMEM users guide - part v: introductory guide, NONMEM Project Group, University of California at San Francisco, 2011.

[20] R.J. Bauer, NONMEM users guide: introduction to NONMEM 7.2.0, ICON Development Solutions, Ellicott City, MD, USA, 2011.

[21] T.M. Ludden, S.L. Beal, L.B. Sheiner, Comparison of the Akaike Information Criterion, the Schwarz criterion and the F test as guides to model selection, J. Pharmacokinet. Biopharm. 22 (1994) 431.

[22] K.H. Owens, P.G. Murphy, N.J. Medlicott, J. Kennedy, M. Zacharias, N. Curran, S. Sreebhavan, M. Thompson-Fawcett, D.M. Reith, Population pharmacokinetics of intravenous acetaminophen and its metabolites in major surgical patients, J. Pharmacokinet. Pharmacodyn. 41 (2014) 211.

[23] A. Kulo, M.Y. Peeters, K. Allegaert, A. Smits, J. de Hoon, R. Verbesselt, L. Lewi, M. van de Velde, C.A. Knibbe, Pharmacokinetics of paracetamol and its metabolites in women at delivery and post-partum, Br. J. Clin. Pharmacol. 75 (2013) 850.

[24] D. Reith, N.J. Medlicott, R. Kumara De Silva, L. Yang, J. Hickling, M. Zacharias, Simultaneous modelling of the Michaelis-Menten kinetics of paracetamol sulphation and glucuronidation, Clin. Exp. Pharmacol. Physiol. 36 (2009) 35.

[25] D.R. Mould, R.N. Upton, Basic concepts in population modeling, simulation, and model-based drug development—part 2: introduction to pharmacokinetic modeling methods, CPT Pharmacometrics Syst. Pharmacol. 2 (2013) e38.

[26] G.J. Schwartz, A. Munoz, M.F. Schneider, R.H. Mak, F. Kaskel, B.A. Warady, S.L. Furth, New equations to estimate GFR in children with CKD, J. Am. Soc. Nephrol. 20 (2009) 629.

[27] L. Zhao, G. Pickering, Paracetamol metabolism and related genetic differences, Drug Metab. Rev. 43 (2011) 41.

[28] A.E. Krasniak, G.T. Knipp, C.K. Svensson, W. Liu, Pharmacogenomics of acetaminophen in pediatric populations: a moving target, Front. Genet. 5 (2014) 314.

[29] C.K. Gelotte, J.F. Auiler, J.M. Lynch, A.R. Temple, J.T. Slattery, Disposition of acetaminophen at 4, 6, and 8 g/day for 3 days in healthy young adults, Clin. Pharmacol. Ther. 81 (2007) 840.

[30] K.H. Owens, N.J. Medlicott, M. Zacharias, N. Curran, S. Chary, M. Thompson-Fawcett, D.M. Reith, The pharmacokinetic profile of intravenous paracetamol in adult patients undergoing major abdominal surgery, Ther. Drug Monit. 34 (2012) 713.

[31] K. Allegaert, R. Verbesselt, M. Rayyan, A. Debeer, J. de Hoon, Urinary metabolites to assess in vivo ontogeny of hepatic drug metabolism in early neonatal life, Methods Find. Exp. Clin. Pharmacol. 29 (2007) 251.

[32] C.D. van der Marel, B.J. Anderson, R.A. van Lingen, N.H. Holford, M.A. Pluim, F.G. Jansman, J.N. van den Anker, D. Tibboel, Paracetamol and metabolite pharmacokinetics in infants, Eur. J. Clin. Pharmacol. 59 (2003) 243.

[33] J.S. Owen, J. Fiedler-Kelly, Introduction to population pharmacokinetic / pharmacodynamic analysis with nonlinear mixed effects models, John Wiley & Sons, Inc., Hoboken, NJ, USA, 2014.

[34] E.I. Ette, Stability and performance of a population pharmacokinetic model, J. Clin. Pharmacol. 37 (1997) 486.

[35] K. Brendel, E. Comets, C. Laffont, F. Mentre, Evaluation of different tests based on observations for external model evaluation of population analyses, J. Pharmacokinet. Pharmacodyn. 37 (2010) 49.

[36] S.L. Beal, Ways to fit a PK model with some data below the quantification limit, J. Pharmacokinet. Pharmacodyn. 28 (2001) 481.

[37] N.H.G. Holford, J.V.S. Gobburu, D.R. Mould, Implications of including and excluding correlation of random effects in hierarchical mixed effects

pharmacokinetic models, Population Approach Group in Europe, Verona, Italy, 2003.

[38] D.H. Salinger, D.K. Blough, P. Vicini, C. Anasetti, P.V. O'Donnell, B.M. Sandmaier, J.S. McCune, A limited sampling schedule to estimate individual pharmacokinetic parameters of fludarabine in hematopoietic cell transplant patients, Clin. Cancer Res. 15 (2009) 5280.

[39] D.T. Lowenthal, S. Oie, J.C. Van Stone, W.A. Briggs, G. Levy, Pharmacokinetics of acetaminophen elimination by anephric patients, J. Pharmacol. Exp. Ther. 196 (1976) 570.

[40] E.K. Johnsrud, S.B. Koukouritaki, K. Divakaran, L.L. Brunengraber, R.N. Hines, D.G. McCarver, Human hepatic CYP2E1 expression during development, J. Pharmacol. Exp. Ther. 307 (2003) 402.

[41] E.H. Krekels, M. Danhof, D. Tibboel, C.A. Knibbe, Ontogeny of hepatic glucuronidation; methods and results, Curr. Drug Metab. 13 (2012) 728.

[42] K. Allegaert, B.J. Anderson, G. Naulaers, J. de Hoon, R. Verbesselt, A. Debeer, H. Devlieger, D. Tibboel, Intravenous paracetamol (propacetamol) pharmacokinetics in term and preterm neonates, Eur. J. Clin. Pharmacol. 60 (2004) 191.

[43] G.M. Palmer, M. Atkins, B.J. Anderson, K.R. Smith, T.J. Culnane, C.M. McNally, E.J. Perkins, G.A. Chalkiadis, R.W. Hunt, I.V. acetaminophen pharmacokinetics in neonates after multiple doses, Br. J. Anaesth. 101 (2008) 523.

[44] C.P. Siegers, W. Loeser, J. Gieselmann, D. Oltmanns, Biliary and renal excretion of paracetamol in man, Pharmacology 29 (1984) 301.

[45] K.S. Jayasinghe, C.J. Roberts, A.E. Read, Is biliary excretion of paracetamol significant in man? Br. J. Clin. Pharmacol. 22 (1986) 363.

[46] K. Allegaert, G. Naulaers, S. Vanhaesebrouck, B.J. Anderson, The paracetamol concentration-effect relation in neonates, Paediatr. Anaesth. 23 (2013) 45.

[47] I.A. Gibb, B.J. Anderson, Paracetamol (acetaminophen) pharmacodynamics: interpreting the plasma concentration, Arch. Dis. Child. 93 (2008) 241.

[48] A. Ohlsson, P.S. Shah, Paracetamol (acetaminophen) for patent ductus arteriosus in preterm or low-birth-weight infants, Cochrane Database Syst. Rev. 3 (2015) CD010061.

CHAPTER 5

CONCLUSIONS

Summary of Findings

This dissertation focused on the exploration of maturational changes in the pharmacokinetics of intravenous acetaminophen and its metabolites in neonates through completion of three primary aims. These aims centered on a prospective clinical trial in which neonates with a clinical indication for intravenous analgesia received acetaminophen (15 mg/kg/dose) for 5 doses at 12-h intervals (<28 weeks' gestation) or for 7 doses at 8-h intervals (≥28 weeks' gestation). Pharmacokinetic samples were collected throughout a 72-h study period.

In the first aim (Chapter 2), novel HPLC–ESI–MS/MS methods were developed for application to the neonatal pharmacokinetic samples. The procedures were successfully validated for simultaneous quantification of acetaminophen, acetaminophen-glucuronide, acetaminophen-sulfate, acetaminophen-glutathione, acetaminophen-cysteine, and acetaminophen-*N*-acetyl-cysteine in small volumes (10 μL) of human plasma and urine. Acetaminophen-d4 and acetaminophen-d3-sulfate were utilized as internal standards. Analytes and internal standards were recovered from plasma by protein precipitation with acetonitrile, and urine samples were prepared by fortification with internal standards followed only by sample dilution. Calibration concentration ranges were carefully tailored to literature values for each analyte in each biological matrix. Prepared samples from plasma and urine were analyzed under the same HPLC–ESI–MS/MS conditions, and chromatographic separation was achieved through use of an Agilent Poroshell 120 EC-C18 column with a 20-min run time per injected sample.

The analytes could be accurately and precisely quantified over 2.0–3.5 orders of magnitude. Across both matrices, mean intra- and inter-assay accuracies ranged from 85–

112%, and intra- and inter-assay imprecision did not exceed 15%. Validation experiments included tests for specificity, recovery and ionization efficiency, inter-individual variability in matrix effects, stock solution stability, and sample stability under a variety of storage and handling conditions (room temperature, freezer, freeze-thaw, and postpreparative). Both methods were found to be sensitive, specific, accurate, precise, and efficient. The reported procedures were successfully applied to the pharmacokinetic study samples.

The second aim (Chapter 3) focused on the development of a population pharmacokinetic model for the parent drug data obtained from the neonatal pharmacokinetic study [1]. Nonlinear mixed effects models were constructed in NONMEM 7.2 using 260 acetaminophen concentration–time points from 35 patients. Potential covariates included body weight, gestational age, postnatal age, postmenstrual age, sex, race, total bilirubin, and estimated glomerular filtration rate. Importantly, there was good representation of extremely preterm, preterm, and term neonates among the study subjects. Data were well described by a one-compartment model with first-order elimination. In neonates ranging from extremely preterm to full-term gestational ages, body weight was the principal predictor of intravenous acetaminophen pharmacokinetics. Clearance and volume of distribution were estimated as 0.348 L/h (5.5% relative standard error; 30.8% between-subject variability) and 2.46 L (3.5% relative standard error; 14.3% between-subject variability), respectively, at the mean subject weight of 2.30 kg.

In an external evaluation of the parent drug model with a dataset from a similar, independent clinical trial, the median prediction error was 10.1% (95% confidence interval: 6.1–14.3%) and the median absolute prediction error was 25.3% (95%

confidence interval: 23.1–28.1%). These figures indicate that the parent drug model performed adequately despite notable study differences in the proportion of extremely preterm neonates, postnatal age, racial composition, and geographic location. Thus, these findings should be generalizable to other similar patient populations.

The results from the second research aim largely reinforce and expand upon previous work that supported the use of a simplified neonatal dosing regimen in which maturational changes in acetaminophen pharmacokinetics could be accommodated using only equivalent per-kilogram dosing, without requiring different doses or dosing intervals dependent upon gestational or postmenstrual age [2]. Our findings suggest that extension of such a parsimonious dosing regimen to extremely preterm neonates is valid.

In the third aim (Chapter 4), a parent–metabolite population pharmacokinetic model was developed using the data obtained from the neonatal pharmacokinetic study. Concentration–time data for acetaminophen, acetaminophen-glucuronide, acetaminophen-sulfate, and the combined oxidative pathway metabolites (acetaminophen-cysteine and acetaminophen-*N*-acetylcysteine) were simultaneously modeled in NONMEM 7.2. The model incorporated 259 plasma and 350 urine samples from 35 neonates. As part of the model development process, an extensive covariate analysis was performed to identify patient characteristics that influenced metabolite pharmacokinetic parameters, with a particular focus on formation clearance of the oxidative pathway metabolites.

Formation clearances for all metabolites increased with weight, and formation clearances for glucuronidation and oxidation also increased with postnatal age. At the mean weight (2.3 kg) and postnatal age (7.5 days), formation clearance estimates

(bootstrap 95% confidence interval; between-subject variability) were 0.049 L/h (0.038–0.062; 62%) for glucuronidation, 0.21 L/h (0.17–0.24; 33%) for sulfation, and 0.058 L/h (0.044–0.078; 72%) for oxidation. Fractional formation clearance of the oxidative pathway metabolites, which are associated with hepatotoxicity, increased slightly (<15%) with weight and postnatal age, but these maturational changes were small relative to between-subject variability. These findings extend the results from the previous aim by showing that the pharmacokinetics of acetaminophen metabolites also support utilization of parsimonious weight-based dosing; however, the large between-subject variability in metabolite pharmacokinetics underscores the importance of continued caution in administration of acetaminophen to neonates.

The collective results from these studies substantially improve our understanding of the factors that influence acetaminophen disposition during the neonatal period, and this knowledge is critical for implementation of informed intravenous acetaminophen dosing strategies in this vulnerable patient population. Nevertheless, several areas of future investigation are warranted.

Future Directions

A major strength of the study reported in Chapter 3 was the incorporation of an external model evaluation. Ideally, such an evaluation would also be performed on the parent–metabolite model presented in Chapter 4; however, because this is the first neonatal study to describe the pharmacokinetics of acetaminophen and its metabolites derived from glucuronidation, sulfation, and oxidation, there are no data available for comparison. A logical and relatively simple future study would be to apply the analytical

methods described in Chapter 2 to pharmacokinetic samples from previous clinical trials of intravenous acetaminophen in neonates in order to acquire metabolite data for external evaluation. Prior to such analysis, optimal design techniques could be applied to data from the present study to minimize the number of samples requiring quantitative analysis while maintaining the essential pharmacokinetic information [3]. Optimal design techniques could also be employed to identify optimal pharmacokinetic sampling schedules for future prospective studies in similar patient populations so that the number of blood samples drawn from each patient could be minimized.

Based on the observed maturational trends in the fraction of acetaminophen undergoing oxidation (Figure 4.5), future work should also be devoted to exploring maturational changes in the pharmacokinetics of acetaminophen and its metabolites in infants. Historically, intravenous acetaminophen has often been administered more conservatively to less mature neonates, but the findings from Chapter 4 revealed that *more mature* neonates clear larger fractions of the drug via oxidation and glucuronidation and a smaller fraction via sulfation. Although the maturational increases in fractional clearance by oxidation were small relative to between-subject variability, it is possible that the observed trend continues into infancy. Moreover, only three neonates with postnatal ages >14 days were included in the present dataset, so the late neonatal period deserves further consideration in this regard, as well.

In the parent–metabolite model, between-subject variability remained especially high for glucuronidation and oxidation (62–72% CV). This was not unexpected given the rapid development of these processes that occurs during early life [4-6]. Even so, future studies should test the influence of additional patient characteristics on metabolite

formation clearances to attempt to reduce between-subject variability. Genetic data represents a particularly promising option for further covariate testing, and a number of genetic polymorphisms have been shown to affect acetaminophen metabolism, primarily in *in vitro* enzyme activity studies with human liver preparations [7].

One potential limitation of the parent–metabolite model is its failure to account for NAPQI that covalently binds proteins to form acetaminophen protein adducts. This fraction of NAPQI is expected to be small relative to the amount conjugated by glutathione, but future studies could explore this point more thoroughly by measuring acetaminophen protein adducts in neonatal study samples and testing for covariate effects on the pharmacokinetics of circulating acetaminophen protein adducts. The material in the Appendix was supplied with such an application in mind. It should be emphasized, however, that the mechanism by which the protein adducts appear in the circulation in the absence of hepatic necrosis is unclear. Hepatic formation [8] and localization [9] of the adducts are highly correlated with toxicity. As hepatic necrosis progresses, acetaminophen protein adducts are released from hepatocytes into the circulation, and the adducts can be detected at high concentrations in the serum/plasma of humans and rodents following supratherapeutic acetaminophen ingestions [10-15]. Serum acetaminophen protein adducts have also been detected at lower concentrations in subjects taking therapeutic doses of the drug [16, 17], but circulating adduct concentrations are not necessarily correlated with hepatic concentrations under such circumstances. Therefore, it would likely be inappropriate to incorporate circulating acetaminophen protein adduct concentrations into a parent–metabolite model in the same fashion as pharmacokinetic data for small molecule metabolites. However, it has been

previously proposed that detection of serum acetaminophen protein adducts above a threshold concentration of 1 nmol/mL is indicative of acetaminophen-induced hepatotoxicity [13], so it might be possible to incorporate the adducts into a model as a toxicodynamic marker based on this threshold.

Perhaps the greatest need for future research related to the use of intravenous acetaminophen in neonates lies in the identification of appropriate pharmacodynamic targets. To date, only one pharmacodynamic study of intravenous acetaminophen has been performed in neonatal patients. Allegaert et al. evaluated their proposed parsimonious dosing regimen [2] (see Table 1.1) in 19 subjects who received intravenous acetaminophen as monotherapy for mild to moderate pain [18]. Pain was assessed using the Leuven Neonatal Pain Score (range: 0–14), which is a previously validated, multidimensional pain scale based on 7 measures (sleep, facial appearance, crying, heart rate, motor tone, movement, and consolability) [19]. A significant trend for lower pain scores within 30 min after administration was observed (repeated measures ANOVA, p = 0.02) along with a nonsignificant increase in pain scores from 5–6 h. The maximum effect was a reduction in pain score of 4.15 units, and an effect compartment concentration of 10 mg/L was associated with a pain score reduction of 3.4 units. These results are encouraging because they agree fairly well with previous estimates obtained from children (9 ± 3 years of age) who received oral acetaminophen prior to tonsillectomy [20]; however, the study design suffered from a number of limitations. The number of subjects was small and observations were particularly sparse. Additionally, the study was not blinded because the primary outcome was collection of pharmacokinetic data. In spite of these limitations, the study findings suggest that it is not inappropriate to

select initial target concentrations for neonatal pharmacodynamic studies based on target concentrations from pharmacodynamic studies performed in older children.

The collection of robust pharmacodynamic data for intravenous acetaminophen in neonates will require substantial effort and resources. The efficacy of acetaminophen is known to be influenced not only by dose, but also by route of administration and indication, which includes variability in efficacy dependent upon the type of painful stimulus [21-23]. Efficacy in neonates may be further complicated by maturational processes. Additionally, neonatal pain assessment presents particular challenges, such as significant subjectivity and interobserver variability. As a consequence of existing limitations in neonatal pain assessment methods, efforts are currently underway to develop and validate improved pain scales that utilize neuroimaging and neurophysiologic techniques [23]. Ultimately, the results from the studies reported in this dissertation will prove most useful when linked to high-quality pharmacodynamic data.

In summary, this dissertation research has elucidated the factors influencing acetaminophen disposition in neonates. At present, findings based on the pharmacokinetics of both parent drug and hepatotoxicity-associated metabolites support cautious implementation of a 20-mg/kg loading dose followed by 10-mg/kg maintenance doses every 6 h for administration of intravenous acetaminophen to neonates ranging from 27–44 weeks' postmenstrual age. Future studies should focus on establishing appropriate pharmacodynamic targets and identifying patient characteristics that can be used to further reduce the amount of unpredictable variability in the pharmacokinetics of acetaminophen and its metabolites.

References

[1] S.F. Cook, J.K. Roberts, S. Samiee-Zafarghandy, C. Stockmann, A.D. King, N. Deutsch, E.F. Williams, K. Allegaert, D.G. Wilkins, C.M. Sherwin, J.N. van den Anker, Population pharmacokinetics of intravenous paracetamol (acetaminophen) in preterm and term neonates: model development and external evaluation, Clin. Pharmacokinet. DOI 10.1007/s40262-015-0301-3 (2015).

[2] K. Allegaert, G.M. Palmer, B.J. Anderson, The pharmacokinetics of intravenous paracetamol in neonates: size matters most, Arch. Dis. Child. 96 (2011) 575.

[3] J.K. Roberts, C. Stockmann, A. Balch, T. Yu, R.M. Ward, M.G. Spigarelli, C.M. Sherwin, Optimal design in pediatric pharmacokinetic and pharmacodynamic clinical studies, Paediatr. Anaesth. 25 (2015) 222.

[4] E.K. Johnsrud, S.B. Koukouritaki, K. Divakaran, L.L. Brunengraber, R.N. Hines, D.G. McCarver, Human hepatic CYP2E1 expression during development, J. Pharmacol. Exp. Ther. 307 (2003) 402.

[5] E.H. Krekels, M. Danhof, D. Tibboel, C.A. Knibbe, Ontogeny of hepatic glucuronidation; methods and results, Curr. Drug Metab. 13 (2012) 728.

[6] I. Vieira, M. Sonnier, T. Cresteil, Developmental expression of CYP2E1 in the human liver: hypermethylation control of gene expression during the neonatal period, Eur. J. Biochem. 238 (1996) 476.

[7] A.E. Krasniak, G.T. Knipp, C.K. Svensson, W. Liu, Pharmacogenomics of acetaminophen in pediatric populations: a moving target, Front. Genet. 5 (2014) 314.

[8] D.J. Jollow, J.R. Mitchell, W.Z. Potter, D.C. Davis, J.R. Gillette, B.B. Brodie, Acetaminophen-induced hepatic necrosis. II. Role of covalent binding in vivo, J. Pharmacol. Exp. Ther. 187 (1973) 195.

[9] D.W. Roberts, T.J. Bucci, R.W. Benson, A.R. Warbritton, T.A. McRae, N.R. Pumford, J.A. Hinson, Immunohistochemical localization and quantification of the 3-(cystein-S-yl)-acetaminophen protein adduct in acetaminophen hepatotoxicity, Am. J. Pathol. 138 (1991) 359.

[10] N.R. Pumford, J.A. Hinson, R.W. Benson, D.W. Roberts, Immunoblot analysis of protein containing 3-(cystein-S-yl)acetaminophen adducts in serum and subcellular liver fractions from acetaminophen-treated mice, Toxicol. Appl. Pharmacol. 104 (1990) 521.

[11] T.J. Davern, 2nd, L.P. James, J.A. Hinson, J. Polson, A.M. Larson, R.J. Fontana, E. Lalani, S. Munoz, A.O. Shakil, W.M. Lee, Measurement of serum acetaminophen-protein adducts in patients with acute liver failure, Gastroenterology 130 (2006) 687.

[12] L.P. James, E.V. Capparelli, P.M. Simpson, L. Letzig, D. Roberts, J.A. Hinson, G.L. Kearns, J.L. Blumer, J.E. Sullivan, Acetaminophen-associated hepatic injury: evaluation of acetaminophen protein adducts in children and adolescents with acetaminophen overdose, Clin. Pharmacol. Ther. 84 (2008) 684.

[13] L.P. James, L. Letzig, P.M. Simpson, E. Capparelli, D.W. Roberts, J.A. Hinson, T.J. Davern, W.M. Lee, Pharmacokinetics of acetaminophen-protein adducts in adults with acetaminophen overdose and acute liver failure, Drug Metab. Dispos. 37 (2009) 1779.

[14] K.L. Muldrew, L.P. James, L. Coop, S.S. McCullough, H.P. Hendrickson, J.A. Hinson, P.R. Mayeux, Determination of acetaminophen-protein adducts in mouse liver and serum and human serum after hepatotoxic doses of acetaminophen using high-performance liquid chromatography with electrochemical detection, Drug Metab. Dispos. 30 (2002) 446.

[15] M.R. McGill, M. Lebofsky, H.R. Norris, M.H. Slawson, M.L. Bajt, Y. Xie, C.D. Williams, D.G. Wilkins, D.E. Rollins, H. Jaeschke, Plasma and liver acetaminophen-protein adduct levels in mice after acetaminophen treatment: dose-response, mechanisms, and clinical implications, Toxicol. Appl. Pharmacol. 269 (2013) 240.

[16] K.J. Heard, J.L. Green, L.P. James, B.S. Judge, L. Zolot, S. Rhyee, R.C. Dart, Acetaminophen-cysteine adducts during therapeutic dosing and following overdose, BMC Gastroenterol. 11 (2011) 20.

[17] L.P. James, A. Chiew, S.M. Abdel-Rahman, L. Letzig, A. Graudins, P. Day, D. Roberts, Acetaminophen protein adduct formation following low-dose acetaminophen exposure: comparison of immediate-release vs extended-release formulations, Eur. J. Clin. Pharmacol. 69 (2013) 851.

[18] K. Allegaert, G. Naulaers, S. Vanhaesebrouck, B.J. Anderson, The paracetamol concentration-effect relation in neonates, Paediatr. Anaesth. 23 (2013) 45.

[19] K. Allegaert, D. Tibboel, G. Naulaers, D. Tison, A. De Jonge, M. Van Dijk, C. Vanhole, H. Devlieger, Systematic evaluation of pain in neonates: effect on the number of intravenous analgesics prescribed, Eur. J. Clin. Pharmacol. 59 (2003) 87.

[20] B.J. Anderson, G.A. Woollard, N.H. Holford, Acetaminophen analgesia in children: placebo effect and pain resolution after tonsillectomy, Eur. J. Clin. Pharmacol. 57 (2001) 559.

[21] S.M. Walker, Neonatal pain, Paediatr. Anaesth. 24 (2014) 39.

[22] I.A. Gibb, B.J. Anderson, Paracetamol (acetaminophen) pharmacodynamics: interpreting the plasma concentration, Arch. Dis. Child. 93 (2008) 241.

[23] R.W. Hall, K.J. Anand, Pain management in newborns, Clin. Perinatol. 41 (2014) 895.

APPENDIX

QUANTIFICATION OF A BIOMARKER OF ACETAMINOPHEN PROTEIN ADDUCTS IN HUMAN SERUM BY HIGH-PERFORMANCE LIQUID CHROMATOGRAPHY–ELECTROSPRAY IONIZATION–TANDEM MASS SPECTROMETRY: CLINICAL AND ANIMAL MODEL APPLICATIONS

Journal of Chromatography B (2015) **985**, 131. Quantification of a Biomarker of Acetaminophen Protein Adducts in Human Serum by High-Performance Liquid Chromatography–Electrospray Ionization–Tandem Mass Spectrometry: Clinical and Animal Model Applications. S. F. Cook, A. D. King, Y. Chang, G. J. Murray, H.-R. K. Norris, R. C. Dart, J. L. Green, S. C. Curry, D. E. Rollins, D. G. Wilkins. Reprinted with permission from Elsevier.

Journal of Chromatography B, 985 (2015) 131–141

Contents lists available at ScienceDirect

Journal of Chromatography B

journal homepage: www.elsevier.com/locate/chromb

Quantification of a biomarker of acetaminophen protein adducts in human serum by high-performance liquid chromatography-electrospray ionization-tandem mass spectrometry: Clinical and animal model applications

Sarah F. Cook[a,*], Amber D. King[a], Yan Chang[a], Gordon J. Murray[a], Hye-Ryun K. Norris[a], Richard C. Dart[b], Jody L. Green[b], Steven C. Curry[c,d], Douglas E. Rollins[a], Diana G. Wilkins[a,e]

[a] Center for Human Toxicology, Department of Pharmacology and Toxicology, University of Utah, 30 South 2000 East, Suite 105, Salt Lake City, UT 84112, USA
[b] Rocky Mountain Poison and Drug Center, Denver Health, 777 Bannock Street, Denver, CO 80204, USA
[c] Department of Medicine, and Center for Toxicology and Pharmacology Education and Research, University of Arizona College of Medicine-Phoenix, 550 East Van Buren Street, Phoenix, AZ 85004, USA
[d] Department of Medical Toxicology, Banner Good Samaritan Medical Center, 925 East McDowell Road, Floor 2, Phoenix, AZ 85028, USA
[e] Division of Medical Laboratory Sciences, Department of Pathology, University of Utah School of Medicine, 15 North Medical Drive, Salt Lake City, UT 84112, USA

ARTICLE INFO

Article history:
Received 6 October 2014
Accepted 19 January 2015
Available online 24 January 2015

Keywords:
Acetaminophen-cysteine
Protein adduct
Hepatotoxicity
Biomarker
Human serum
HPLC-ESI-MS/MS

ABSTRACT

The aims of this study were to develop, validate, and apply a high-performance liquid chromatography-electrospray ionization-tandem mass spectrometry (HPLC-ESI-MS/MS) method for quantification of protein-derived 3-(cystein-*S*-yl)-acetaminophen (APAP-Cys) in human serum. Formation of acetaminophen (APAP) protein adducts is thought to be a critical, early event in the development of APAP-induced hepatotoxicity, and quantification of these protein adducts in human serum represents a valuable tool for assessment of APAP exposure, metabolism, and toxicity. In the reported procedure, serum samples were first dialyzed or passed through gel filtration columns to remove APAP-Cys not covalently bound to proteins. Serum eluates were then subjected to enzymatic protease digestion to liberate protein-bound APAP-Cys. Norbuprenorphine-D_3 was utilized as an internal standard (IS). APAP-Cys and IS were recovered from digested serum by protein precipitation with acetonitrile, and sample extracts were analyzed by HPLC-ESI-MS/MS. The method was validated by assessment of intra- and inter-assay accuracy and imprecision on two different analytical instrument platforms. APAP-Cys could be accurately quantified from 0.010 to 10 μM, and intra- and inter-assay imprecision were <15% on both analytical instruments. APAP-Cys was stable in human serum for three freeze-thaw cycles and for 24 h at ambient temperature. Extracted samples were stable when stored in refrigerated autosamplers for the typical duration of analysis or when stored at −20 °C for six days. Results from process efficiency and matrix effect experiments indicated adequate recovery from human serum and insignificant ion suppression or enhancement. The utility and sensitivity of the reported procedure were illustrated by analysis of clinical samples collected from subjects taking chronic, therapeutic doses of APAP. Applicability to other biological matrices was also demonstrated by measurement of protein-derived APAP-Cys in plasma collected from APAP-treated mice, a common animal model of APAP-induced hepatotoxicity.

1. Introduction

Acetaminophen (APAP) is one of the most commonly used medications in the United States [1–4]. When used as indicated, APAP is an effective and well-tolerated analgesic and antipyretic

* Corresponding author. Tel.: +1 8015815117.
E-mail address: cook.sarah@utah.edu (S.F. Cook).

http://dx.doi.org/10.1016/j.jchromb.2015.01.028
1570-0232/

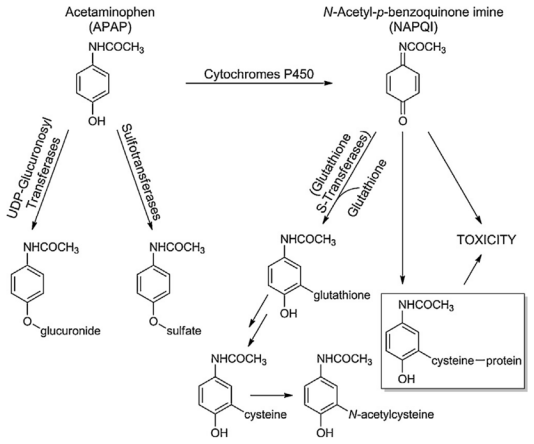

Fig. 1. Major APAP metabolic pathways with relationship to APAP protein adducts and toxicity.

agent [5–7]. However, at supratherapeutic doses, the drug has long been known to produce liver injury [8–11], and APAP overdose is currently the leading cause of acute liver failure in the United States [12]. Consequently, APAP is frequently utilized as a model hepatotoxicant [13–15], and the precise mechanistic pathways that ultimately result in APAP-induced liver injury are still under investigation [16]. Recent evidence of transient, asymptomatic elevations of liver enzymes in the serum of human subjects receiving APAP in a chronic, therapeutic fashion (2–4 g/day for ≥3 days) has also raised interest in studying the hepatic effects of such treatment [17–21].

Drug metabolism plays a pivotal role in APAP-induced hepatotoxicity (Fig. 1). APAP metabolism occurs primarily in the liver, where the drug undergoes glucuronidation and sulfation. The non-toxic glucuronide and sulfate metabolites are efficiently excreted in the urine. APAP can also be oxidized by hepatic cytochrome P450 enzymes to form the reactive intermediate *N*-acetyl-*p*-benzoquinone imine (NAPQI). At therapeutic doses, only a small portion (5–15%) of APAP is bioactivated to yield NAPQI; at higher doses, the glucuronidation and sulfation pathways are saturated, and greater amounts of NAPQI can form. This electrophilic species can be detoxified by conjugation with glutathione. However, the glutathione detoxification pathway is also saturable, and excess NAPQI instead binds to hepatic proteins. The relative capacity for bioactivation versus detoxification is reflected in the amount of NAPQI that is able to bind proteins covalently to form APAP protein adducts [22,23]. Hepatic formation [24] and localization [25] of the adducts are highly correlated with toxicity, which is thought to result from a combination of inactivation of critical hepatic proteins via NAPQI binding and oxidative stress [13,16].

As APAP-induced hepatic necrosis progresses, hepatic APAP protein adducts are released into the circulation and have been detected at high concentrations in the serum/plasma of humans and rodents following supratherapeutic APAP doses [26–31]. Serum APAP protein adducts have also been detected at lower concentrations in subjects taking therapeutic doses of the drug [32,33], although the mechanism by which the protein adducts appear in the circulation in the absence of hepatic necrosis is unclear. Because it is rarely possible to obtain liver tissue samples in studies involving human subjects, measurement of serum APAP protein adducts represents a valuable tool for assessment of APAP exposure and metabolism. It has also been proposed that detection of serum APAP protein adducts above a threshold concentration may be indicative of APAP-induced hepatotoxicity [29].

Early studies of APAP protein adducts relied on radiometric [24,34] and immunochemical [26,35–39] methods for qualitative and quantitative detection. Muldrew et al. later developed a sensitive high-performance liquid chromatography-electrochemical detection (HPLC-ECD) assay that obviated the use of radiolabeled drug or antibodies [27,30]. The actual analyte detected by the assay was a biomarker of APAP protein adducts, protein-derived 3-(cystein-*S*-yl)-acetaminophen (or acetaminophen-cysteine, APAP-Cys). Measurement of protein-derived APAP-Cys is expected to provide an accurate marker for quantification of APAP protein adducts because NAPQI has been shown to bind proteins primarily at the thiol moiety of cysteine residues [40,41]. In the method developed by Muldrew et al., aliquots of biological matrix were first dialyzed to remove non-protein-bound APAP-Cys, which is a metabolite of NAPQI (see Fig. 1). Dialyzed samples were subjected to digestion with a broad-spectrum protease and then prepared for HPLC-ECD analysis by protein precipitation with trichloroacetic acid [30].

James et al. optimized the efficiency and sensitivity of the original HPLC-ECD assay [28,29]. The improved assay replaced the dialysis step with a more efficient centrifugal gel filtration procedure for removal of non-protein-bound APAP-Cys [29]. We sought to adapt this method for analysis by HPLC-electrospray ionization-tandem mass spectrometry (HPLC-ESI-MS/MS) to provide enhanced specificity and sensitivity for detection of protein-derived APAP-Cys in human serum.

Herein we report a novel procedure for quantification of protein-derived APAP-Cys in human serum by HPLC-ESI-MS/MS. The assay has been validated on two different analytical instrument platforms. Details of the methods are provided along with validation results. The utility of the assay is illustrated by a brief summary of the analysis of serum samples collected from human subjects taking chronic, therapeutic doses of APAP. Additionally, because mice are frequently used in animal models of APAP-induced hepatotoxicity, we demonstrate application of the assay to plasma samples collected from mice that received a range of APAP doses.

2. Materials and methods

2.1. Materials

APAP-Cys powder (3-cysteinylacetaminophen trifluoroacetic acid salt, ≥95% purity) was obtained from Toronto Research Chemicals (Toronto, ON, Canada). Norbuprenorphine-D_3 (NBup-D_3) solution (100 μg/mL in methanol) was obtained from Cerilliant (Round Rock, TX). Analyte-free human serum and mouse plasma (sodium heparin; pooled from male C57BL/6 mice) were obtained from BioChemed Services (Winchester, VA). Spectra/Por 6 dialysis membrane (standard grade, regenerated cellulose, 3500 Da molecular weight cut-off, in 0.05% sodium azide, 18 mm width, 11.5 mm diameter) was obtained from Spectrum Laboratories (Rancho Dominguez, CA). Bio-Spin 6 Tris columns (6000 Da molecular weight cut-off) were obtained from Bio-Rad Laboratories (Hercules, CA). Protease type XIV from *Streptomyces griseus* (≥3.5 units/mg solid) and acetaminophen (analytical standard) were obtained from Sigma–Aldrich (St. Louis, MO). Ultrafree-MC centrifugal filter devices (Durapore PVDF, 0.22 μm) were obtained from EMD Millipore (Billerica, MA). Phosphate buffered saline pH 7.4 was obtained from Teknova (Hollister, CA). Sodium heparin solution (5000 USP units/mL, from porcine intestinal mucosa, APP Pharmaceuticals) was obtained from the University of Utah Hospital Pharmacy (Salt Lake City, UT). Sodium acetate trihydrate (ACS grade, BDH Chemicals) was obtained from VWR (Radnor, PA). Formic acid (88%) was obtained from Fisher Scientific (Pittsburgh, PA). LC–MS grade

acetonitrile and methanol were obtained from Honeywell Burdick and Jackson (Morristown, NJ). Glacial acetic acid was obtained from Spectrum Chemicals (New Brunswick, NJ). Ultrapure water (18.2 MΩ) for preparation of aqueous solutions was obtained by passage of deionized water through a Milli-Q Gradient A10 filtration system equipped with a Q-Gard 2 purification pack (EMD Millipore, Billerica, MA). Silanized glassware was prepared by vapor-phase silanization with hexamethyldisilazane (Pierce, Rockford, IL) under vacuum in an oven at 250 °C for 2 h.

2.2. Authentic clinical serum samples for assay verification

Clinical samples were collected from subjects enrolled in an Institutional Review Board-approved study (Colorado Multiple Institutional Review Board number 05-0139) in which APAP was administered in a chronic, therapeutic fashion (4 g/day). On day 0 (pre-dose) and after various numbers of treatment days, blood samples were obtained through venipuncture and collected in 5-mL, additive-free Vacutainer tubes (BD, Franklin Lakes, NJ). Blood samples were typically allowed to clot for a period of 15–20 min before centrifugation for 10 min at 3500 rpm in a swinging bucket centrifuge. In rare instances when blood could not be centrifuged shortly after clotting, samples were refrigerated until centrifugation, which was usually performed within 1–6 h. Serum supernatants were transferred to cryovials and stored at −80 °C. De-identified serum samples were shipped overnight on dry ice to the Center for Human Toxicology at the University of Utah and immediately stored at −80 °C until the time of preparation for analysis.

2.3. Authentic mouse plasma samples for assay verification

All animal procedures were approved by the Institutional Animal Care and Use Committee of the University of Utah. Male C57BL/6 mice (4 months old; 25–32 g) were obtained from the National Institute on Aging aged rodent colony (maintained by Charles River Laboratories, Wilmington, MA). For at least one week following shipment, mice were kept in a temperature-controlled facility with a 12-h light/dark cycle and ad libitum food and water access. Animals were not fasted prior to treatment. APAP was dissolved in warm phosphate buffered saline and administered via intraperitoneal injection at doses of 0, 75, 150, or 300 mg/kg (n = 5–7). APAP dosing solution concentrations were adjusted so that each animal received approximately the same volume. Two hours after dosing, mice were anesthetized with isoflurane in an induction chamber until non-responsive to tail pinch and then sacrificed by cervical dislocation. Blood samples were drawn from the inferior vena cava using syringes that were pre-rinsed with heparin solution. Following centrifugation at 3000 rpm for 10 min, plasma supernatants were isolated and then stored at −80 °C until the time of preparation for analysis.

2.4. Calibration standards and quality control (QC) samples

Stock solutions of APAP-Cys were prepared at 1 mM in methanol using a Mettler Toledo XS3DU microbalance (Columbus, OH) and silanized class-A volumetric flasks. APAP-Cys working solutions at 10, 1.0, and 0.10 μM were prepared by serial dilution of the stock in methanol/water (1/1, v/v). Separate sets of APAP-Cys stock and working solutions were prepared for calibrator and QC applications. APAP-Cys reference standard was not available in sufficient purity from different sources or lot numbers; however, calibrator and QC solution sets were prepared by different analysts. Internal standard (IS) working solution was prepared by dilution of the methanolic NBup-D_3 reference solution to 2 μM in water. All stock and working solutions were stored at −20 °C in silanized glass tubes.

To identify appropriate human serum lots for use as analyte-free matrix, individual lots were dialyzed or gel-filtered (see Sections 2.5.1 and 2.6.1), digested, extracted, analyzed, and confirmed to be negative. Appropriate human serum lots were then stored at −20 °C until use for preparation of calibrators and QC samples.

Calibrators and triplicate sets of QC samples were freshly prepared in silanized glass tubes for analysis with each validation or study sample batch. Calibrators were prepared by fortification of 100 μL dialyzed or gel-filtered (see Sections 2.5.1 and 2.6.1), analyte-free human serum with APAP-Cys calibrator working solutions to yield effective serum concentrations of 0.010, 0.020, 0.025, 0.050, 0.10, 0.25, 0.50, 1.0, 2.5, 5.0, and 10 μM. Similarly, QC samples were prepared by fortification of 100 μL dialyzed or gel-filtered, analyte-free human serum with APAP-Cys QC working solutions to yield effective serum concentrations of 0.030, 0.30, and 7.5 or 7.8 μM. Two additional dialyzed or gel-filtered, analyte-free human serum samples accompanied each batch for preparation with and without IS.

2.5. Method 1: Thermo Surveyor HPLC-TSQ Quantum triple-quadrupole mass spectrometer

2.5.1. Sample preparation

For method 1, calibrator, QC, validation, and study samples were prepared with dialyzed matrix. Analyte-free human serum (3 mL) was dialyzed (3500 Da molecular weight cut-off) against 3× 4 L of 10 mM aqueous sodium acetate pH 6.5 for 22 h at 5 °C, with replacement of dialysis buffer at 2 and 5 h. In cases where smaller volumes of individual serum lots were needed, dialysis was performed similarly but with 0.5 mL serum dialyzed against 3× 1 L of buffer. Dialyzed serum was stored frozen in silanized glass tubes until use.

Following fortification of calibrator and QC samples, 100 μL of 8 units/mL protease type XIV in water was added to each sample. Sample tubes were capped with PTFE-lined screw tops, vortexed gently to mix, and digested by incubation at 37 °C for 24 h in a thermostat-controlled water bath. After digestion, sample tubes were kept on ice whenever possible for the duration of sample extraction. IS working solution (20 μL) was added to each sample, and samples were vortexed briefly. To control for the addition of solvent that occurred during fortification of calibrator and QC samples with APAP-Cys working solution, all samples were brought to a total volume of 320 μL by addition of methanol/water (1/1/, v/v). Protein precipitation was performed by addition of acetonitrile (400 μL), vortex mixing, and equilibration of samples on ice for 10 min. Samples were then transferred to 1.5-mL microcentrifuge tubes and centrifuged for 10 min at 16,000 rpm, 5 °C in a Sorvall RC-5B refrigerated superspeed centrifuge (DuPont Instruments) fitted with an F-20/MICRO rotor. Sample supernatants were transferred to silanized glass tubes and evaporated to dryness under a 10–15 psi airstream in a TurboVap LV Evaporator (Zymark) with the water bath set to 50 °C. Sample residues were reconstituted with 200 μL of 0.1% aqueous formic acid and vortex mixed. Reconstituted samples were transferred to Ultrafree-MC filter devices and centrifuged for 2 min at 10,000 rpm, 5 °C in the Sorvall RC-5B centrifuge. Sample filtrates were transferred to conical polypropylene autosampler vials and stored in the refrigerated autosampler prior to HPLC-ESI-MS/MS analysis.

2.5.2. HPLC-ESI-MS/MS analysis

For analysis method 1, HPLC-ESI-MS/MS was conducted on a Surveyor HPLC system (LC Pump Plus with built-in vacuum degasser and quaternary pump, and autosampler with thermostatted sample tray and column compartment) interfaced with a TSQ Quantum triple-quadrupole mass spectrometer (Thermo Fisher Scientific Inc., Waltham, MA). Xcalibur software (version

1.4, Thermo Fisher Scientific Inc., Waltham, MA) was used for instrument control, data acquisition and analysis, and ESI-MS/MS parameter optimization.

Prepared samples were stored in the autosampler tray at 10 °C, and injection volume was 20 μL in partial loop mode. Samples were injected in the following order: calibration standards (ascending concentrations), analyte-free samples with and without IS, QC set 1, approximately half of the validation/study samples, QC set 2, remaining validation/study samples, QC set 3. Between injections, the autosampler needle was washed with methanol/water (1/1, v/v). Chromatographic separation was achieved with a YMC ODS-AQ HPLC column (2.0 × 50 mm, 3.0 μm particle size, YMC America, Inc., Allentown, PA) at ambient temperature and using a gradient mobile phase consisting of 0.1% formic acid in water (A) and methanol (B) at a flow rate of 0.25 mL/min. Mobile phase was held at 2% B for 6 min, increased linearly to 50% B over 1 min, held at 50% B for 6 min, decreased linearly to 2% B over 1 min, and then re-equilibrated at 2% B for 6 min, yielding a total run time of 20 min/injection. Typical retention times for APAP-Cys and NBup-D_3 were 11.5 and 13.7 min, respectively. The MS diverter valve was only directed to the ion source during the anticipated retention time range for analyte and IS.

The mass spectrometer was operated in ESI mode with positive polarity and selective reaction monitoring (SRM). Capillary temperature was set to 280 °C, and source collision energy was set to 5 V. High-purity nitrogen was used for sheath and auxiliary gas. Q2 collision-induced dissociation was achieved with ultra-high-purity argon at 1.5 mTorr. Ion source and MS/MS parameters were routinely re-optimized by infusion of approximately 30 μM solutions of APAP-Cys and NBup-D_3 in methanol at 20 μL/min into a 0.25 mL/min mobile phase flow of 50% B. Typical settings were: ion spray voltage: 3900 V; sheath gas pressure: 25 mTorr; and auxiliary gas: 20 mTorr. APAP-Cys was monitored using the 271.0 → 140.0 *m/z* transition with typical tube lens and collision energy voltages of 90 and 30 V, respectively. NBup-D_3 was monitored using the 417.0 → 417.0 *m/z* transition with typical tube lens and collision energy voltages of 100 and 22 V, respectively. The following SRM parameter settings were applied to all transitions: scan width: 1.000 amu; scan time: 0.20 s; and Q1 and Q3 peak widths (FWHM): 0.70 amu.

2.6. Method 2: Agilent 1260 Infinity HPLC-6460 triple-quadrupole mass spectrometer

2.6.1. Sample preparation

For method 2, calibrator, QC, cross-validation, and study samples were prepared with gel-filtered matrix. To provide sufficient analyte-free human serum for fortification of calibrator, QC, and validation samples, 150-μL aliquots of analyte-free human serum were filtered through two separate Bio-Spin 6 columns according to the manufacturer's instructions. Prior to serum filtration, buffer exchange was performed with three washes of 10 mM aqueous sodium acetate pH 6.5. Analyte-free serum filtrates were pooled in silanized glass tubes. Gel filtration of study samples was performed similarly except that 150 μL of each serum sample was filtered (two times per sample), and 100 μL of each filtrate was then transferred to a silanized glass tube to be used for protein digestion and sample extraction. When gel filtration was performed prior to the day of protein digestion, serum filtrates were stored frozen until use.

Following fortification of calibrator and QC samples and gel filtration of study samples, incubation with protease was performed exactly as detailed for Method 1 in Section 2.5.1. After protein digestion, sample extraction was carried out similarly to the Method 1 procedure, with the following minor simplifications: sample tubes were not kept on ice at any point; protein precipitation was performed by addition of 600 μL acetonitrile followed by 30 s vigorous vortex mixing; and samples were kept in silanized glass tubes after protein precipitation and centrifuged for 15 min at 1100 × *g*, ambient temperature in an IEC FL40 swing-out rotor centrifuge (Thermo Fisher Scientific Inc., Waltham, MA). The remainder of the preparation procedure agrees exactly with that detailed for Method 1.

2.6.2. HPLC-ESI-MS/MS analysis

For analysis method 2, HPLC-ESI-MS/MS was conducted on an Agilent 1260 Infinity HPLC system (inline solvent micro-degasser, binary LC pump, high-performance thermostatted autosampler, and 1290 Infinity thermostatted column compartment) interfaced with an Agilent 6460 triple-quadrupole mass spectrometer (Agilent Technologies, Santa Clara, CA). MassHunter Workstation software (Agilent Technologies, Santa Clara, CA) was used for instrument control, data acquisition, and ESI-MS/MS parameter optimization (version B.03.01) and for data analysis (version B.04.00).

Prepared samples were stored in the autosampler tray at 5 °C, and injection volume was 10 μL. Samples were injected in the same order as for Method 1. Between injections, the autosampler needle was washed with methanol/water (1/1, v/v). Chromatographic separation was achieved with an Agilent Poroshell 120 SB-C18 HPLC column (2.1 × 100 mm, 2.7 μm particle size, Agilent Technologies, Santa Clara, CA) maintained at 25 °C and using a gradient mobile phase consisting of 0.1% formic acid in water (A) and 0.1% formic acid in methanol (B) at a flow rate of 0.2 mL/min. Mobile phase was held at 3% B for 12.5 min, increased linearly to 95% B over 0.5 min, held at 95% B for 8 min, decreased linearly to 3% B over 0.5 min, and then re-equilibrated at 3% B for 4.5 min, yielding a total run time of 26 min/injection. Typical retention times for APAP-Cys and NBup-D_3 were 12.4 and 16.9 min, respectively. The MS diverter valve was only directed to the ion source during the anticipated retention time range for analyte and IS.

The mass spectrometer was operated in ESI + Agilent Jet Stream mode with positive polarity and multiple reaction monitoring (MRM). Ultra-high-purity nitrogen was used for source and collision cell gas. Ion source and MS/MS conditions were optimized by infusion of analyte and IS under similar conditions as described for Method 1. Optimal settings were: gas temperature: 350 °C; gas flow: 10 L/min; nebulizer pressure: 30 psi; sheath gas temperature: 400 °C; sheath gas flow: 9 L/min; capillary voltage: 3500 V; and nozzle voltage: 500 V. APAP-Cys was monitored using a quantification transition of 271.0 → 140.0 *m/z* (fragmentor voltage: 80 V; collision energy: 22 V) and a qualification transition of 271.0 → 96.0 *m/z* (fragmentor voltage: 80 V; collision energy: 45 V). NBup-D_3 was monitored using a quantification transition of 417.0 → 417.0 *m/z* (fragmentor voltage: 100 V; collision energy: 34 V). The following settings were applied to all transitions: MS1 resolution: widest (FWHM approximately 2.5 amu); MS2 resolution: wide (FWHM approximately 1.2 amu); and dwell time: 200 ms.

2.7. Quantitation calculations and acceptance criteria

Throughout method validation and sample analysis, calibration curves were constructed using the APAP-Cys/NBup-D_3 peak area ratio versus nominal APAP-Cys concentration. Curves were fit by quadratic regression with 1/*x* weighting. Back-calculated calibrator and QC concentrations determined by interpolation were required to be within 20% of the nominal concentration. Calibration standards that failed to meet this criterion were excluded from regression, and at least 75% of the calibrators were required to be included in regression. The lower limit of quantification (LLOQ) was defined as the lowest concentration of analyte with acceptable imprecision (≤20%) and accuracy (±20% of nominal concentration). At each QC concentration, at least two of the three replicates were

required to meet the ±20% accuracy criterion in order for a sample batch to pass.

2.8. Method validation

2.8.1. Method 1: Full validation

The method was validated by assessment of LLOQ, intra- and inter-day imprecision and accuracy, overall process efficiency, stock solution stability, sample stability, specificity, and matrix effect.

To identify an appropriate, reproducible LLOQ, analyte-free human serum was fortified with APAP-Cys at several concentrations ranging from 0.010 to 0.10 μM ($n = 3$ for each concentration). Fortified samples were prepared and analyzed according to Method 1.

Imprecision and accuracy of the method were determined from replicate samples of analyte-free human serum fortified with APAP-Cys at 0.030, 0.30 and 7.5 μM, corresponding to low, medium, and high QC concentrations, respectively. Intra-assay imprecision and accuracy at each concentration were determined from five replicate samples assayed within the same analytical batch. Inter-assay imprecision and accuracy at each concentration were calculated from a total of 18 replicates assayed over four separate analytical batches. Imprecision is expressed as percent coefficient of variation (% CV) and accuracy as a percent of the nominal concentration.

Overall process efficiency (recovery plus ion suppression/enhancement) for extraction of APAP-Cys from human serum was determined at low, medium, and high QC concentrations. Process efficiency for extraction of NBup-D_3 from human serum was determined at 0.5 μM. Analyte-free human serum was fortified with APAP-Cys or NBup-D_3 and prepared as detailed in Section 2.5.1 ($n = 5$). Unextracted samples representing 100% recovery and 0% ion suppression/enhancement of the same analyte and IS amounts were prepared by fortification of 0.1% aqueous formic acid with appropriate amounts of APAP-Cys and NBup-D_3 ($n = 5$). Process efficiencies (%) were calculated by dividing the mean peak area of analyte or IS in extracted samples by the corresponding mean peak area in unextracted samples.

Stability of APAP-Cys stock solution (1 mM in methanol) was assessed by comparison of freshly dissolved stock solution to stock solutions that had been stored at various temperatures for varying lengths of time. Stock solutions were diluted in 0.1% aqueous formic acid to a concentration appropriate for injection on the HPLC-ESI-MS/MS ($n = 5$ for each stock), and the solutions were analyzed as described in Section 2.5.2. The following storage conditions were tested: 17 h at room temperature and approximately 2, 7, and 9 months at −20 °C. Stability (%) was calculated by dividing the mean APAP-Cys peak areas from test solutions prepared from stored stocks by the mean APAP-Cys peak area from test solutions prepared from the fresh stock.

Matrix stability experiments were performed by analysis of analyte-free human serum fortified with APAP-Cys at low and high QC concentrations of 0.030 and 7.5 μM, respectively. Five replicates at each concentration were subjected to a variety of storage and handling conditions, and the stored QC samples were compared to freshly prepared calibrator and QC samples. Stability of APAP-Cys in human serum at room temperature was assessed by preparation of samples that were stored at room temperature for 24 h. Stability in human serum was also assessed by preparation of samples that were subjected to three cycles of freezing (at least 12 h storage at −80 °C) and thawing (60 min at room temperature). Stability of prepared samples was assessed following storage in the autosampler (10 °C) for 48 h and at −20 °C for six days.

Specificity of the method was assessed by analysis of human serum from six APAP-abstinent individuals. To allow for identification of potential interfering peaks co-eluting with either APAP-Cys or IS, serum samples were prepared in triplicate according to the usual procedure (see Section 2.5.1), and one sample from each individual was prepared similarly but without IS fortification. For samples prepared with IS, the specificity acceptance criterion for each lot was that the mean peak area ratio of any peak at the analyte retention time (271.0 → 140.0 *m/z* transition) to the IS peak must be <20% of the corresponding mean peak area ratio from concurrently assayed duplicate LLOQ samples. For samples prepared without IS, any peak area at the IS retention time (417.0 → 417.0 *m/z* transition) was required to be <5% of the mean IS peak area in the LLOQ samples in order to meet acceptance criterion.

The effect of biological matrix on analyte and IS ionization was evaluated using a post-column infusion method [42]. Analyte- and IS-free human serum was prepared and injected onto the HPLC column. Simultaneously, a solution of 10 μM APAP-Cys and 2 μM IS in methanol was introduced into the post-column effluent via a T connector, and the intensities of analyte and IS SRM transitions were visually monitored in real time.

2.8.2. Method 2: Cross-validation

Method 2 was validated by assessment of LLOQ, intra- and inter-day imprecision and accuracy, and stability of prepared samples stored in the autosampler. As an additional cross-validation measure, four sample batches were injected onto both HPLC-ESI-MS/MS systems for analysis by Methods 1 and 2.

To evaluate a potential LLOQ of 0.010 μM, analyte-free human serum was fortified with APAP-Cys at 0.010 μM on three separate days ($n = 3$ for each day) and then prepared and analyzed according to Method 2.

Imprecision and accuracy of Method 2 were determined as for Method 1. Intra-assay imprecision and accuracy were determined from five replicate samples assayed within the same analytical batch at low, medium, and high QC concentrations of 0.030, 0.30, and 7.8 μM, respectively. Inter-assay imprecision and accuracy at each concentration were calculated from a total of 18 replicates assayed over six separate analytical batches.

Autosampler stability for Method 2 was assessed similarly to the procedure used for Method 1. Three replicate samples at low and high QC concentrations of 0.030 and 7.8 μM, respectively, were prepared and analyzed according to Method 2. Following initial analysis, the prepared samples were stored in the autosampler (5 °C) for 72 h and then compared to freshly prepared calibrator and QC samples.

Method 2 was further cross-validated with Method 1 by comparison of four sample batches that were prepared according to Method 2 and then injected onto both systems for HPLC-ESI-MS/MS analysis by Methods 1 and 2. Each batch included two to three sets of QC samples along with human serum samples from clinical study participants.

2.9. Application of method for analysis of mouse study samples

Calibrator and QC samples were prepared with analyte-free mouse plasma that was diluted 10-fold in 10 mM aqueous sodium acetate pH 6.5 (dialysis buffer) and then subjected to one round of gel filtration as described for Method 2 in Section 2.6.1. Fortification of analyte-free matrix with APAP-Cys calibrator and QC working solutions was performed as detailed in Section 2.4. Mouse study samples were diluted 10-fold in ultrapure water and dialyzed as described for Method 1 in Section 2.5.1 (0.5 mL sample volume procedure). Aliquots (150 μL) of dialyzed samples were then subjected to two rounds of gel filtration as detailed for Method 2. The remainder of the sample preparation procedure was performed according to Method 2.

2.10. Statistical software

Correlation and mouse dose-response analyses were performed in GraphPad Prism 6 (GraphPad Software, Inc., La Jolla, CA). All other calculations were performed in Excel (version 14.0, Microsoft Corp., Redmond, WA).

3. Results and discussion

3.1. Method development

At the time of initial method development, deuterated APAP-Cys was unavailable in sufficient purity (≥95%) for use as an IS. NBup-D_3 was selected as the IS based on the laboratory's previous experience with the chromatographic and mass spectral properties of the compound. A deuterated form of norbuprenorphine was selected to avoid interference with norbuprenorphine, a metabolite of the drug buprenorphine.

The mass transition for analyte quantification (271.0 → 140.0 *m/z*) was selected because it provided acceptable specificity and because the abundance of the product ion provided adequate sensitivity. The same mass transition has also been employed for quantification of non-protein-bound APAP-Cys in human plasma using triple quadrupole linear ion trap MS detection [43]. Method 2 incorporated an additional provision for APAP-Cys identification through inclusion of an analyte qualification transition (271.0 → 96.0 *m/z*). Samples were required to have a qualifier ion peak with signal-to-noise greater than 3 in order for a quantifiable APAP-Cys concentration to be reported, and this was particularly helpful for samples with concentrations near the LLOQ. For NBup-D_3, monitoring of a single precursor ion transition (417.0 → 417.0 *m/z*) provided adequate IS specificity.

3.2. Validation of analysis method 1: Thermo Surveyor HPLC-TSQ Quantum triple-quadrupole mass spectrometer

Based on the criteria described in Section 2.7, the LLOQ for Method 1 was determined to be 0.020 μM. The mean observed concentration for this LLOQ was 0.021 μM, with 106.7% accuracy and 9.76% CV. Calibration curves were fit well by quadratic regression with 1/*x* weighting over the concentration range of 0.020–10 μM. Back-calculation of calibrator and QC concentrations by interpolation yielded values within ±20% of nominal concentration, and coefficients of determination (R^2) for calibration curves were ≥0.99. No evidence of chromatographic carryover was observed when analyte-free human serum samples were injected immediately after the highest calibration standard.

Imprecision, accuracy, and process efficiency data for Method 1 are summarized in Table 1. The method was found to be highly precise and accurate. Across all three QC concentrations, intra-assay imprecision did not exceed 5% CV, and inter-assay imprecision did not exceed 10% CV. Mean intra- and inter-assay accuracies were within ±6% and ±9% of nominal concentrations, respectively. Additionally, mean overall process efficiencies for APAP-Cys and NBup-D_3 ranged from 80 to 110%, suggesting adequate recovery and insignificant ion suppression or enhancement from human serum.

Methanolic APAP-Cys stock solution appeared stable (within ±20% of freshly prepared solution) following overnight storage at room temperature and up to seven months of storage at −20 °C, but significant deterioration was clearly evident by nine months of storage at −20 °C (mean ± standard deviation was 73.3 ± 3.3% of freshly prepared solution). Based on these results, it was determined that analyte stock solution should be used within six months of preparation.

APAP-Cys was adequately stable in human serum and prepared samples. At low and high QC concentrations, mean accuracies were within ±20% of nominal concentrations following storage of fortified human serum at room temperature for 24 h, three freeze–thaw cycles of fortified human serum, and storage of prepared samples in the autosampler at 10 °C for 48 h or at −20 °C for six days (Table 2).

Analysis of human serum from six APAP-abstinent individuals demonstrated that the assay provides requisite specificity. In samples fortified with IS, mean peak area ratios (analyte/IS) were all <5% of the mean LLOQ peak area ratio. Similarly, in samples that were not fortified with IS, peak areas in the 417.0 → 417.0 *m/z* IS transition were all <0.5% of the mean IS peak area from the LLOQ samples.

The post-column infusion method for assessment of matrix effect showed neither signal suppression nor enhancement at the analyte and IS retention times.

3.3. Cross-validation of analysis method 2: Agilent 1260 Infinity HPLC-6460 triple-quadrupole mass spectrometer

Subsequent to validation of Method 1 with analysis on a Thermo Surveyor HPLC-TSQ Quantum system, the laboratory acquired a new instrument for application of this assay. The method was cross-validated on an Agilent 1260 Infinity HPLC-6460 triple-quadrupole system (Method 2), which was thereafter used for routine analysis. The validation results for both methods are presented in this paper to illustrate the versatility of the assay on two different HPLC-ESI-MS/MS platforms. The transition between instruments also coincided closely with the adoption of a centrifugal gel filtration procedure for removal of non-protein-bound APAP-Cys; therefore, the details of that procedure are provided with Method 2 in Section 2.6.1.

Based on the criteria described in Section 2.7, the LLOQ for Method 2 was determined to be 0.010 μM. Calibration curves were fit well by quadratic regression with 1/*x* weighting over the concentration range of 0.010–10 μM. Back-calculation of calibrator and QC concentrations by interpolation yielded values within ±20% of nominal concentration, and R^2 values for calibration curves were ≥0.99. No evidence of chromatographic carryover was observed when analyte-free human serum samples were injected immediately after the highest calibration standard. Representative MRM chromatograms are provided for analyte- and IS-free serum (Fig. 2a), analyte-free serum fortified with IS (Fig. 2b), and a 0.010 μM APAP-Cys calibration standard (LLOQ) (Fig. 2c).

Imprecision and accuracy data for Method 2 are summarized in Table 3. The method was found to be highly precise and accurate. Across all three QC concentrations, intra-assay imprecision did not exceed 6% CV, and inter-assay imprecision did not exceed 8% CV. Mean intra- and inter-assay accuracies were within ±13% and ±4% of nominal concentrations, respectively.

APAP-Cys was stable in prepared samples stored in the autosampler at 5 °C for 72 h (Table 2). At low and high QC concentrations, mean accuracies were within ±13% of nominal concentrations.

Imprecision and accuracy data are provided in Table 4 for low, medium, and high QC samples from four batches that were prepared according to Method 2 and then analyzed by both Methods 1 and 2. For Method 1, imprecision and mean accuracies ranged from 5–13% and 95–107%, respectively. Results for Method 2 were similar and slightly improved compared to Method 1, with imprecision and mean accuracies ranging from 4–5% and 98–102%, respectively. The four sample batches that were analyzed by both methods also included 87 human serum samples from clinical study participants. Of these samples, 35 were determined to be <LLOQ by both methods, and two were <LLOQ by Method 1 but quantifiable by Method 2. For the remaining 50 samples, protein-derived APAP-Cys

Table 1
Intra- and inter-assay imprecision/accuracy and process efficiency for determination of APAP-Cys in human serum by Method 1.

Nominal concentration (μM)	Intra-assay imprecision and accuracy ($n = 5$)			Inter-assay imprecision and accuracy ($n = 18$)			Process efficiency (%)[b]
	Observed concentration (μM)[a]	Imprecision (% CV)	Mean accuracy (%)	Observed concentration (μM)[a]	Imprecision (% CV)	Mean accuracy (%)	
0.030	0.029 ± 0.001	4.22	96.7	0.030 ± 0.002	7.15	101.1	110.0 ± 8.9
0.30	0.312 ± 0.003	0.89	103.9	0.30 ± 0.02	5.10	100.0	92.9 ± 10.8
7.5	7.9 ± 0.1	1.88	105.7	8.1 ± 0.5	6.27	108.6	79.8 ± 4.2
0.5 (IS)	n/a	n/a	n/a	n/a	n/a	n/a	97.1 ± 10.4

[a] Reported values are mean concentration ± standard deviation.
[b] Reported values are mean % process efficiency ± standard deviation.

Table 2
Stability of APAP-Cys in human serum.

Nominal concentration (μM)	Stability in human serum (%)[a]		Stability in prepared samples (%)[a]		
	24 h at room temperature	3 freeze–thaw cycles	48 h at 10 °C (autosampler, Method 1)	72 h at 5 °C (autosampler, Method 2)	6 days at −20 °C
0.030	100.0 ± 5.8	116.0 ± 12.3	92.7 ± 5.5	108.0 ± 2.8	110.0 ± 5.3
7.5	96.6 ± 1.2	114.2 ± 5.7	114.6 ± 0.7	87.4 ± 0.6	110.6 ± 3.8

[a] Reported values are mean % nominal concentration ± standard deviation.

Table 3
Intra- and inter-assay imprecision/accuracy for determination of APAP-Cys in human serum by Method 2.

Nominal concentration (μM)	Intra-assay imprecision and accuracy ($n = 5$)			Inter-assay imprecision and accuracy ($n = 18$)		
	Observed concentration (μM)[a]	Imprecision (% CV)	Mean accuracy (%)	Observed concentration (μM)[a]	Imprecision (% CV)	Mean accuracy (%)
0.030	0.032 ± 0.001	2.96	107.8	0.030 ± 0.002	6.12	102.7
0.30	0.33 ± 0.02	5.33	112.7	0.29 ± 0.02	5.62	97.8
7.8	8.0 ± 0.1	1.06	103.6	7.5 ± 0.6	7.74	96.7

[a] Reported values are mean concentration ± standard deviation.

Table 4
Cross-validation of Method 1 and Method 2 for determination of APAP-Cys in human serum.

Nominal concentration (μM)	Method 1 ($n = 11$)			Method 2 ($n = 11$)		
	Observed concentration (μM)[a]	Imprecision (% CV)	Mean accuracy (%)	Observed concentration (μM)[a]	Imprecision (% CV)	Mean accuracy (%)
0.030	0.029 ± 0.004	13.03	95.0	0.031 ± 0.001	4.26	102.4
0.30	0.32 ± 0.02	5.25	106.8	0.30 ± 0.01	3.73	101.3
7.5	7.7 ± 0.7	9.56	102.1	7.4 ± 0.3	4.66	98.4

[a] Reported values are mean concentration ± standard deviation.

concentrations from Methods 1 and 2 were highly correlated, with a Pearson correlation coefficient of 0.91 (Fig. 3).

3.4. Application to clinical samples

The methods presented in this paper have been successfully applied for determination of protein-derived APAP-Cys in the serum of clinical study participants taking chronic, therapeutic doses of APAP. Representative MRM chromatograms from Method 2 show undetectable protein-derived APAP-Cys in serum collected prior to APAP ingestion (Fig. 4a) and protein-derived APAP-Cys quantified at 0.10 μM in serum collected from the same subject on day 7 of the 4 g APAP/day regimen (Fig. 4b). For this application, the methods provided suitable, adequately sensitive quantitative ranges. Of 500 consecutive study samples collected after at least two days of APAP ingestion, 77% were >0.020 μM (Method 1 LLOQ) and 79% were >0.010 μM (Method 2 LLOQ). None of the 500 samples had concentrations that fell above the upper limit of quantification.

3.5. Application to mouse model samples

Since mice are frequently used in animal models of APAP-induced hepatotoxicity, the application of Method 2 for determination of protein-derived APAP-Cys in mouse plasma is also demonstrated. For these illustrative purposes, plasma was used in place of serum because plasma tends to be collected more often than serum in murine studies. APAP was administered to mice in sub-toxic (75 mg/kg) to toxic (300 mg/kg) doses, and protein-derived APAP-Cys plasma concentrations were well within the quantitative limits of the assay in samples collected two hours after drug administration (Fig. 5). In all plasma samples collected from mice treated with vehicle control, protein-derived APAP-Cys concentrations were <LLOQ. Interestingly, the observed concentration range of protein-derived APAP-Cys in the 300 mg/kg treatment group (1–7 μM) is fairly consistent with recent results obtained through an alternative approach for measuring a specific APAP protein adduct. Switzar et al. [44] measured APAP-mouse serum

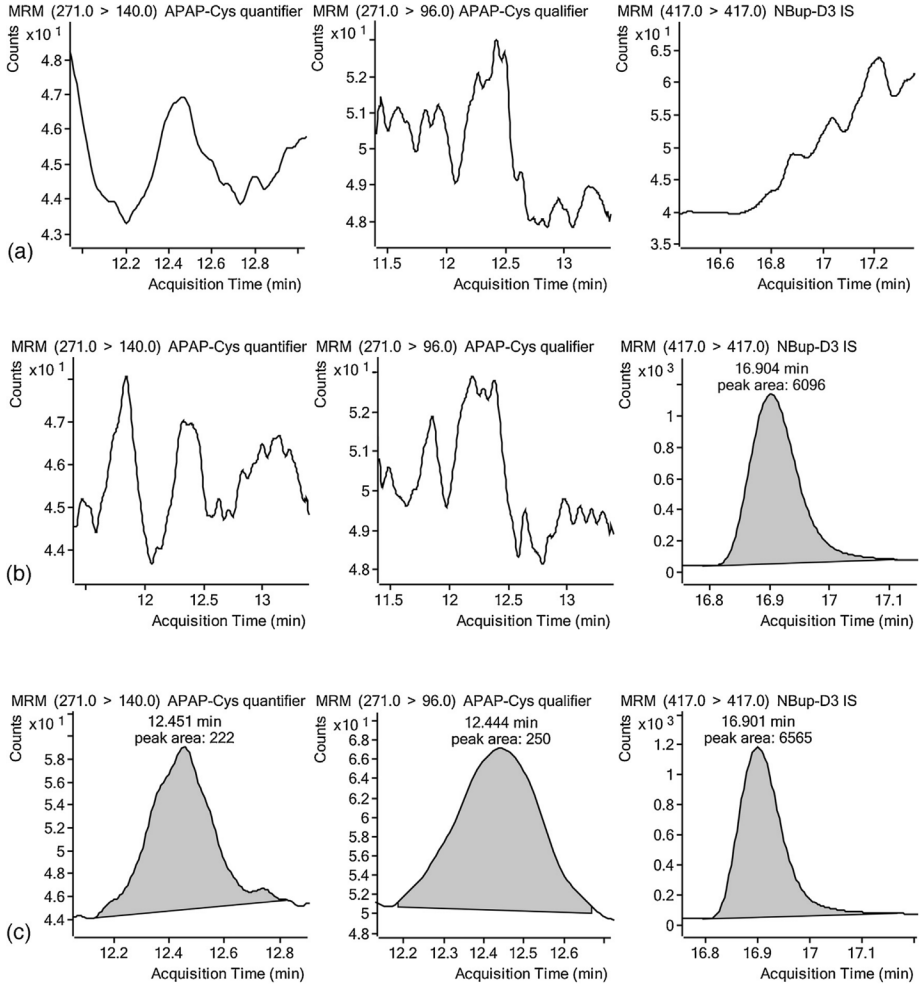

Fig. 2. Representative MRM chromatograms for determination of APAP-Cys in human serum by Method 2. (a) Analyte- and IS-free serum. (b) Analyte-free serum fortified with IS at 0.5 μM. (c) Serum fortified with APAP-Cys at LLOQ of 0.010 μM and IS at 0.5 μM.

albumin adducts by utilizing affinity chromatography, gel filtration, tryptic digestion, and LC–MS analysis. Despite this methodological variation and significant experimental differences (mouse strain and sex, APAP dosing route, biological matrix, and sample collection time), mouse serum samples collected 1 day after treatment with 300 mg/kg APAP had a mean concentration of approximately 2 μM APAP-mouse serum albumin.

3.6. Additional considerations

Although this paper focuses on the validation and application of the reported methods for quantification of protein-derived APAP-Cys in human serum, the assay is equally applicable to other matrices of interest. For example, we have successfully utilized the procedure for determination of protein-derived APAP-Cys in mouse liver and kidney tissue [31] and in culture medium and cell lysates collected from hepatic cell lines [45]. Several features of the methods described herein warrant special consideration prior to application of this procedure to any given study. As much as possible, these concerns should be addressed at the beginning of a particular study so that specimen processing can be maintained consistently across the samples to be compared within the study.

First, since the assay quantifies protein-derived APAP-Cys as a biomarker of APAP protein adducts, it is critical that non-protein-bound APAP-Cys be thoroughly removed prior to the protein digestion step. The adequacy of an approach for removal of non-protein-bound APAP-Cys can easily be tested by applying the given technique (e.g., dialysis or gel filtration) to a representative range of biological samples from a particular study and then omitting the protein digestion step from the sample preparation procedure. With this modified preparation, the absence of quantifiable APAP-Cys from all test samples would suggest that the technique is sufficient; the presence of any quantifiable analyte suggests that additional measures are required for removal of non-protein-bound APAP-Cys. For instance, in the present report, it was determined that two gel filtration passages provided adequate removal of non-protein-bound APAP-Cys from the serum of subjects taking chronic, therapeutic APAP; however, when this

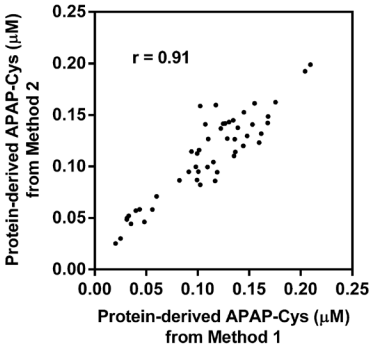

Fig. 3. Correlation between 50 protein-derived APAP-Cys concentrations determined by Methods 1 and 2 in serum samples from clinical study subjects. Not reflected in the figure are 35 samples that were determined to be <LLOQ by both methods and two samples that were quantifiable by Method 2 but determined to be <LLOQ by Method 1.

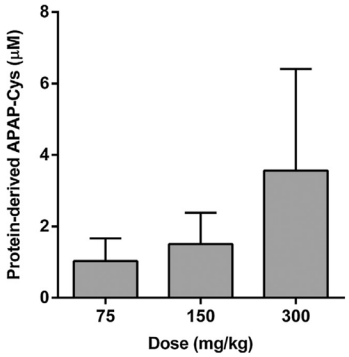

Fig. 5. Determination of protein-derived APAP-Cys plasma concentrations by Method 2 in mice treated with varying doses of APAP. Data are expressed as mean ± SD of $n = 5–7$ animals. Protein-derived APAP-Cys concentrations in the plasma of all mice treated with vehicle control were <LLOQ.

assay was applied to serum samples collected from APAP overdose patients, the lengthier, more labor-intensive dialysis step had to be included in order to achieve satisfactory non-protein-bound APAP-Cys removal (data not shown). Similarly, dialysis had to be included when processing plasma samples from mice treated with a toxic APAP dose (300 mg/kg), and plasma samples from mice treated with lower doses were handled equivalently in order to control for potential matrix effects.

A second consideration, which is closely related to the first, is the choice of an appropriate technique for preparation of analyte-free matrix. The biological matrix used for calibrator and QC samples is generally analyte-free even prior to dialysis or gel filtration; however, the procedures used for removal of non-protein-bound APAP-Cys can alter the composition of the biological matrix, and it is desirable to process the analyte-free matrix in a similar fashion in order to control for potential matrix effects. Nevertheless, these procedures are costly (gel filtration), lengthy (dialysis), and labor intensive (dialysis), so it is preferable to identify the minimum amount of processing that provides adequate control of matrix effects. This can be achieved by comparison of a reference set of QC samples prepared from analyte-free matrix that has been processed equivalently to study samples with a test set of QC samples prepared from analyte-free matrix that has undergone reduced processing. The reduced procedure can be considered appropriate if the test and reference QC results are similar in terms of accuracy, imprecision, and absolute peak areas of analyte and IS. For example,

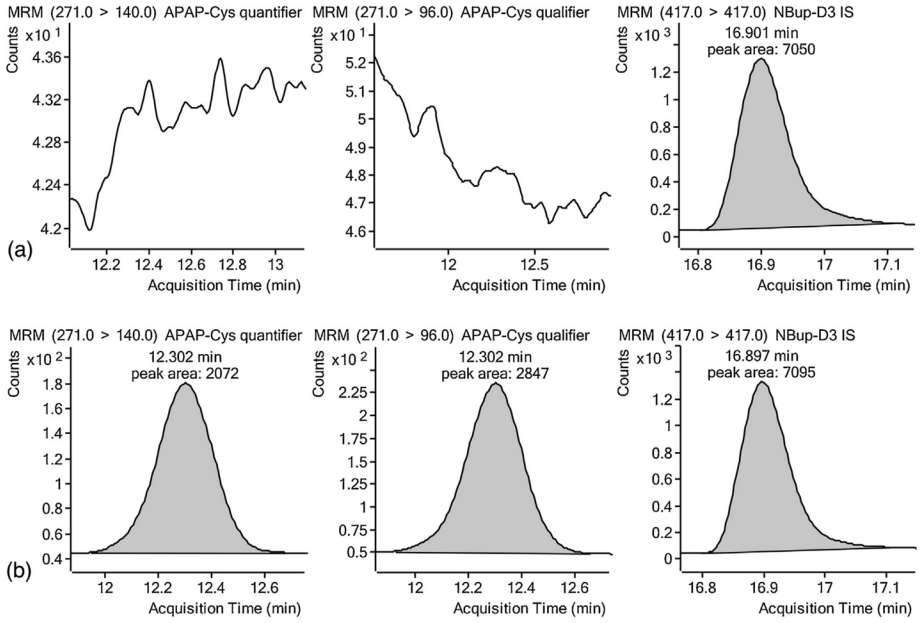

Fig. 4. Representative MRM chromatograms for determination of protein-derived APAP-Cys in human serum by Method 2. (a) Undetectable protein-derived APAP-Cys in a day 0 (pre-dose) sample from a clinical study participant. (b) Protein-derived APAP-Cys quantified at 0.10 μM in a day 7 sample from the same clinical study participant receiving 4 g APAP/day.

in the application of this method to analysis of mouse study samples, it was possible to omit the dialysis step and one of the two gel filtration passages from the preparation of analyte-free matrix used for calibration standards and QC samples.

Finally, the amount of protease required for adequate protein digestion may vary from study to study. Since the assay does not assess the extent of protein digestion in a given sample, it should be established that the amount of protease used in sample preparation for a particular study provides maximal release of protein-derived APAP-Cys within the anticipated concentration range. However, in our experience, the ion source becomes visibly dirtier when greater amounts of protease are used, so it is also prudent to avoid excessive protease in order to maintain the cleanliness and sensitivity of the analytical instrument. An appropriate protease concentration can be identified by digesting samples in the expected concentration range with varying amounts of protease. If necessary, individual samples can be pooled first to provide sufficient volume for multiple incubations. The optimal amount of protease will be the lowest concentration that provides plateau values for protein-derived APAP-Cys in the anticipated concentration range of the study. For instance, in the reported application of this assay to clinical samples, addition of 8 units/mL protease provided adequate protein digestion in serum collected from subjects taking chronic, therapeutic doses of APAP: With addition of 8 units/mL protease, quantification of protein-derived APAP-Cys from a pooled serum sample was found to be highly reproducible ($n = 5$; mean: 0.09 μM; CV: 5%), and the mean concentration of protein-derived APAP-Cys did not increase when the same pooled sample was prepared with addition of 24 units/mL protease ($n = 5$; mean: 0.08 μM; CV: 5%). However, application of this assay to serum samples collected from APAP overdose patients required addition of 40 units/mL protease in order to achieve maximal release of protein-derived APAP-Cys (data not shown).

4. Conclusion

A novel procedure for quantification of protein-derived APAP-Cys in human serum by HPLC-ESI-MS/MS was developed and successfully validated on two different analytical instrument platforms. The utility and sensitivity of the assay were demonstrated by analysis of samples collected from human subjects taking APAP in a chronic, therapeutic fashion. Applicability to other biological matrices was also illustrated in a mouse model study. In summary, the reported methods were found to be sensitive, specific, accurate, precise, and efficient for quantification of protein-derived APAP-Cys, a biomarker of APAP protein adducts.

Authors' contributions

DGW, DER, RCD, JLG, and SCC secured funding. RCD and JLG designed and performed the clinical study. DER and SFC designed and performed the mouse study. ADK, SFC, YC, GJM, and HKN developed, validated, and applied the analytical methods. SFC performed the statistical analysis. SFC, DGW, and DER drafted the manuscript, and all authors contributed to manuscript revisions and reviewed the final version.

Acknowledgements

This work was supported by a contract for analytical laboratory services from McNeil Consumer Healthcare (Division of McNEIL-PPC, Inc., Fort Washington, PA) (to DGW and DER), by investigator-initiated research grants from McNeil Consumer Healthcare (to RCD, JLG, and SCC), and by a pilot grant from the University of Utah Center on Aging (to DER). McNeil Consumer Healthcare did not participate in the design, performance, analysis, or interpretation of this work. SFC received stipend support from the American Foundation for Pharmaceutical Education (predoctoral fellowship) and the Howard Hughes Medical Institute (Med into Grad Initiative).

References

[1] D.W. Kaufman, J.P. Kelly, L. Rosenberg, T.E. Anderson, A.A. Mitchell, Recent patterns of medication use in the ambulatory adult population of the United States: the Slone survey, JAMA 287 (2002) 337.
[2] R. Paulose-Ram, R. Hirsch, C. Dillon, K. Losonczy, M. Cooper, Y. Ostchega, Prescription and non-prescription analgesic use among the US adult population: results from the third National Health and Nutrition Examination Survey (NHANES III), Pharmacoepidemiol. Drug Saf. 12 (2003) 315.
[3] R. Paulose-Ram, R. Hirsch, C. Dillon, Q. Gu, Frequent monthly use of selected non-prescription and prescription non-narcotic analgesics among U.S. adults, Pharmacoepidemiol. Drug Saf. 14 (2005) 257.
[4] L. Vernacchio, J.P. Kelly, D.W. Kaufman, A.A. Mitchell, Medication use among children <12 years of age in the United States: results from the Slone Survey, Pediatrics 124 (2009) 446.
[5] R.C. Dart, E. Bailey, Does therapeutic use of acetaminophen cause acute liver failure? Pharmacotherapy 27 (2007) 1219.
[6] A.M. Larson, Acetaminophen hepatotoxicity, Clin. Liver Dis. 11 (2007) 525.
[7] G.G. Graham, M.J. Davies, R.O. Day, A. Mohamudally, K.F. Scott, The modern pharmacology of paracetamol: therapeutic actions, mechanism of action, metabolism, toxicity and recent pharmacological findings, Inflammopharmacology 21 (2013) 201.
[8] E.M. Boyd, G.M. Bereczky, Liver necrosis from paracetamol, Br. J. Pharmacol. Chemother. 26 (1966) 606.
[9] D.G. Davidson, W.N. Eastham, Acute liver necrosis following overdose of paracetamol, Br. Med. J. 2 (1966) 497.
[10] J.S. Thomson, L.F. Prescott, Liver damage and impaired glucose tolerance after paracetamol overdosage, Br. Med. J. 2 (1966) 506.
[11] B. McJunkin, K.W. Barwick, W.C. Little, J.B. Winfield, Fatal massive hepatic necrosis following acetaminophen overdose, JAMA 236 (1976) 1874.
[12] A.M. Larson, J. Polson, R.J. Fontana, T.J. Davern, E. Lalani, L.S. Hynan, J.S. Reisch, F.V. Schiodt, G. Ostapowicz, A.O. Shakil, W.M. Lee, Acetaminophen-induced acute liver failure: results of a United States multicenter, prospective study, Hepatology 42 (2005) 1364.
[13] H. Jaeschke, M.R. McGill, A. Ramachandran, Oxidant stress, mitochondria, and cell death mechanisms in drug-induced liver injury: lessons learned from acetaminophen hepatotoxicity, Drug Metab. Rev. 44 (2012) 88.
[14] M.J. Tunon, M. Alvarez, J.M. Culebras, J. Gonzalez-Gallego, An overview of animal models for investigating the pathogenesis and therapeutic strategies in acute hepatic failure, World J. Gastroenterol. 15 (2009) 3086.
[15] B. Fromenty, Bridging the gap between old and new concepts in drug-induced liver injury, Clin. Res. Hepatol. Gastroenterol. 37 (2013) 6.
[16] J.A. Hinson, D.W. Roberts, L.P. James, Mechanisms of acetaminophen-induced liver necrosis, Handb. Exp. Pharmacol. (2010) 369.
[17] K.J. Heard, J.L. Green, R.C. Dart, Serum alanine aminotransferase elevation during 10 days of acetaminophen use in nondrinkers, Pharmacotherapy 30 (2010) 818.
[18] K. Heard, J.L. Green, V. Anderson, B. Bucher-Bartelson, R.C. Dart, A randomized, placebo-controlled trial to determine the course of aminotransferase elevation during prolonged acetaminophen administration, BMC Pharmacol. Toxicol. 15 (2014) 39.
[19] P.B. Watkins, N. Kaplowitz, J.T. Slattery, C.R. Colonese, S.V. Colucci, P.W. Stewart, S.C. Harris, Aminotransferase elevations in healthy adults receiving 4 grams of acetaminophen daily: a randomized controlled trial, JAMA 296 (2006) 87.
[20] E.K. Kuffner, A.R. Temple, K.M. Cooper, J.S. Baggish, D.L. Parenti, Retrospective analysis of transient elevations in alanine aminotransferase during long-term treatment with acetaminophen in osteoarthritis clinical trials, Curr. Med. Res. Opin. 22 (2006) 2137.
[21] M.J. Prior, D.D. Harrison, M.E. Frustaci, A randomized, double-blind, placebo-controlled 12 week trial of acetaminophen extended release for the treatment of signs and symptoms of osteoarthritis, Curr. Med. Res. Opin. 30 (2014) 2377.
[22] M.R. McGill, H. Jaeschke, Metabolism and disposition of acetaminophen: recent advances in relation to hepatotoxicity and diagnosis, Pharm. Res. 30 (2013) 2174.
[23] L.P. James, P.R. Mayeux, J.A. Hinson, Acetaminophen-induced hepatotoxicity, Drug Metab. Dispos. 31 (2003) 1499.
[24] D.J. Jollow, J.R. Mitchell, W.Z. Potter, D.C. Davis, J.R. Gillette, B.B. Brodie, Acetaminophen-induced hepatic necrosis. II. Role of covalent binding in vivo, J. Pharmacol. Exp. Ther. 187 (1973) 195.
[25] D.W. Roberts, T.J. Bucci, R.W. Benson, A.R. Warbritton, T.A. McRae, N.R. Pumford, J.A. Hinson, Immunohistochemical localization and quantification of the 3-(cystein-S-yl)-acetaminophen protein adduct in acetaminophen hepatotoxicity, Am. J. Pathol. 138 (1991) 359.
[26] N.R. Pumford, J.A. Hinson, R.W. Benson, D.W. Roberts, Immunoblot analysis of protein containing 3-(cystein-S-yl)acetaminophen adducts in serum and subcellular liver fractions from acetaminophen-treated mice, Toxicol. Appl. Pharmacol. 104 (1990) 521.

[27] T.J. Davern 2nd, L.P. James, J.A. Hinson, J. Polson, A.M. Larson, R.J. Fontana, E. Lalani, S. Munoz, A.O. Shakil, W.M. Lee, Measurement of serum acetaminophen-protein adducts in patients with acute liver failure, Gastroenterology 130 (2006) 687.
[28] L.P. James, E.V. Capparelli, P.M. Simpson, L. Letzig, D. Roberts, J.A. Hinson, G.L. Kearns, J.L. Blumer, J.E. Sullivan, Acetaminophen-associated hepatic injury: evaluation of acetaminophen protein adducts in children and adolescents with acetaminophen overdose, Clin. Pharmacol. Ther. 84 (2008) 684.
[29] L.P. James, L. Letzig, P.M. Simpson, E. Capparelli, D.W. Roberts, J.A. Hinson, T.J. Davern, W.M. Lee, Pharmacokinetics of acetaminophen-protein adducts in adults with acetaminophen overdose and acute liver failure, Drug Metab. Dispos. 37 (2009) 1779.
[30] K.L. Muldrew, L.P. James, L. Coop, S.S. McCullough, H.P. Hendrickson, J.A. Hinson, P.R. Mayeux, Determination of acetaminophen-protein adducts in mouse liver and serum and human serum after hepatotoxic doses of acetaminophen using high-performance liquid chromatography with electrochemical detection, Drug Metab. Dispos. 30 (2002) 446.
[31] M.R. McGill, M. Lebofsky, H.R. Norris, M.H. Slawson, M.L. Bajt, Y. Xie, C.D. Williams, D.G. Wilkins, D.E. Rollins, H. Jaeschke, Plasma and liver acetaminophen-protein adduct levels in mice after acetaminophen treatment: dose-response, mechanisms, and clinical implications, Toxicol. Appl. Pharmacol. 269 (2013) 240.
[32] K.J. Heard, J.L. Green, L.P. James, B.S. Judge, L. Zolot, S. Rhyee, R.C. Dart, Acetaminophen-cysteine adducts during therapeutic dosing and following overdose, BMC Gastroenterol. 11 (2011) 20.
[33] L.P. James, A. Chiew, S.M. Abdel-Rahman, L. Letzig, A. Graudins, P. Day, D. Roberts, Acetaminophen protein adduct formation following low-dose acetaminophen exposure: comparison of immediate-release vs extended-release formulations, Eur. J. Clin. Pharmacol. 69 (2013) 851.
[34] W.Z. Potter, D.C. Davis, J.R. Mitchell, D.J. Jollow, J.R. Gillette, B.B. Brodie, Acetaminophen-induced hepatic necrosis. III. Cytochrome P-450-mediated covalent binding in vitro, J. Pharmacol. Exp. Ther. 187 (1973) 203.
[35] D.W. Roberts, N.R. Pumford, D.W. Potter, R.W. Benson, J.A. Hinson, A sensitive immunochemical assay for acetaminophen-protein adducts, J. Pharmacol. Exp. Ther. 241 (1987) 527.
[36] J.B. Bartolone, K. Sparks, S.D. Cohen, E.A. Khairallah, Immunochemical detection of acetaminophen-bound liver proteins, Biochem. Pharmacol. 36 (1987) 1193.
[37] J.B. Bartolone, W.P. Beierschmitt, R.B. Birge, S.G. Hart, S. Wyand, S.D. Cohen, E.A. Khairallah, Selective acetaminophen metabolite binding to hepatic and extrahepatic proteins: an in vivo and in vitro analysis, Toxicol. Appl. Pharmacol. 99 (1989) 240.
[38] N.R. Pumford, J.A. Hinson, D.W. Potter, K.L. Rowland, R.W. Benson, D.W. Roberts, Immunochemical quantitation of 3-(cystein-S-yl)acetaminophen adducts in serum and liver proteins of acetaminophen-treated mice, J. Pharmacol. Exp. Ther. 248 (1989) 190.
[39] P.A. Webster, D.W. Roberts, R.W. Benson, G.L. Kearns, Acetaminophen toxicity in children: diagnostic confirmation using a specific antigenic biomarker, J. Clin. Pharmacol. 36 (1996) 397.
[40] A.J. Streeter, D.C. Dahlin, S.D. Nelson, T.A. Baillie, The covalent binding of acetaminophen to protein. Evidence for cysteine residues as major sites of arylation in vitro, Chem. Biol. Interact. 48 (1984) 349.
[41] A.M. Matthews, D.W. Roberts, J.A. Hinson, N.R. Pumford, Acetaminophen-induced hepatotoxicity. Analysis of total covalent binding vs. specific binding to cysteine, Drug Metab. Dispos. 24 (1996) 1192.
[42] T.M. Annesley, Ion suppression in mass spectrometry, Clin. Chem. 49 (2003) 1041.
[43] D. Tonoli, E. Varesio, G. Hopfgartner, Quantification of acetaminophen and two of its metabolites in human plasma by ultra-high performance liquid chromatography-low and high resolution tandem mass spectrometry, J. Chromatogr. B: Analyt. Technol. Biomed. Life Sci. 904 (2012) 42.
[44] L. Switzar, L.M. Kwast, H. Lingeman, M. Giera, R.H. Pieters, W.M. Niessen, Identification and quantification of drug-albumin adducts in serum samples from a drug exposure study in mice, J. Chromatogr. B: Analyt. Technol. Biomed. Life Sci. 917–918 (2013) 53.
[45] M.R. McGill, H.M. Yan, A. Ramachandran, G.J. Murray, D.E. Rollins, H. Jaeschke, HepaRG cells: a human model to study mechanisms of acetaminophen hepatotoxicity, Hepatology 53 (2011) 974.